POLITECNICO DI MILANO

Scuola di Ingegneria dei Sistemi

Corso di Laurea Magistrale in Ingegneria Biomedica

Design and development of a 3D Ewing's sarcoma model and a compression bioreactor as innovative *in vitro* tools for Cancer Tissue Engineering.

Relatore: Prof.ssa Manuela Teresa Raimondi
Correlatore: Prof.ssa Gordana Vunjak-Novakovic

Tesi di Laurea di
Alessandro Marturano Matr. 766118

Anno Accademico 2012-2013

Contents

INDEX OF FIGURES, TABLES and GRAPHS

SUMMARY

Introduction and background

Maintenance of homeostasis at the tissue level involves the integration and response to signals from within the tissue itself and from its surroundings, and disruption at any of the detection, the transduction or the response steps may lead to uncontrolled growth, producing what is called a neoplasm or tumor. More precisely, cancer denotes diseases that give rise to abnormal cells that proliferate indefinitely, and that can invade nearby tissues and spread to other parts of the body through the blood and lymph systems.

For over a century our understanding of cancer processes and stages has been derived from detailed studies of the histopathology of tumors. In parallel with this approach, both the two-dimensional (2D) culture and *in vivo* models of cancer have been actively used to unravel the complex mechanisms and molecular pathways of cancer pathogenesis. It is although known that cancer cells lose many of their relevant properties in 2D culture, presumably due to the lack of the native-like physiological milieu with 3D extracellular matrix (ECM), other cells and regulatory factors. As a result, 2D cultures are not predictive of antitumoral drug effects in the human being [1] [2]. Additionally, it has been proven that also animal models have their own limitations in representing human disease [3], necessitating the use of clinical data [4]. Bioengineering methods are just starting to enter the field of cancer research, offering simple 3D models of cancer – such as tumor spheroids, cell inserts, and cell encapsulation in hydrogels or in porous scaffolds [5] [6, 7]. While these models are an advance over monolayer cultures, cancer cells still remain deprived of native tumor environments where cancer cell-nonmalignant cell interactions are crucial for tumor biology [8]. Indeed, the microenvironment can both inhibit and facilitate tumor growth and metastatic dissemination to distant organs [9]. However, current approaches are far from replicating the native *in vivo* milieu in which tumors develop, a necessary condition for advancing cancer research and translating novel therapies into clinical practice. **Aim 1** of this thesis is to develop a model of human bone cancer (Ewing's sarcoma) engineered by introducing tumor cell spheroids into their resident bone tissue environment that has been formed by culturing human mesenchymal stem cells in decellularized bone matrix. This innovative model allows not only the cross-

talk between the cancer cells, but also the interactions of cancer cells with the human bone cells and the mineralized bone matrix. Within such native-like environment, cancer cells (*i*) re-express focal adhesion and cancer related genes that are highly expressed in tumors but lost in monolayer cultures, (*ii*) recapitulate the original hypoxic and glycolytic tumor phenotypes, and (*iii*) acquire angiogenic capacity and vasculogenic mimicry that favor tumor initiation and adaptation. Furthermore, tumor cells and healthy cells embedded in an *in vivo* tissue, continuously sense the biochemical and mechanical state of their environment, transduce the extracellular signals into intracellular signals, integrate these signals, and respond accordingly. It has become likely, that this process called mechanotransduction signaling has a crucial role in the maintenance of many mechanically stressed tissues, such as muscle, bone, cartilage and blood vessels [10]. In order to emulate such external inputs, a broad number of research groups have developed devices, commonly referred as bioreactors, capable of inducing physiological-like stimuli.

For the last decade, bioreactors have been extensively employed in the Tissue Engineering field with the promise of obtaining implantable viable tissue constructs [11]. However, after a rapid improving and some optimistic results – mostly in the field of bone and cartilage tissue engineering [12, 13] – the translation of experimental *in vitro* findings into a clinical approach still remains a vast challenge. Although their clinical applications in regenerative medicine tend to receive most of the attention, in this work an innovative application for bioreactors has been proposed. In fact, **aim 2** of this project is the design and development of a compression bioreactor for Cancer Tissue Engineering that can provide mechanical loading to 24 independent samples, easy to assemble, with a user friendly interface and suitable for drug studies. Since several studies have shown that changes in the ECM stiffness can regulate tumor growth, and in particular the one of Tse *et al.* that has shown that compressive stress stimulates migration of mammary carcinoma cells, this device could provide deeper insights on the effects that mechanical stimuli have on tumor cells. For these reasons, the tissue engineered Ewing's sarcoma is stimulated using the compression bioreactor to investigate whether or not mechanical loading – kept in a physiological range – inhibits or enhances tumor cells' motility and invasiveness. In particular, tumor proliferation and spreading could be induced by the re-expression of some focal adhesion genes such as RHOA and CDC42 and the formation of f-actin stress fibers (**aim 3).**

The specific aims of this thesis can be summarized as follow:

Aim 1. Tissue engineered Ewing's sarcoma: development, validation and characterization of a novel 3D Ewing's sarcoma model that *(i)* re-express focal adhesion and cancer related genes, (*ii*) recapitulates the original hypoxic and glycolytic tumor phenotypes and (*iii*) acquire angiogenic capacity and vasculogenic mimicry that favor tumor initiation and adaptation.

Aim 2. Compression bioreactor: design and validation of a compression bioreactor that allows *(i)* operating with a statistically significant number of independent samples, *(ii)* that is easy to assemble, with *(iii)* a user-friendly interface and *(iv)* that is suitable for drug studies.

Aim 3. Effects of compressive stimuli on the TE-ES model: study the effects of physiological mechanical stimuli on tumor cells behavior, applying dynamic compression to the tissue engineered Ewing's sarcoma (TE-ES) via the compression bioreactor.

Materials and methods

Aim 1: tissue engineered Ewing's sarcoma.

Cell culture scaffolds (4 mm diameter x 4 mm high plugs) were prepared from fully decellularized bone as in previous studies [14] [15]. The scaffolds were seeded with 1.5 x106 hMSCs (passage 3) and cultured in 6 mL of osteogenic medium for 4 weeks. After 4 weeks, the scaffolds were bisected; one half was seeded with Ewing's sarcoma cells (3 spheroids per scaffold) (TE-ES) and the other half was used as a control (TE-bone).Three tumor models were formed using three different tumor cell lines: RD-ES, SK-N-MC and EWS-GFP. The three models have been characterized and validated using several types of techniques. First, to assess the re-expression of focal adhesion genes (**aim 1** (i)) a high-throughput micro-array analysis has been performed comparing the gene expression of Ewing's sarcoma cell lines and tumor harvested from patients. A set of genes related to focal adhesion and tumorigenesis up-regulated in real tumors but not in 2D cell lines were selected, and their expression in the TE-ES was measured using qRT-PCR. Second, to evaluate the expression of hypoxic and glycolytic tumor phenotypes (**aim 1** (ii)) the necrotic areas in the inner part of TE-ES models were identified by Hematoxylin and Eosin staining and the apoptotic cells were quantified using TUNEL immunofluorescent staining

in the TE-RDES, TE-SK-N-MC and TE-EW-GFP. Hypoxia was further studied using qRT-PCR technique to measure the mRNA expression levels of HIF1a. Moreover, glycolytic phenotype was confirmed by immunohistochemical (IHC) staining of GLUT-1 in the TE-RDES, TE-SK-N-MC and TE-EW-GFP. Finally, angiogenesis and vasculogenic mimicry (**aim 1** (iii)) were first assessed measuring the mRNA levels of VEGFa by qRT-PCR. Then, angiogenesis-related proteins were detected in TE-ES culture media using an ELISA assay and compared with expression levels in the TE-bone counterparts. Finally PAS-stained sections from TE-bone and TE-ES models confirmed the vasculogenic mimicry.

Aim 2: compression bioreactor.

After individuating what were the aspects of previous bioreactors intended to improve with this device and after exploring a few different options, the three main modules of the system were defined:

The culture module: includes the main platform with the culture chambers that provide the mechanical stimuli. The stimulus results from the vertical uni-directional motion of a plunger in direct contact with the scaffold.
The compression module: comprises the stepper motor and the linear actuator that provide the linear motion.
The control module and user interface: involves the microcontroller through which all the culture and the stimulation parameters can be inserted and adjusted.

The *Culture module* is build by assembling several parts together:

1) *The Fluid Exchange layer*: this component is needed to add and remove independently the medium from each culture well. By this mean, it is also possible to add growing factors or drugs to each sample, individually. It is made with stereolitography technique casting liquid PDMS (polydimethylsiloxane) mixture inserted into a custom-designed mold.
2) *The Clamping system*: with a combination of special springs called Belleville springs and cam levers, the plunger can easily be clamped and released. Without the clamping

force, the plungers will then fall freely upon the scaffold giving a precise “zero” positioning.

3) *The Lid*: this is the supporting part for the *Clamping system* and the *Fluid Exchange layer*.
4) *The Well insert*: this component sits at the bottom of each well and is meant to hold the scaffold in the correct position.
5) *The Grommet*: this is a boundary of soft silicone that is meant to seal the chambers and to bear the loading that derives from the vertical motion. It is attached to a modified version of a 24-well plate cover.
6) *The 24-well plate*: this component represents the base of the bioreactor, providing 24 independent culture wells.

The *Compression module*, on the other hand, is the part responsible of the vertical motion that results in compression loading when the plungers are in contact with the scaffolds. The unidirectional motion is provided by an integrated stepper motor/linear actuator. A stepper motor is a brushless, synchronous, electric motor that converts digital pulses into mechanical shaft rotation. Then the rotary motion can be converted into linear motion using a lead screw/worm gear drive system (linear actuator). The linear actuator (*Compression module*) and *Lid (Culture module)* are connected by a rigid shaft coupling, which is a unit of hardware used to join two shafts within a motor or mechanical system. In particular, the shaft coupling connects the linear actuator’s rod with a thumb screw that is stably screwed into the *Lid*. Thus, this solution allows the operator to easily fasten the two pieces (the linear actuator and the *Lid*) using the shaft coupling and also makes it possible to adjust the four set screws to ensure a tight coupling. The loader control system (*Control module*) consists of an Arduino Pro Mini and an A4988 stepper motor driver IC. The A4988 allows the Arduino to control the motion of the actuator with just two microcontroller digital output pins. One pin sets the direction of motion and the other causes the actuator to take one step every time that it is pulsed. In addition, four other digital output pins are used to send a four-bit binary number to the stepper driver indicating the desired micro-stepping resolution. Within an intuitive graphical user interface, the operator selects a governing waveform for the loading. The options are: triangular, sinusoidal, and trapezoidal waveforms. Then, the operator specifies the frequency,

amplitude, and resolution of the motion. After the parameters are finalized and the operator clicks the update button, the computer serially transmits several bytes of data to the Arduino that characterize the chosen profile. After all of this is accomplished, the operator no longer plays a role and all actuator control is executed by the Arduino.

In order to validate the system, first the accuracy of platen displacement was assessed by comparing expected results with those obtained. To monitor the displacement of the *Lid* an electronic dial indicator mounted on the bioreactor was used. Different magnitudes of displacement in millimeters were configured for the individual application of compressive loading for the three different waveforms (triangular, trapezoid and sinusoidal). Frequency was held constant first at 0.1 Hz and then at 1 Hz. The applied displacements were then plotted against the measured displacements to assess the correlation between these variables. Secondly, a simulation on COMSOL® Multiphysics 4.2a of a basic experimental setup to evaluate the stress field within our culture chamber has been operated. Briefly, using the software 3D drawing tools, the culture well with, well insert, scaffold and plunger were recreated. The motion waveform designed was a sine wave with 14 μm of amplitude (0.7% of strain with a 2X4 mm scaffold) at 1 Hz frequency. The bone scaffold was supposed linear elastic [16] and the material properties such as Young Modulus (50 MPa), density (434 kg/m^3) and Poisson ratio (0.3) were used according to the paper published by Marcos-Campos *et al.* [17]. Finally, a *Quasi-static analysis* that solves a time-dependent problem, assuming the structural mechanics part being static was performed.

Aim 3: effects of compressive stimuli on the TE-ES model.

After the technical validation, where the reliability and the consistence of the system have been evaluated, it has been decided to use the compression bioreactor in a pilot study. The TE-ES was generated by using the established protocol previously described and the samples were stimulated using the compression loading of the bioreactor. The compression protocol consisted in twenty-four hours of culture in the bioreactor with three loading inputs. The application consisted of 0.7% of strain (for a 2 mm thick scaffold it equals 14 μm of displacement amplitude), applied using a sinusoidal wave form for the vertical motion at 1 Hz frequency for 1800 loading cycles (equivalent of 30 minutes of stimulation). The same stimulation protocol was applied to TE-bone constructs that served

as control samples. First the re-expression of focal adhesion genes, such as RHOA and CDC42 was measured by qRT-PCR. The expression levels in the stimulated TE-ES SK-N-MC models were compared to those of the SK-N-MC 2D cell lines, the ES tumor samples from patients and the TE-ES SK-N-MC non-stimulated models. Finally, an f-actin staining provided qualitative information on the polymerization of actin stress fibers.

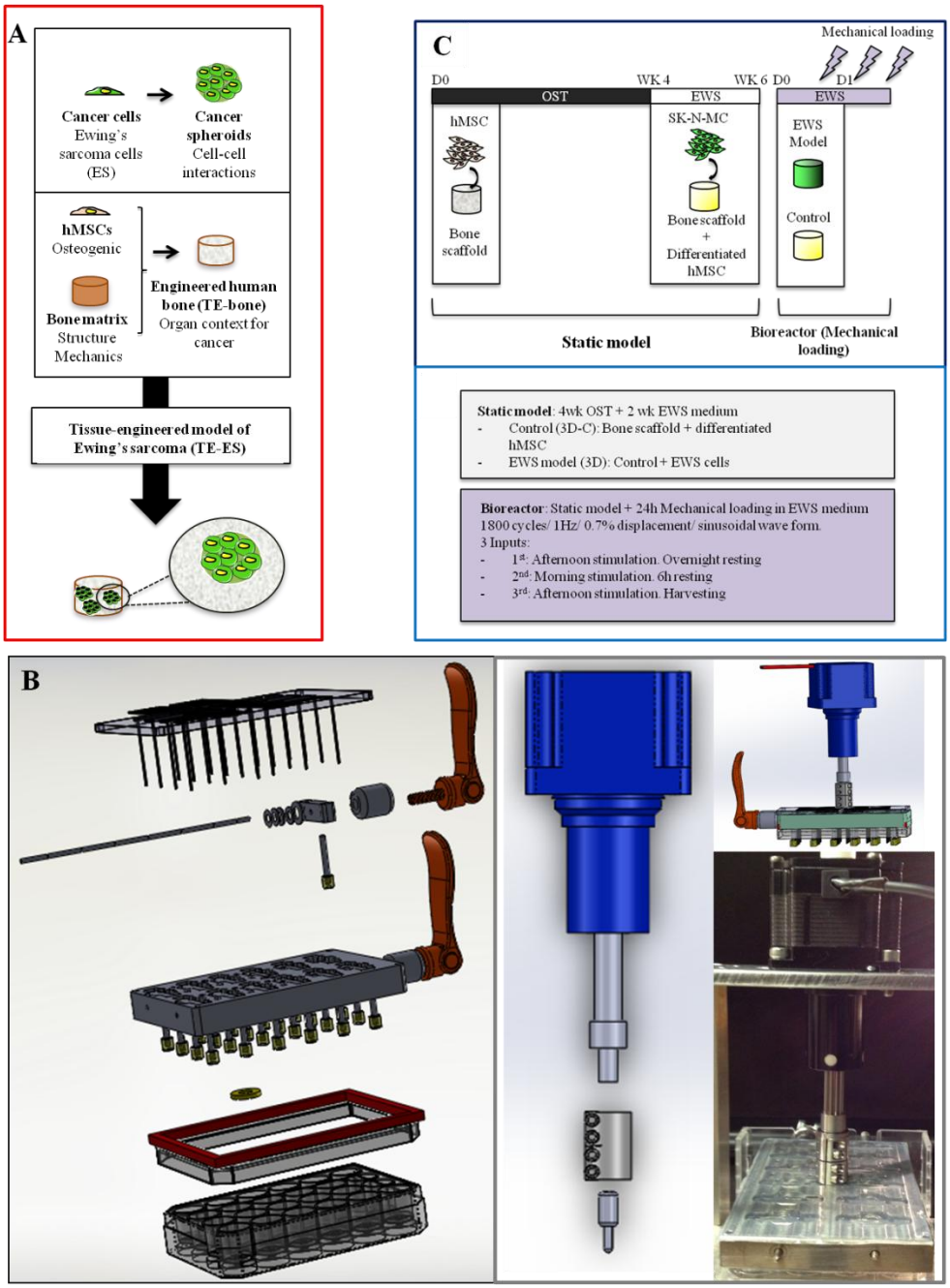

Figure I. General overview of the three aims of this project. (A) Generation of a 3D TE-ES (**aim 1**). (B) Compression bioreactor assembly (**aim 2**). (C) Experimental set-up of the pilot study (**aim 3**)

Results and discussion

In order to validate the TE-ES model, histological sections were analyzed by hematoxylin-eosin staining, allowing the detection of large areas with small-round cells that were CD99 positive and surrounded by bone cells and ECM (**fig. II A1**). Gene expression profiles of cell lines cultured in monolayers and native tumors was compared, with focus on differentially expressed focal adhesion genes and cancer pathways. A group of twelve differentially expressed genes in both TE-RD-ES and TE-SK-N-MC models evidenced a major role of microenvironment in the acquirement of tumor expression profile (**fig. II A2**). This model could therefore be used for the characterization of differentially expressed genes and could then help identify new tumor targets. The primary bone tumor RD-ES cell line seemed to perfectly mimic the ESFT signature, the *in vitro*-generated EWS-GFP cell line only in part and the metastatic SK-N-MC cell line was not able to recapitulate many of the tumor characteristics. These differences, correlated to the expression levels of HIF1-α (low in RD-ES cells, and high in SK-N-MC and EWS-GFP cells), suggesting that HIF1-α might play a protective role in the adaptation of tumor cells to hypoxia (**fig. II B1**). TUNEL assays after 4 weeks of cultivation revealed higher cell death in the middle of the TE- SK-N-MC tumor model (73 ± 36%) relatively to TE-RD-ES (29± 3%) and/or TE-EW-GFP(16± 2%) (**fig. II B2**). Tumor cells respond to oxygen and nutrient deprivation by promoting vascularization that maintains tumor growth and survival [18]**.** Induction of vascular endothelial growth factor (VEGFA) is an essential feature of tumor angiogenesis that is driven by hypoxia and mediated by HIF1α. High induction of VEGFA in TE-RD-ES was found at week 2 compared to the RD-ES cell line and TE-bone. Then, by an ELISA assay it has been attempted to identify angiogenic proteins secreted by TE-ES tumors (**fig. II C2**). This analysis demonstrated that 8 proteins (Angiopoietin, CXCL16, Endothelin-1, FGF-7, IGFBP1-1, PIGF, TGF- β1 and TIMP4) were highly expressed in TE-RD-ES and TE-EW-GFP tumor models compared to TE-bone (fold change >3). In contrast, none of these proteins was detected in the TE-SK-N-MC tumor model. Interestingly, Endothelin-1 is implicated in ES proliferation and invasion while IGFBP1-1 prolongs the half-life of

IGF-1, a well-known target gene of EWS-FLI and TGF-β1. These observations are consistent with previous studies, validating the system object of this work. Native ES is featured by the presence of blood lakes and PAS positive cells expressing endothelium-associated genes [19]. Tissue sections stained with PAS revealed positive areas in all the TE-ES models (except in TE-EW-GFP at week 2), as compared to negative-PAS TE-bone (**fig. II C1)**. All the data point to a new direction in tumor modeling, where tumor cells are studied within the 3D niche – engineered to mimic the native host tissue.

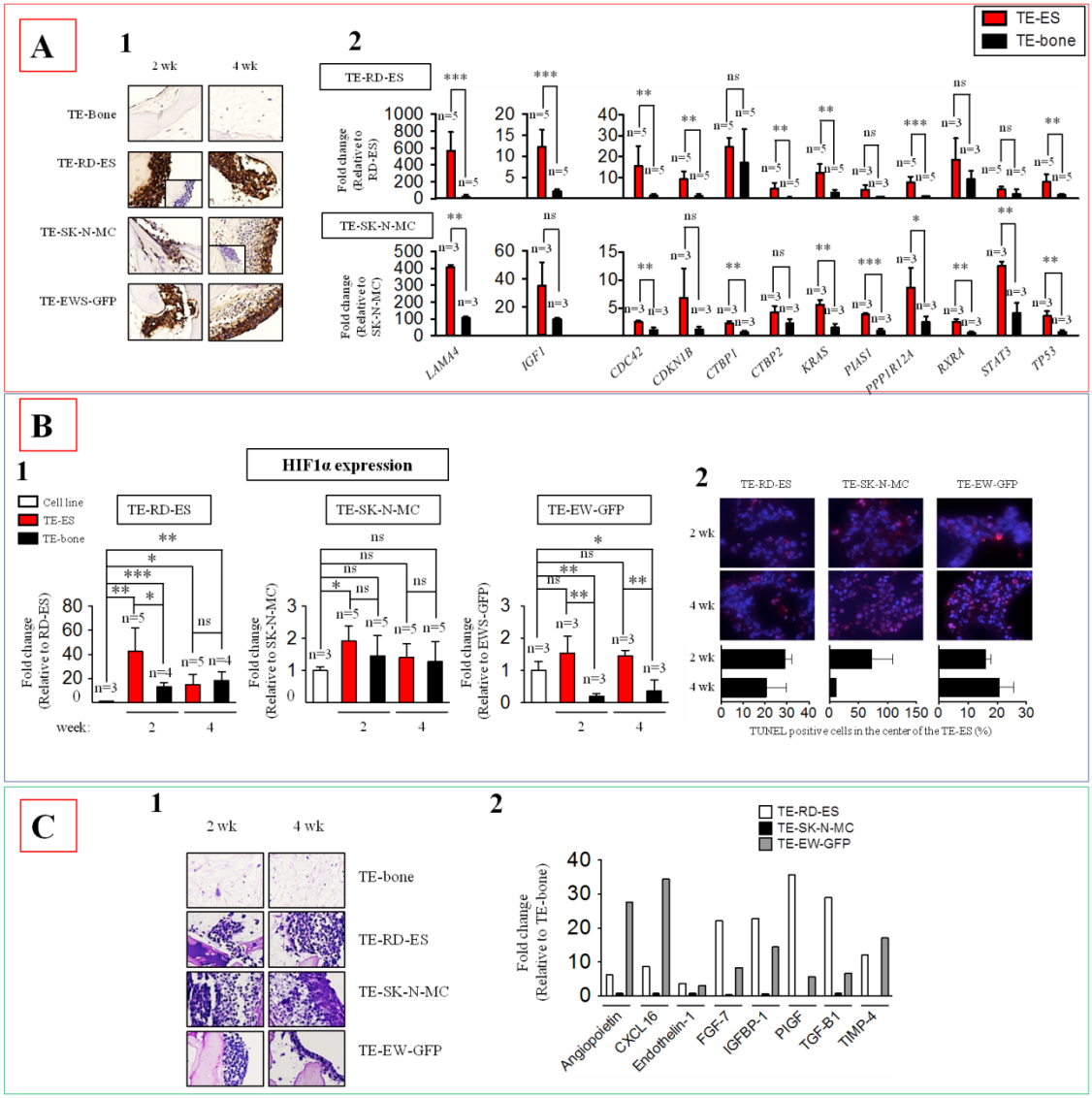

Figure II. TE-ES characterization. (A) Re-activation of focal adhesion pathways analyzed by CD99 staining (1) and mRNA expression levels in TE-ES compared to 2D cell lines (2). (B) Hypoxia and glycolitic phenotype evaluated via mRNA expression of HIF1α (1) and TUNEL staining (2). (C) Angiogenesis and vasculogenic mimicry evaluated through PAS staining (1) and ELISA assay (3).

In order to assess the reliability of the device, making it suitable for the pilot study, a technical validation has been performed. It consisted in the evaluation of the accuracy of the *Lid's* displacement (measured value) compared to the value given as an input by the operator (reference value). In most cases, the accuracy was higher than 90% and became less only when the motor had to perform displacement in the range of a few microns. Using COMSOL® Multiphysics, a finite element analysis of the stress field, arising in the bone scaffold as a response to dynamic compression, was performed. Solving Von Mises' tensor, the stress field generated in the construct was calculated and the stresses were in the range of $2.5x10^5$ - $5.0x10^5$ [Pa], depending on the position within the plug. It is likely that the cells within the scaffold sense these physical stimuli, and that they integrate these signals activating the mechanotransduction process. It is, hence, interesting to evaluate whether or not tumor cells react to these stimuli, for example by expressing focal adhesion genes and by forming f-actin stress fibers. Hence, in the proposed pilot study (**aim 3**), the TE-ES model was stimulated during 24 hours for three times at physiological values. The stimulation not only induced further expression of the already re-expressed CDC42 (compared to cell lines), but the fold change was comparable to the one seen in real tumors. Moreover, along with an increase of RHOA expression, F-actin staining demonstrated that the cells under mechanical compression – in TE-SK-N-MC but not in TE-bone – had a polarized shape and were highly oriented. Similar to these results are the results obtained by Tse *et al.* that showed how compressive stress induced a subset of "leader cells" to extend filopodia enhancing migration of mammary carcinoma cells [20].

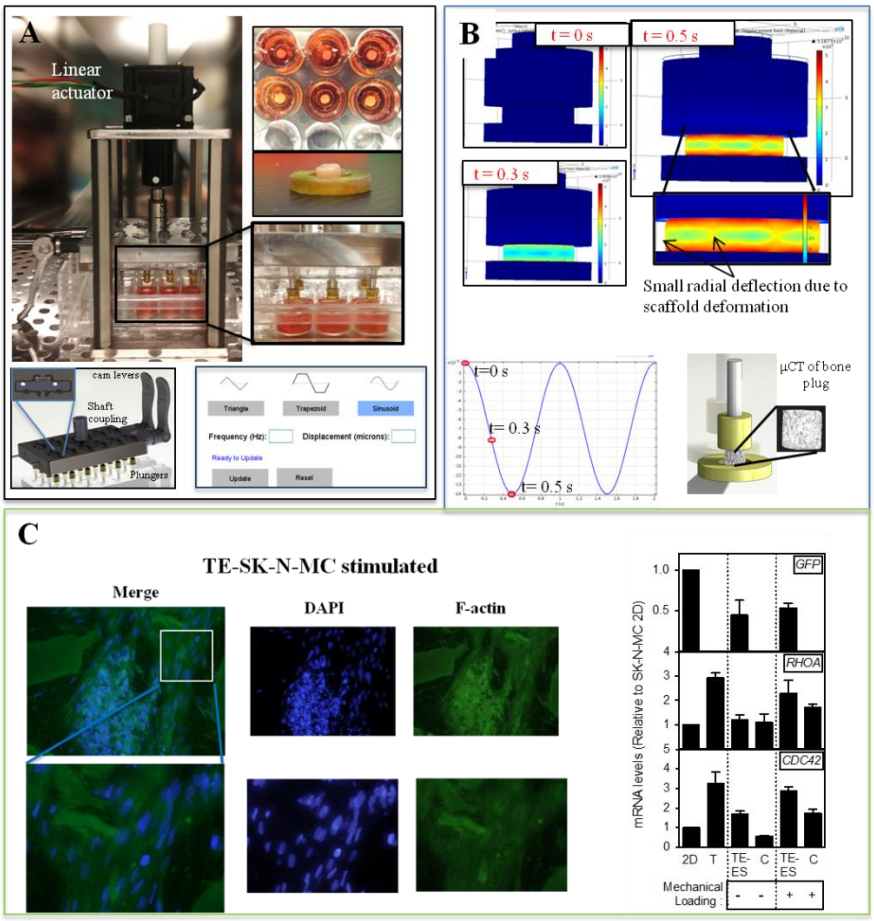

Figure III. Pilot study and COMSOL® simulations. (A) Bioreactor setup with TE-ES samples. (B) Stress field analysis in TE-Bone. (C) F-actin staining and focal adhesion genes expression in TE-ES.

Based on the specific goals of this work, it is possible to conclude that, **Aim 1** (TE-ES model) and **Aim 2** (compression bioreactor) have been fully achieved while preliminary work has been carried out for **Aim 3** (pilot study). Here, a bioengineered model of human Ewing's sarcoma that mimics the *in vivo* bone tumor niche with high biological fidelity is described. In this model, cancer cells that have lost their transcriptional profiles after monolayer culture re-express genes related to focal adhesion and cancer pathways. The bioengineered model recovers the original hypoxic and glycolytic tumor phenotype, and leads to re-expression of angiogenic and vasculogenic mimicry features that favor tumor adaptation. Moreover, a novel compression bioreactor has been designed and validated allowing to operate with a statistically significant number of independent samples, easy to assemble, with a user-friendly interface and suitable for drug studies. Finally, the pilot study provides deeper insights on the effects of mechanical loading on the TE-ES model. In the future, it will be important to optimize and fully validate both the Ewing's sarcoma

experimental model and the compression bioreactor. The ultimate goal will be to establish an enabling technology for cancer research, in form of a bioengineering platform for studies of cancer biology and high-throughput screening of model *in vitro*. In order to develop the proposed platforms with bioengineered human tumors, for an advanced cancer research, it is possible to pursue three specific directions in a highly integrated fashion. First, to improve the actual model the TE-bone should be pre-vascularized with HUVECs; second, it will be important to integrate the compression bioreactor with a perfusion system that could provide controlled oxygen and nutrient supply to the constructs; third, it would be advisable to develop bioengineering platforms for high-throughput screenings of therapeutic ES targets, scaling down the TE-ES models.

Sommario

Introduzione e contesto

Il mantenimento dell'omeostasi a livello tessutale prevede l'integrazione e la risposta a segnali presenti nel tessuto stesso e nell'ambiente circostante. La rottura, in una qualsiasi delle fasi di rilevazione, di trasduzione e di risposta, può portare ad una crescita incontrollata, producendo una cosiddetta neoplasia o tumore.

Più precisamente, il cancro definisce un gruppo di malattie che danno origine a cellule anomale che proliferano indefinitamente, e che possono invadere tessuti vicini diffondendosi in altre parti del corpo attraverso il sangue e il sistema linfatico. Per oltre un secolo, la comprensione dei processi tumorali è derivata da studi dettagliati dell'istopatologia dei tumori. Parallelamente a quest'approccio, sono stati utilizzati intensamente sia le culture bidimensionali (2D) che i modelli *in vivo* di tumore per investigare i complessi meccanismi e le vie molecolari della patogenesi del cancro. Eppure, le cellule tumorali perdono molte delle loro proprietà più rilevanti nella cultura 2D – presumibilmente a causa della mancanza del "milieu" fisiologico nativo che comprende la matrice 3D extracellulare (ECM), altre cellule e fattori regolatori. Le culture 2D, dunque, possono essere considerate non predittive degli effetti che i farmaci antitumorali potranno avere nell'essere umano [1 134] [2 107].

È stato inoltre dimostrato come persino i modelli animali non siano spesso rappresentativi delle malattie presenti nell'uomo [3 135], richiedendo quindi l'ausilio di ulteriori dati clinici [4 136]. Recentemente, alcuni metodi di bioingegneria stanno iniziando ad entrare nel campo della ricerca finalizzata allo studio sul cancro offrendo semplici modelli 3D della malattia, come: sferoidi tumorali, inserti cellulari e incapsulamento di cellule in idrogel o *scaffold* sintetici [5 9] [6 137, 7 138]. Anche se questi modelli sono considerati un miglioramento rispetto alle colture monostrato, le cellule tumorali rimangono ancora prive degli ambienti rispecchianti la realtà nella quale le interazioni cellula maligna-cellula sana sono d'importanza cruciale per la sopravvivenza e la progressione della malattia [8 125].

In effetti, il microambiente é in grado sia di inibire sia di facilitare la crescita del tumore e la diffusione metastatica – messa in atto al fine di colonizzare anche organi distanti [9 39]. Tuttavia, gli approcci attuali sono tutt'altro che adeguati per replicare la complessità dell'ambiente nativo presente *in vivo*, in cui si sviluppano i tumori. Quest'ultima, però è una condizione necessaria per far progredire la ricerca sul cancro e permettere l'adozione di terapie avanzate nella pratica clinica.

L'obiettivo 1 di questa tesi è, quindi, quello di sviluppare un modello di tumore osseo umano (sarcoma di Ewing) ingegnerizzato reintroducendo degli sferoidi di cellule tumorali nel loro ambiente osseo, ottenuto dalla coltura di cellule staminali mesenchimali umane in una matrice ossea decellularizzata. Questo modello innovativo non solo permette il "cross-talk" tra le cellule tumorali, ma anche le interazioni delle cellule tumorali con le cellule ossee umane e, infine, la matrice ossea mineralizzata. Queste cellule tumorali, inserite in un contesto più vicino a quello nativo:(i) fanno ri-esprimere geni associati all'adesione focale e al cancro, e che sono comunemente espressi in tumori, ma non in colture monostrato, (ii) ricapitolano il fenotipo tumorale ipossico e glicolitico originario, e (iii) acquisiscono capacità angiogenica e di mimica vascolare che favorisce l'iniziazione e l'adattamento del tumore. Inoltre, in un tessuto *in vivo* le cellule maligne e le cellule sane sono in grado di rilevare continuativamente lo stato biochimico e meccanico del loro ambiente, trasducendo i segnali extracellulari in segnali intracellulari, integrando questi segnali e rispondendo a essi. E' sempre più evidente che questo processo, chiamato meccanotrasduzione, ha un ruolo cruciale nel mantenimento di molti tessuti come muscolo scheletrico, osso, cartilagine e vasi sanguigni soggetti a carichi di tipo meccanico [18]. Per emulare tali input esterni, un ampio numero di gruppi di ricerca ha sviluppato dispositivi, comunemente indicati come bioreattori, in grado di indurre stimoli fisiologici simili a quelli presenti *in vivo*. Nell'ultima decade, i bioreattori sono, quindi, stati largamente impiegati nel settore dell'ingegneria dei tessuti, con l'obiettivo ultimo di ottenere costrutti di tessuto vitale impiantabili in pazienti [64]. Tuttavia, dopo un rapido miglioramento e alcuni risultati ottimistici - per lo più nel campo dell'ingegneria tessutale di ossa e cartilagine [65,70] - la traduzione dei risultati ottenuti *in vitro* in pratica clinica rimane ancora una realtà lontana. Anche se l'impiego di bioreattori per applicazioni cliniche finalizzate alla medicina rigenerativa tende a ricevere la maggior parte dell'attenzione, in questo lavoro ne è stata proposta un'applicazione innovativa. L'**obiettivo 2** di questa tesi è,

infatti, la progettazione e lo sviluppo di un bioreattore per l'ingegneria dei tessuti tumorali in grado di fornire un carico meccanico a 24 campioni indipendenti, facile da montare, con un'interfaccia semplice, e consono per l'investigazione degli effetti dei farmaci su modelli ingegneristici. Questo dispositivo, inoltre, potrebbe fornire maggiori approfondimenti sugli effetti che gli stimoli meccanici hanno sulle cellule tumorali; difatti, alcuni studi hanno dimostrato che lievi cambiamenti nella rigidità dell'ECM possono regolare la crescita del tumore e, in particolare, Tse *et al.* ha dimostrato che la sollecitazione compressoria stimola la migrazione di cellule di carcinoma mammario.

In questa tesi, il modello ingegnerizzato Ewing sarcoma sarà stimolato utilizzando il nuovo bioreattore per indagare se il carico meccanico - mantenuto in un intervallo fisiologico - inibisca o favorisca la motilità e l'invasività delle cellule tumorali. In particolare, la proliferazione tumorale e la diffusione potrebbero essere promosse dalla ri-espressione di alcuni geni legati all'adesione focale come RHOA e CDC42 e la formazione di filamenti di actina indotti dallo stress meccanico (**obiettivo 3)**.

Gli obiettivi specifici di questa tesi possono essere riassunti come segue:

Obiettivo 1. Generazione di un modello ingegnerizzato di Ewing sarcoma: lo sviluppo, la validazione e la caratterizzazione di un innovativo modello 3D di Ewing sarcoma a partire da tre differenti linee cellulari in grado di (i) ri-esprimere geni correlati all'adesione focale e al cancro, (ii) ricapitolare il fenotipo tumorale ipossico e glicolitico originario e (iii) acquisire capacità angiogenica e mimica vascolare favorendo l'iniziazione e l'adattamento del tumore.

Obiettivo 2. Bioreattore per compressione: progettazione e validazione di un bioreattore per compressione che consenta (i) di operare con un numero statisticamente significativo di campioni indipendenti, (ii) che sia di facile montaggio, con (iii) un'interfaccia "user-friendly" e (iv) adatto per lo studio degli effetti di farmaci.

Obiettivo 3. Studio degli effetti di stimoli di compressione su un modello di TE-ES: impiego del bioreattore per compressione al fine di studiare gli effetti di stimoli meccanici fisiologici sul comportamento delle cellule tumorali presenti nel tessuto ingegnerizzato di Ewing sarcoma (TE-ES).

Materiali e metodi.

Obiettivo 1: Generazione di un modello ingegnerizzato di Ewing sarcoma. Gli *scaffold*, impiegati nel modello di Ewing sarcoma (diametro 4x4 mm), sono stati ricavati da osso trabecolare bovino completamente decellularizzato, seguendo il protocollo validato in studi precedenti [76] [77]. Gli *scaffold* sono stati, in seguito, seminati con 1,5 $x10^6$ hMSCs (al passaggio 3) e, dopo quattro settimane di cultura, i campioni sono stati divisi: una metà è stata seminata con cellule di Ewing sarcoma (3 sferoidi per *scaffold*) (TE-ES) e l'altra metà è stata utilizzata come controllo (TE-osso).

Tre modelli tumorali sono stati formati usando tre linee cellulari tumorali: RD-ES, SK-N-MC e EWS-GFP. I modelli sono stati caratterizzati e validati utilizzando una grande varietà di tecniche. Inizialmente, per valutare la ri-espressione di geni legati a processi di adesione focale (**obiettivo 1** (i)), è stato utilizzato un micro-array, che permette di confrontare l'espressione genica di linee cellulari rispetto a campioni di Ewing sarcoma estratti da pazienti. Un gruppo di geni legati all'adesione focale e tumorigenesi altamente espressi in tumori nei pazienti, ma non in cellule 2D, è stato selezionato e, utilizzando la tecnica di qRT-PCR, è stata misurata l'espressione del mRNA in ognuno dei TE-ES. In secondo luogo, utilizzando uno "staining" di ematossilina-eosina sono state individuate le aree necrotiche per la maggior parte presenti nella superficie interna dei campioni. Inoltre, le cellule apoptotiche sono state individuate e quantificate mediante immunofluorescenza TUNEL nel TE-RDES, TE-SK-N-MC e TE-EW-GFP. L'ipossia è stata ulteriormente studiata utilizzando la tecnica qRT-PCR al fine di misurare i livelli di espressione di mRNA di HIF1a. In aggiunta, il fenotipo glicolitico è stato confermato tramite una colorazione immunoistochimica (IHC) di GLUT-1 in TE-RDES, TE-SK-N-MC e TE-EW-GFP. Queste analisi hanno perciò permesso di confermare l'espressione del fenotipo ipossico e glicolitico nei diversi modelli (**obiettivo 1** (ii)). Infine, l'angiogenesi e la mimica vascolare (**obiettivo 1** (iii)) sono stati inizialmente studiati tramite un'analisi qRT-PCR misurando l'espressione di mRNA relativo al VEGFA; in seguito, è stato eseguito un saggio ELISA prelevando dal terreno di cultura delle TE-ES un cluster di proteine associate al processo di angiogenesi; e infine, sono state colorate delle sezioni dei modelli TE-ES con una reazione PAS (acido periodico - reattivo di Schiff) confermando la presenza di mimica vascolare.

Obiettivo 2: bioreattore per compressione. Dopo l'identificazione degli aspetti che richiedevano un miglioramento nei bioreattori esistenti , è stato possibile definire i tre moduli principali che dovrebbero comporre un dispositivo innovativo:
Il modulo di coltura che include la piattaforma principale con le camere di coltura che forniscono gli stimoli meccanici. Lo stimolo è trasmesso dal movimento unidirezionale di un pistone in diretto contatto con lo *scaffold*.

Il modulo di compressione che racchiude sia il motore passo-passo sia l'attuatore lineare, responsabili del movimento verticale.

Il modulo di controllo e l'interfaccia utente che comprende il microcontrollore attraverso il quale i parametri di cultura e di stimolazione possono essere inseriti e regolati.

Il *modulo di Cultura* è stato realizzato assemblando più parti insieme:

1) *Lo strato per lo scambio di fluidi*: componente necessario per aggiungere e rimuovere in modo indipendente il medium da ogni pozzetto di cultura. Grazie ad esso, è anche possibile aggiungere fattori di crescita o farmaci singolarmente ad ogni campione. Il pezzo è stato realizzato tramite la tecnica di stereolitografia in cui del PDMS (polidimetilsilossano) liquido viene fatto indurire in uno stampo opportunamente realizzato.
2) *Il sistema di serraggio*: con una combinazione di speciali molle chiamate "molle Belleville" e di leve a camma, il pistone può essere facilmente bloccato e rilasciato. Senza la forza di serraggio trasmessa dalle molle, i pistoni sono invece liberi di cadere sugli *scaffold* garantendo una posizione iniziale precisa e ripetibile.
3) *Il coperchio*: parte di supporto per il *sistema di serraggio* e lo *strato per lo scambio di fluido*, dove tutti i pezzi sono assemblati insieme.
4) *Base*: siede sul fondo di ciascun pozzetto e ha il compito mantenere lo *scaffold* in posizione centrata durante la stimolazione.
5) *La guarnizione*: bordo di silicone morbido con il compito di sigillare le camere e di supportare il carico che deriva dal movimento verticale. È collegato a una versione modificata di un coperchio per una comune piastra di coltura.
6) *La piastra di cultura a 24 pozzetti*: base del bioreattore, fornisce 24 pozzetti di coltura indipendenti tra loro.

Il *modulo di compressione,* invece, è la parte responsabile del movimento verticale che, quando i pistoni sono in contatto con gli *scaffold,* risulta in un carico di compressione. Un motore passo-passo, integrato con un attuatore lineare, è incaricato di generare il moto unidirezionale. Un motore passo-passo é un motore elettrico che converte degli impulsi digitali in rotazione, che a sua volta vengono tradotti in movimento lineare tramite, appunto, l'attuatore lineare. Quest'ultimo e il coperchio, parte rispettivamente del *modulo di compressione* e del *modulo di cultura* sono connessi tra loro tramite un'unità di hardware comunemente utilizzata per unire due alberi meccanici all'interno di un motore chiamata appunto "accoppiatore di alberi". In particolare, esso connette l'albero dell'attuatore lineare con una vite che è stabilmente avvitata al centro del coperchio. Questa soluzione permette all'operatore di fissare agevolmente i due pezzi (l'attuatore lineare e il coperchio); inoltre, regolando le quattro viti su di esso, si assicura un serraggio stretto.

Il sistema di controllo del motore (*modulo di controllo*) è costituito da un Arduino Pro Mini e un driver dedicato al motore passo-passo. Esso, infatti, permette all'Arduino di controllare il moto dell'attuatore con solo due pin di uscita digitali. In particolare, un pin imposta la direzione del moto mentre l'altro consente all'attuatore di compiere un passo per ogni impulso. Inoltre, altri quattro pin di uscita digitali sono utilizzati per inviare un numero binario a quattro bit al driver che controlla la risoluzione del "micro-stepping" che, dunque, permette spostamenti di dimensioni micrometriche. Grazie ad un'interfaccia grafica intuitiva, l'operatore può selezionare facilmente la forma d'onda desiderata che verrà eseguita dal motore. Le possibili opzioni di forma d'onda sono: triangolare, sinusoidale e trapezoidale. In sintesi, l'operatore imposta la frequenza, l'ampiezza, e la risoluzione del movimento e, in seguito, il computer trasmette serialmente diversi byte di dati all'Arduino che mette in moto il motore con il profilo scelto.
Per validare il sistema, prima è stata verificata la precisione dello spostamento del *modulo di coltura* confrontando i valori selezionati con quelli realmente ottenuti. Per misurare l'ampiezza di spostamento è stato utilizzato un sensore elettronico opportunamente montato sul bioreattore. In questo caso, sono stati fissati molteplici valori di spostamento per ognuna delle tre diverse forme d'onda (triangolare, trapezoidale e sinusoidale), mentre la frequenza é stata tenuta costante prima a 0.1 Hz e poi a 1 Hz. I valori teorici sono stati riportati graficamente contrapposti agli spostamenti misurati ed è stato poi calcolato il coefficiente di correlazione tra di essi. In secondo luogo, è stato simulato, grazie all'aiuto

di un software (COMSOL Multiphysics® 4.2) un settaggio sperimentale tipico al fine di valutare il campo di stress presente durante un ciclo di stimolazione all'interno della camera di coltura. In breve, utilizzando gli strumenti di disegno 3D integrati nel software, sono stati ricreati il pozzetto di cultura, la base, lo *scaffold* e il pistone. La forma d'onda sinusoidale avente 14 micron di ampiezza (corrispondente a 0,7% di deformazione con uno *scaffold* spesso 2 mm) e 1 Hz di frequenza è stata anch'essa ricreata nel software. Lo *scaffold* osseo è stato modellizzato come materiale lineare elastico [84] e le sue proprietà, quali il modulo di Young (50 MPa), la densità (434 kg / m ^ 3) e il coefficiente di Poisson (0.3), sono stati selezionati usando come riferimento uno studio condotto da Marcos-Campos *et al*. [79]. Infine, è stata eseguita un'analisi quasi-statica di un problema tempo dipendente, assumendo la parte strutturale meccanica statica.

Obiettivo 3: effetti degli stimoli compressivi sul modello TE-ES. Dopo la validazione tecnica, tramite la quale è stato possibile studiare l'affidabilità e la consistenza del sistema, si è deciso di utilizzare il bioreattore per compressione in uno studio preliminare. Il TE-ES è stato generato utilizzando il protocollo in precedenza descritto e i campioni sono stati stimolati con un carico di compressione del bioreattore. Il protocollo di stimolazione consisteva in 24 ore di cultura nel bioreattore con tre stimoli equivalenti a 0,7% di deformazione (per uno *scaffold* avente 2 mm di spessore pari a 14 micron di ampiezza), aventi forma d'onda sinusoidale e frequenza di 1 Hz per la durata di 1800 cicli di carico (equivalente a 30 minuti di stimolazione). Lo stesso protocollo di stimolazione è stato applicato ai costrutti TE-osso che servivano come campioni di controllo. Inizialmente, mediante qRT-PCR, si è misurata la ri-espressione di geni di adesione focale, come RHOA e CDC42. In seguito, i livelli d'espressione nei campioni di TE-ES-SK-N-MC stimolati sono stati confrontati con quelli delle linee cellulari in 2D e ai campioni di tumore prelevati da pazienti. Infine, una colorazione di f-actina ha permesso di estrarre informazioni qualitative sul grado di polimerizzazione delle catene di actina in seguito alla stimolazione meccanica.

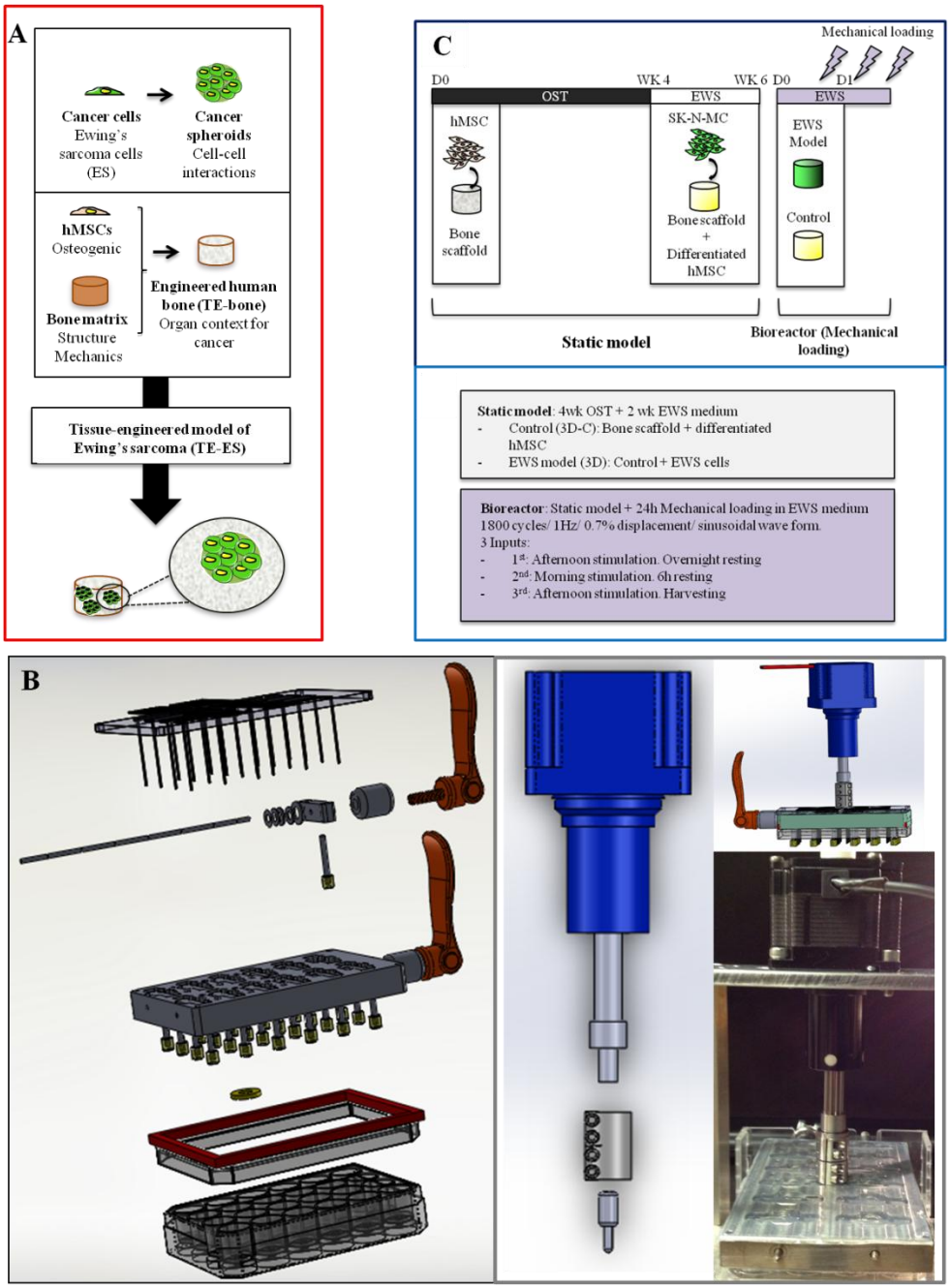

Figura I. Panoramica generale dei tre obiettivi di questo progetto. (A) Generazione di un modello 3D di TE-ES. (**obiettivo 1**). (B) Assemblaggio del bioreattore per compressione. (**obiettivo 2**). (C) Settaggio sperimentale dello studio preliminare (**obiettivo 3**).

Risultati e discussione.

Al fine di validare il modello di TE-ES, sono state analizzate delle sezioni istologiche mediante colorazione ematossilina-eosina, permettendo l'individuazione di grandi aree caratterizzate dalla presenza di piccole cellule CD99 positive e circondate da cellule ossee e matrice extracellulare (**fig. II A1**). Sono stati confrontati i profili di espressione genica delle linee cellulari coltivate in monostrato e delle cellule tumorali estratte dai pazienti, focalizzando l'attenzione sull'espressione di geni correlati ai "pathway" di adesione focale e tumorigenesi. In seguito, è stato possibile distinguere un set di geni diversamente espressi presenti in entrambi i modelli TE-SK-N-MC e TE-RD-ESe, evidenziando un ruolo importante del microambiente circostante nella ri-acquisizione del profilo di espressione tumorale (**fig. II A2**).

Questo modello può, quindi, essere utile al fine di caratterizzare e studiare dei geni finora inibiti dall'ambiente in due dimensioni e dalla mancanza di altre cellule. Tali geni, infine, potrebbero permettere di identificare nuovi target terapeutici su cui testare dei potenziali farmaci chemioterapici. La linea cellulare RD-ES, derivata da un tumore primario, sembra in grado di emulare perfettamente le caratteristiche che caratterizzano la famiglia di tumori associati all'Ewing sarcoma (ESFT). Inoltre, la linea cellulare EWS-GFP generata *in vitro* sembra adattarsi solo in parte all'ambiente circostanze e, infine, la linea cellulare SK-N-MC, di origine metastatica, non è stata in grado di riacquisire molte delle caratteristiche del tumore. Queste differenze sono correlabili ai livelli di espressione di HIF1-α (bassi livelli di espressione nelle cellule RD-ES, altamente espresse nelle linee cellulari di SK-N-MC e EWS-GFP), suggerendo che HIF1-α potrebbe svolgere un ruolo protettivo per l'adeguamento delle cellule tumorali alle condizioni d'ipossia (**fig. II B1**). L'analisi del test TUNEL, dopo 4 settimane di coltura, ha permesso di identificare la presenza di morte cellulare diffusa nel centro del modello TE-SK-N-MC (73 ± 36%) rispetto a TE-RD-ES (29 ± 3%) e / o TE-EW -GFP (16 ± 2%) (**fig. II B2**). Le cellule tumorali, infatti, rispondono alle privazioni di ossigeno e di nutrienti nell'ambiente circostante promuovendo il processo di neo-vascolarizzazione che permette la crescita della massa tumorale e la sua sopravvivenza [94]. L'induzione del fattore di crescita vascolare endoteliale (VEGFA) è una caratteristica essenziale dell'angiogenesi tumorale guidata da condizioni d'ipossia e mediata dall'espressione di HIF1α. E' possibile osservare alla settimana 2, nel modello TE-RD-ES un'elevata espressione di VEGFA rispetto alla linea cellulare RD-ES e al controllo (TE-osso). Infine, mediante saggio ELISA, si è cercato di

individuare tra le proteine secrete dai TE-ES quelle associate a processi di angiogenesi (**fig. II C2**). Tale analisi ha permesso di dimostrare che otto proteine (Angiopoietina, CXCL16, endotelina-1, FGF-7, IGFBP1-1, PIGF, TGF-β1 e TIMP4), sono altamente espresse nei modelli TE-EW-GFP e TE-RD-ES rispetto al TE-bone (fold change> 3). Al contrario, nessuna di queste proteine è stata rilevata nel modello di tumore TE-SK-N-MC. È, inoltre, interessante osservare che l'endotelina-1 nell'Ewing sarcoma è implicata nella proliferazione e invasione mentre IGFBP1-1 prolunga l'emivita di IGF-1, un noto gene bersaglio di EWS-FLI e TGF-β1. Queste osservazioni sono coerenti con gli studi precedenti, e convalidano perciò il sistema oggetto di questo lavoro.

I tessuti tumorali di Ewing sarcoma estratti da pazienti sono, nella maggior parte dei casi, caratterizzati dalla presenza di "blood lakes" (laghi di sangue) e di cellule PAS positive che esprimono geni endotelio-associati [96]. Le sezioni di tessuto colorate tramite PAS rivelano la presenza di aree positive in tutti i modelli TE-ES (tranne TE-EW-GFP alla settimana 2), rispetto al PAS-negativo TE-osso (**fig. II C1**).

La totalità dei dati ottenuti rappresenta un grande passo in avanti nella modelizzazione di tumori *in vitro*, in cui le cellule tumorali sono studiate all'interno della nicchia 3D ingegnerizzata - progettata per imitare il tessuto *in vivo* che ospita le cellule maligne.

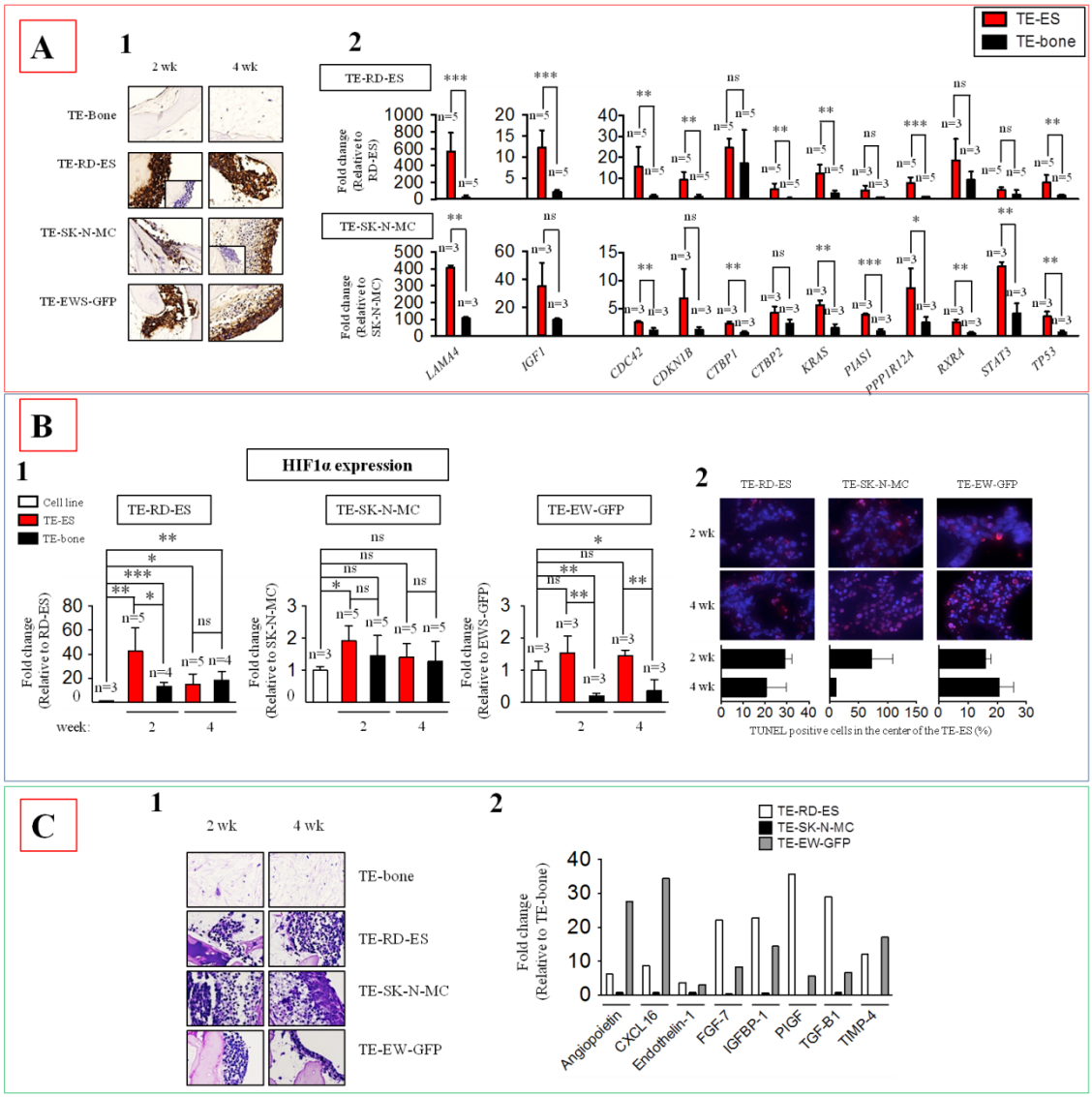

Figura II. Caratterizzazione del TE-ES. (A) Riattivazione di processi di adesione focale analizzati tramite colorazione di CD99 (1) e i livelli di espressione di mRNA nei TE-ES rispetto alle linee cellulari 2D (2). (B) Valutazione dei fenotipi ipossico e glicolitico tramite l'espressione del gene HIF1α (1) e colorazione TUNEL (2). (C) Descrizione dei processi di angiogenesi e mimica vasulogenica tramite colorazione PAS (1) e saggio ELISA (3).

Una validazione tecnica è stata, infine, eseguita per valutare l'affidabilità del dispositivo al fine di renderlo idoneo per uno studio preliminare. Essa consisteva nella valutazione della precisione dello spostamento del coperchio (valore misurato) rispetto al valore dato come input dall'operatore (valore di riferimento). Nella maggior parte dei casi, la precisione era superiore al 90%, e diventa inferiore solo quando il motore si è trovato a compiere

spostamenti nell'intervallo pochi micron. Usando COMSOL Multiphysics®, è stata effettuata un'analisi a elementi finiti del campo di stress derivante nello *scaffold* di osso in risposta ad una compressione dinamica. Risolvendo il tensore di Von Mises, è stato possibile calcolare il campo di stress generato nel costrutto e le sollecitazioni misurate erano nell'intervallo di 2.5x105 - 5.0x105 [Pa], secondo la posizione di riferimento all'interno del cilindro. E' probabile che le cellule all'interno dello *scaffold* "sentano" questi stimoli fisici, e che integrino questi segnali attivando il processo di meccanotransduzione. Risulta, quindi, interessante valutare se le cellule tumorali reagiscano o meno a questi stimoli, ad esempio mediante l'espressione di geni legati all'adesione focale e formando filamenti di actina. Perciò, nello studio preliminare proposto (**obiettivo 3**), il modello TE-ES è stato stimolato durante 24 ore per tre volte utilizzando dei parametri considerati fisiologici. La stimolazione non solo ha indotto un'ulteriore espressione della CDC42 già ri-espresso (rispetto alle linee cellulari), ma si è osservato che il *fold-change* é paragonabile a quello visto in tumori prelevati da pazienti. Inoltre, insieme ad un aumento di espressione di RHOA, facente parte della famiglia delle GTP-asi, una colorazione dei filamenti di actina, tramite F-actin *staining*, ha evidenziato come le cellule sotto compressione meccanica - in TE-SK-N-MC, ma non in TE-bone - assumono una forma polarizzata e altamente orientata. Questi risultati sono simili a quelli ottenuti dallo studio di Tse *et al*. in cui dimostra come una sollecitazione di tipo compressorio induce un sottoinsieme di "cellule leader" a estendere delle protrusioni citoplasmatiche, chiamate filopodi, che permettono una migliore migrazione delle cellule di carcinoma [23].

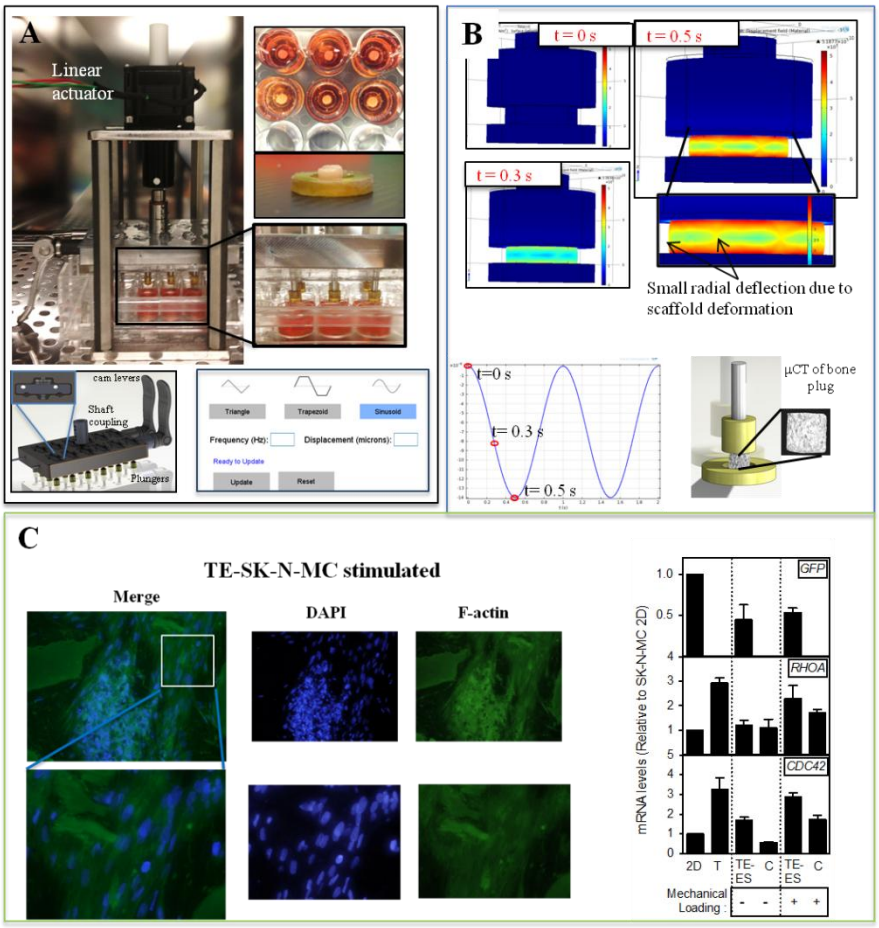

Figura III. Studio preliminare e simulazione COMSOL® . (A) Settaggio del bioreattore in cui sono stati coltivati I campioni di TE-ES. (B) Analisi del campo di stress nel TE-osso. (C) F-actin *staining* ed espressione di geni di adesione focale nel TE-ES.

Sulla base degli obiettivi specifici di questo lavoro, è possibile concludere che, l'**Obiettivo 1** (modello TE-ES) e **l'Obiettivo 2** (bioreattore compressione) sono stati pienamente raggiunti, mentre è stato eseguito del lavoro preliminare per l'**Obiettivo 3** (studio preliminare).

In questa tesi, è stato descritto un modello bioingegneristico di Ewing sarcoma in grado di simulare la nicchia tumorale presente nell'osso *in vivo*. Nel modello, le cellule tumorali che hanno perso i loro profili trascrizionali dopo la coltura in monostrato, ri-esprimono i geni legati all' adesione focale e ai meccanismi tumorali. Qui sono riattivati i fenotipi tumorali ipossico e glicolitico originari, e si ha l'induzione di meccanismi legati all'angiogenesi e alla formazione di nuovi vasi sanguigni, che favoriscono l'adattamento del tumore. Inoltre,

è stato progettato e validato un innovativo bioreattore per compressione che permette di operare con un numero statisticamente significativo di campioni indipendenti, facile da montare, con un'interfaccia user-friendly e adatto per studiare nuovi farmaci. Infine, lo studio preliminare fornisce una più approfondita comprensione sugli effetti del carico meccanico sul modello di TE-ES.

In futuro, sarà importante ottimizzare e validare ulteriormente sia il modello sperimentale di Ewing sarcoma che il bioreattore per compressione. L'obiettivo finale sarà quello di stabilire una tecnologia all'avanguardia per la ricerca sul cancro, tramite lo sviluppo di una piattaforma bioingegneristica per lo studio della biologia della malattia. Al fine di sviluppare tale piattaforma, sarà possibile perseguire tre direzioni specifiche in un modo altamente integrato.

Innanzitutto, sarà necessario migliorare il modello di TE-osso pre-vascolarizzandolo con cellule HUVEC; in secondo luogo, sarà importante integrare nel bioreattore un sistema di perfusione che fornisca ossigeno e nutrienti in maniera controllata e uniforme a tutto il costrutto; in ultimo, sarebbe opportuno sviluppare piattaforme di bioingegneria per analisi *high-throughput* che permetterebbero lo studio di *target* terapeutici per la cura dell'Ewing sarcoma.

Chapter 1 - Introduction and Background

Tumors have recently been described as very complex organs provided with vasculature, stem cells and other important stromal components. In the past decades, an enormous body of work has been produced to study and thus better understand the cancer proliferation and spreading - from the genetic mutations to the metastasis. Most of the work has been carried out on tumor cells cultured in monolayer or on *in vivo* animal models. Both have their own limitations and drawbacks, such as the loss of the tumor signature or high cost and reproducibility, laying the basis for new research approaches.

In this chapter, after a brief but exhaustive introduction on tumors, the processes that drive cancer invasion will be described. Moreover, it is known that tumors alike healthy cells, continuously sense the extracellular matrix (ECM) and they tend to transduce biochemical and biophysical signals; therefore, it will also be discussed how all these cues influence a tumor's fate.

In the second paragraph, an overview of Ewing's sarcoma family of tumors (ESFT) is given, focusing on the genetic mutation that leads to an uncontrolled growth and to malignancy.

Finally, after a thorough description of the currently established approaches in cancer studies – that emphasize the need of more advanced *in vitro* models – bioreactors will be suggested as novel research tools in Cancer Tissue Engineering.

1.1 Introducing tumors.

Cells embedded in an *in vivo* tissue continuously sense the biochemical and mechanical state of their environment, transduce the extracellular signals into intracellular signals,

integrate these signals, and respond accordingly [21]. The response at the cell level may involve changes in metabolic state, gene expression, growth, differentiation, cell division, cell movement, or apoptosis. Maintenance of homeostasis at the tissue level involves the integration and response to signals from within the tissue itself and its surroundings, and disruption at any of the detection, transduction or response steps may lead to uncontrolled growth, producing what is called a neoplasm or tumor. Tumors can be benign, pre-malignant or malignant, and when they become malignant they become a cancer. More precisely, cancer denotes diseases that give rise to abnormal cells that proliferate indefinitely, and that can invade nearby tissues and spread to other parts of the body through the blood and lymph systems. A decade ago Hanahan and Weinberg identified six essential characteristics of cancer that are summarized as follows (**Fig 1.1**) [22].

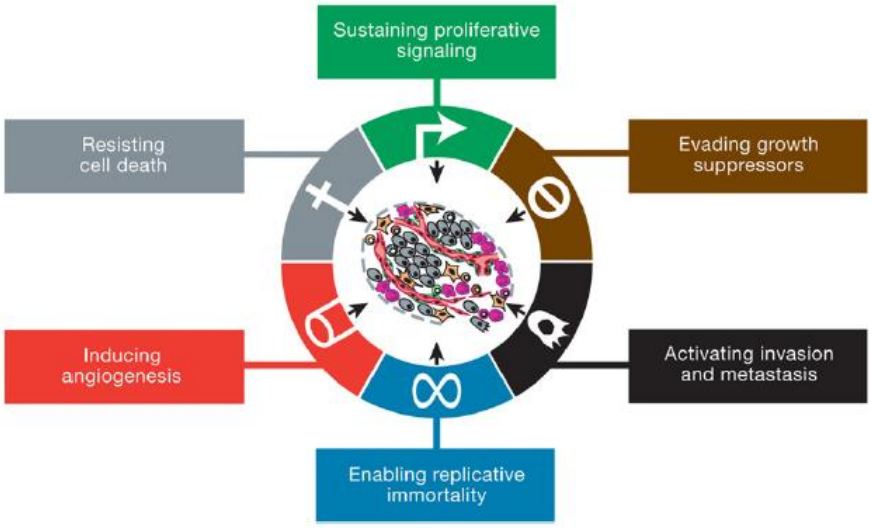

Figure 1.1. The Hallmarks of Cancer. Representation of the six hallmarks that characterize tumor development. (image adapted from [22])

- Self-sufficiency in growth signals: healthy cells require a signal to enter the proliferative state, and many oncogenes mimic such growth signals.
- Insensitivity to anti-growth signals: where cells ignore the external and internal signals that regulate cell proliferation.
- Evasion of apoptosis: cells circumvent programmed cell death.

- Unlimited ability to divide: in normal tissue cells typically double 50–80 times (the Hayfllick limit), but cancer cells can divide considerably more by, e. g., suppressing p53.
- Sustained angiogenesis: tumor cells can induce production of capillary sprouts from nearby vessels, which then provide nutrients and a pathway to the circulatory system.
- Tissue invasion and metastasis: without this characteristic tumors, remain benign, but with it they can spread to other tissues and organs, via the circulatory system or the lymph system.

The first four of these characteristics are also typical of a benign tumor, while the fifth one is a necessary condition for the unlimited growth of the tumor at the location where it initiated. Thus the primary characteristic of cancer cells is, in fact, their ability to invade and metastasize.

There are numerous environmental causes of cancer, which is initiated with either mutations or viral or bacterial agents. Most tissues in the human body can give rise to cancer, some even yield several types, and each cancer has unique features. For instance, a *carcinoma* is a cancer that begins in the skin or in tissues that line or cover internal organs; while a *sarcoma* is a cancer that begins in bone, cartilage, fat, muscle, blood vessels, or other connective or supportive tissue. *Leukemia*, on the contrary, is a cancer that starts in blood-forming tissue such as the bone marrow, and that causes large numbers of abnormal blood cells to be produced and spread in the blood. *Lymphoma* and *multiple myeloma* are two cancers that begin in the cells of the immune system. Lasts but not least, the *central nervous system cancers* are a type of cancers that begin in the tissues of the brain and spinal cord.

Given the complexity of normal embryonic development and the multitude of steps and checkpoints involved, it is unsurprising that there are numerous steps at which the homeostatic balance in a tissue can be upset. While the hallmarks of cancers like the one listed earlier focus on specific properties of the cancer cells, cancer development *in vivo* is context-dependent, since the environmental factors play a major role in the transition from normal cell to benign tumor to, eventually, cancer.

1.1.1 Fundamental processes in tumor development.

The fundamental processes that characterize tumor development can be resumed as follows:

1) Transformation and initiation: multiple genetic changes that accumulate with successive cell divisions.

   These changes are facilitated by the 'immortalization' of cells (the ability to divide indefinitely) via, e. g., activation of telomerase, an enzyme that prevents shortening of chromosomes during cell division. This can lead to clones capable of neoplastic growth wherein genetic errors can arise and accumulate with each cell division. It can also involve activation of growth promoting oncogenes, inactivation of cancer suppressor genes, and changes in the expression of genes that regulate apoptosis. [21]

2) Neoplastic growth**:** a higher than normal density at which growth saturates, usually lower than normal nutritional requirements in the growth medium, and a loss of contact inhibition of growth, are the two principal characteristics of this type of growth.

   Tumor cells may face hypoxia, acidity, and limited nutrient availability as they grow, and some types can develop adaptive responses to cope with metabolic and other types of stress. Under normal conditions cells use the Krebs cycle for generating ATP, but tumor cells shift their metabolism toward high levels of glucose consumption and lactate production (the Warburg Effect). [23, 24] One adaptive response to ensure an adequate glucose supply is to stimulate angiogenesis in nearby vessels and to migrate toward these vessels. In this phase tumor cells may also produce chemoattractants to attract stromal cells such as macrophages to them, which provide more growth factors. Thus tumor cells can pursue strategies of metabolic adaptation to survive periods of metabolic stress and maintain viability as cells accumulate. [25] In addition to the multitude of biochemical signals to which

cells within a tissue are exposed, they are also subject to external forces that arise from cell-cell or cell-substrate (fluid or ECM) interactions, and to internal forces generated in the cytoskeleton. These can be either contractile or tensile, and either tangential or normal to the cell boundary. Tangential, or shear forces, involve relative motion of adjacent regions of the cell and can thereby open mechanosensitive channels and deform the cytoskeleton. While biochemical signaling pathways still receive the most attention, it is widely recognized in molecular biology that forces within a cell and between a cell and its environment, whether the environment is other cells in an epithelial sheet or the ECM in the tissue context, give rise to an additional mode of signaling that can influence the cell growth, the differentiation, and the morphology of a tissue or an organ [21]. Whether forces act directly by suppressing growth or gene expression, or indirectly by activating intracellular biochemical pathways, depends on the context.

3) Angiogenesis: defined as the physiological process through which new blood vessels form from pre-existing vessels.

   Initially solid tumors are avascular (they do not have their own blood supply), and rely on diffusion from the surrounding vasculature to supply oxygen and nutrients and to remove waste products. As the tumor grows, nutrient demand increases until the flux of nutrients through the surface of the tumor is too small to supply the entire mass of cells. A necrotic core of dead cells may develop at the center and eventually the tumor stops growing and reaches a steady state size of ~1–3 mm, in which the number of dying cells counterbalances the number of proliferating cells. Growth can resume only if the tumor becomes vascularized (if it becomes permeated with a network of capillaries).

4) Invasion: it occurs when cells start to leave the primary tumor site and invade the surrounding ECM.

   Cell-cell interactions modulated by cadherins, a family of calcium-binding transmembrane glycoproteins that interact with members of the same type on adjacent cells, are critical for tissue formation and homeostasis. As with integrins, cadherins interact with the cytoskeleton via adapter proteins, and are an integral part of what are called adheren junctions between cells. These junctions encircle each cell in a belt-like structure that contains myosin II and tropomyosin. The

tension created by these belts stabilizes tissues, and maintains their integrity. The first stage of single-cell invasion involves detachment of epithelial cells from the primary tumor by loss of expression or function of the adhesion molecule E-cadherin, which leads to loss of connections with neighboring cells and reorganization of the actin cytoskeleton into actin stress fibers anchored to the focal adhesion complexes that are essential for traction during cell migration. [21]

Cancer cells invade the surrounding tissue either as individuals or as small groups of cells, and may secrete enzymes that degrade the ECM to facilitate passage of cells. Migration is to nearby vessels (if the tumor is vascularized it may enter the circulatory system directly) or to the lymph system. In the first case it may involve chemotaxis to attractants released by nearby stromal cells in response to stimuli from the tumor. Movement is a very complex process that involves the spatiotemporal control and integration of a number of sub-processes, including the transduction of chemical or mechanical signals from the environment, intracellular biochemical responses, and translation of the intra- and extracellular signals into a mechanical response [26].

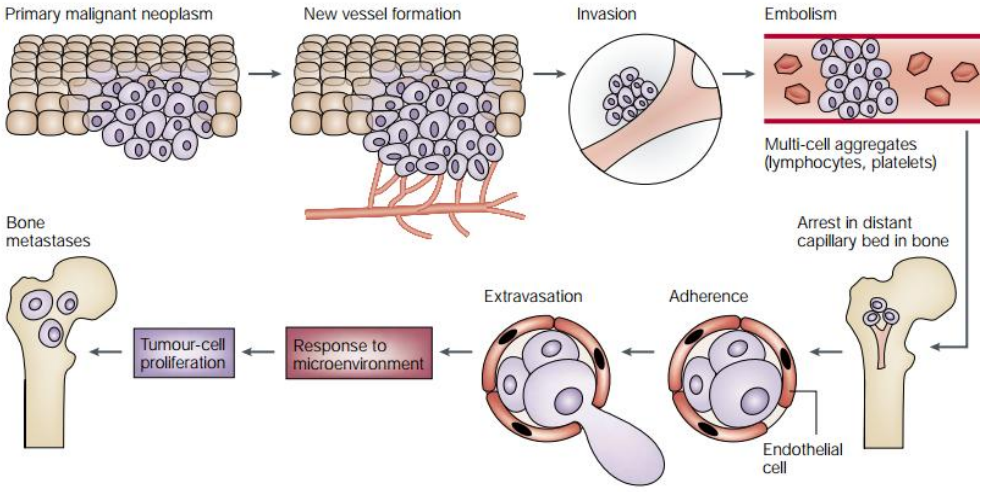

Figure 1.2. From primary tumor to metastasizing cancer. Primary malignant neoplasm as a consequence of genetic mutations and environmental signals, induces new vascular capillaries, invading them and beginning the journey to distant tissues e.g. the bone **(**adapted from [27])

1.1.2 Tumor microenvironment, mechanotransduction and force sensing.

Cancer was long viewed as a cell-autonomous process, in which successive acquisition of mutations in oncogenes and tumor suppressor genes resulted in progressively enhanced proliferation and resistance to cell death. It is now well known that additional cell types and the soluble and insoluble factors they produce make a vital contribution to tumorigenesis [28]. The demonstration by Judah Folkman [29] that tumors had the power to stimulate the growth of new blood vessels provided further convincing evidence that tumorigenesis could not proceed without active cooperation from non-malignant cells. Similarly, Cunha and co-workers showed that fibroblasts from reactive stromal regions of tumors had the capacity to transform otherwise non-malignant prostate epithelial cells [30]. A work in the 1980's showed that expression of the viral Src oncogene did not result in cellular transformation in the developing chick embryo, yet dissociated cells were demonstrably transformed in culture[31]. These studies led to the realization that even the expression of a potent oncogene was not sufficient for the process of transformation and that additional factors, such as disruption of tissue architecture by wounding, may be necessary [31]. Hence, tumor progression is the product of an evolving crosstalk between different cell types (e.g. endothelial cells, macrophages, and mesenchymal stem cells), within the tumor and its surrounding supporting tissue, or tumor stroma (**fig 1.3)**. [32]

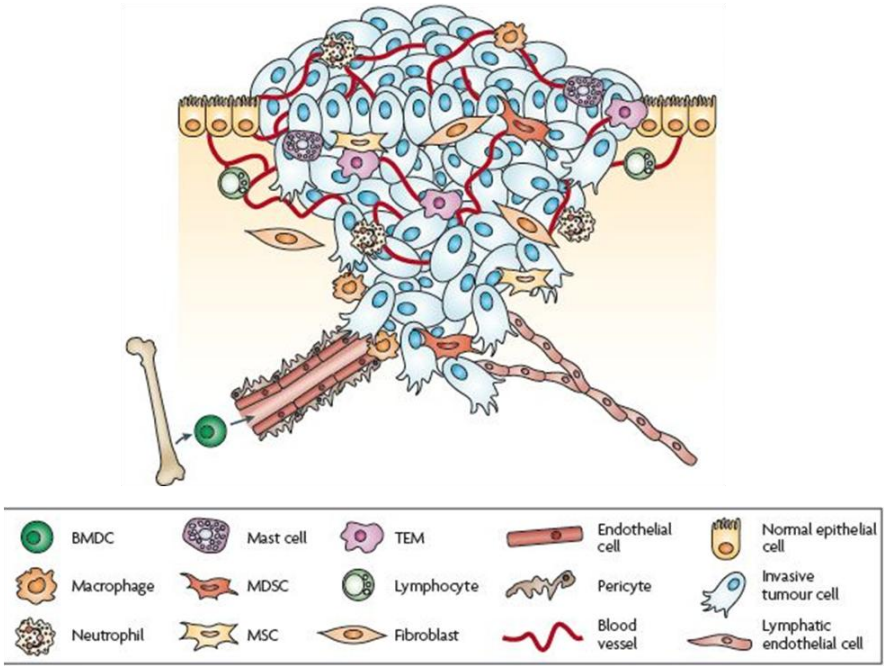

Figure 1.3. Cancer heterogeneous microenvironment Cancer cells in primary tumors are surrounded by a complex microenvironment comprising numerous cells including endothelial cells of the blood and lymphatic circulation, stromal fibroblasts, macrophages, myeloid-derived suppressor cells (MDSCs), monocytes and mesenchymal stem cells (MSCs).(adapted from [33])

Mesenchymal stem cells (MSCs), amongst other cells play an important role in tumor development. They can alternatively be defined as multipotent mesenchymal stromal cells, being a heterogeneous population of cells that proliferate in vitro as plastic-adherent cells, having fibroblast-like morphology, forming colonies in vitro and being able to differentiate towards several lineages (**fig 1.4**.) [34].

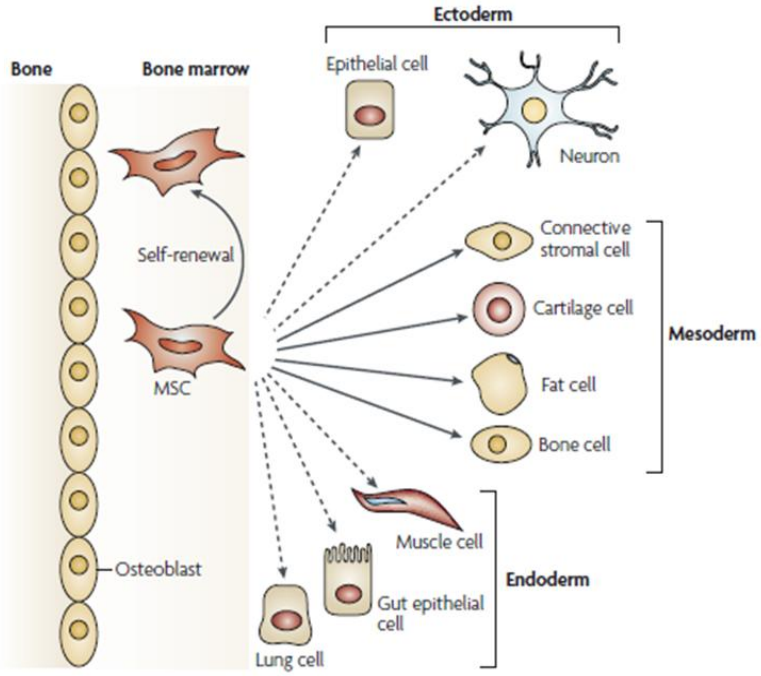

Figure 1.4. The multipotentiality of MSCs. Ability of mesenchymal stem cells (MSCs) in the bone-marrow cavity to self-renew (curved arrow) and to differentiate (straight, solid arrows) towards the mesodermal lineage. The reported ability to transdifferentiate into cells of other lineages (ectoderm and endoderm) is shown by dashed arrows, as transdifferentiation is controversial *in vivo*. (Adapted from [34])

This type of cell is also known for its ability to repair injured tissue. They circulate in the blood like sentinels until they are called to sites of injury, where they differentiate into bone, cartilage, fat or muscle cells to repair or replace damaged tissue. In fact Spaeth *et al.* have studied how MSC migrate, behaving like immune cells, towards the tumor site, often referred as the "wound that never heals". It has been suggested the employment of this cells as vehicles to deliver antitumor proteins or suppress their migration to reduce tumor growth [35]. A team led by Robert Weinberg [36] reported evidence that these cells can also promote metastasis. The researchers injected mice with human breast cancer cells labeled with green fluorescent protein either with or without MSCs. Mice given both cell types developed many more lung metastases (up to seven times more) than animals injected only with the cancer cells (**fig 1.5**). [37]

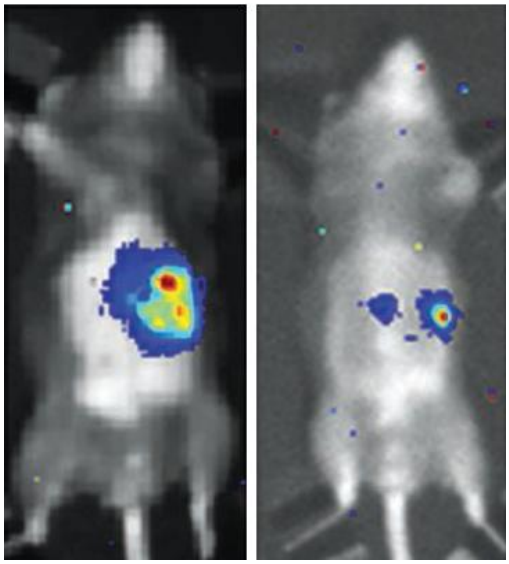

Figure 1.5. MSC aiding cancer metastasis. *In vivo* experiment showing how MSC can participate in tumor invasion promoting cells spreading. Rat injected with cancer cells and MSC (left) and cancer cells injected alone (right). (adapted from [37])

It is, at this point very clear that all the components of the ECM, including biophysical and biochemical signals, play an important role in tumor behavior. For the purposes of this work it is important to focus in particular on mechanotransduction defined as the translation of mechanical stimuli into biochemical signals, enabling cells to adapt to their physical surroundings (ECM). Research in mechanotransduction has often focused on sensory cells, such as hair cells in the inner ear (specialized in transducing mechanical inputs into biochemical signals by opening ion channels in response to applied forces) that provide a good model to study cellular mechanosensing. Due to these models, it has become likely that mechanotransduction signaling has a crucial role in the maintenance of many mechanically stressed tissues, such as muscle, bone, cartilage and blood vessels [10]. Generally, almost all cells respond to mechanical stimulation with adaptive changes in cell function. These changes include short-term responses (such as increases/decreases in intracellular tension, adhesion, spreading or migration) as well as changes in long-term effects (such as in protein synthesis and secretion, structural reorganization, proliferation and viability). These effects are often mediated through multiple, overlapping and crosstalking signaling pathways. Moreover, stem cells can be steered towards specific fates during differentiation on the basis of the geometry and stiffness of the substrate on which

the cells are grown [38]. Several mechanisms involved in mechanotransduction have been resumed in **Figure 1.6** and they are activated in concert or independently.

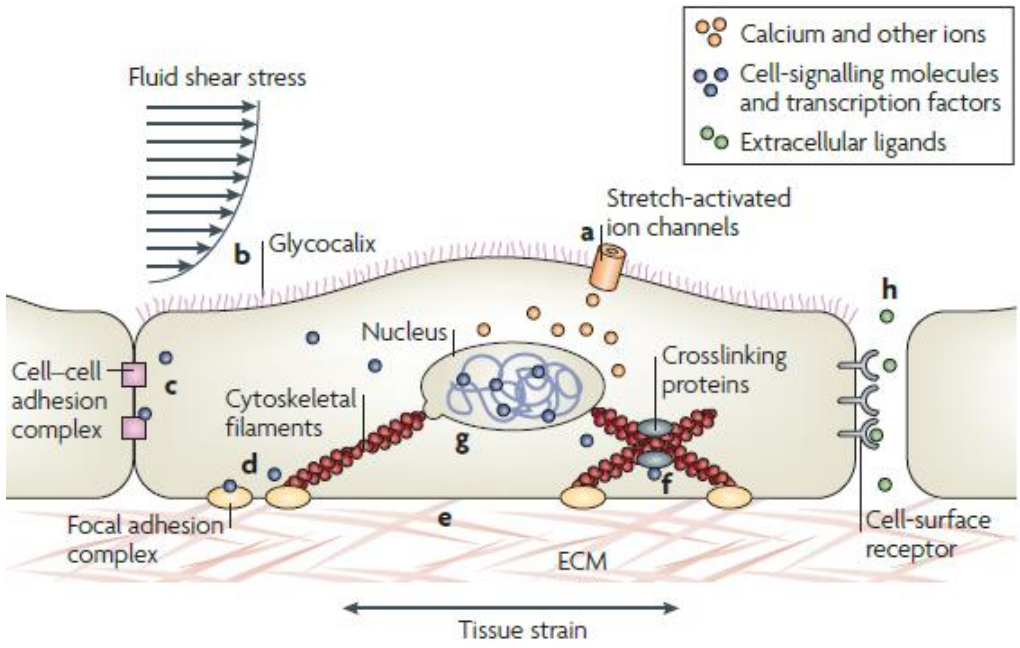

Figure 1.6. Several types of mechanosensors. Several biological components, not mutually exclusive, have been proposed to act as cellular mechanosensors. Note that most of these features can be found in many cell types, although some (for example, changes in intercellular space) might only be relevant in a subset of cells. (adapted from [10])

For example, in response to membrane strain, stretch-activated ion channels in the plasma membrane open and allow the influx of calcium and other ions (**fig. 1.6a**). In endothelial cells, the glycocalix (carbohydrate-rich proteins on the cell surface), mediate mechanotransduction signaling in response to fluid shear stress (**fig. 1.6b**). Cell–cell junctional receptors or extracellular matrix (ECM)–cell focal adhesions allow cells to sense their environments and force-induced unfolding of ECM proteins, such as fibronectin, can initiate mechanotransduction signaling outside the cell (**fig. 1.6c, d and e**). Intracellular strain might induce conformational and geometrical changes in cytoskeletal elements, thereby changing binding affinities to specific molecules and activating signaling pathways (**fig. 1.6f)**. Furthermore, intracellular deformations can alter chromatin conformation in the nucleus, and modulate access to transcription factors or transcriptional machinery (**fig.**

1.6g). Finally, compressing intercellular space could alter the effective concentration of autocrine and paracrine signaling molecules (**fig. 1.6h**).

A common denominator of many mechanobiology diseases is a disruption in the intricate force transmission between the extracellular matrix (ECM), the cytoskeleton and the interior of the nucleus. Hence, any changes in normal intracellular force transmission through changes in cellular (or extracellular) structure and organization can lead to altered molecular forces acting on these proteins, resulting in attenuated or increased mechanosensitive signals. Examples include mutations in proteins that are involved in intracellular calcium signaling or members of the **Rho** or mitogen activated protein kinase (MAPK) pathways.

Several studies have shown that changes in the ECM stiffness can regulate tumor growth morphogenesis, and integrin adhesions. For example Paszek *et al*. found that tumors are rigid because they have a stiff stroma and elevated Rho-dependent cytoskeletal tension that drives focal adhesions, disrupts adherens junctions, perturbs tissue polarity, enhances growth, and hinders lumen formation [39].

Not only ECM stiffness but also other mechanical inputs, such as tumor expansion leading to tissue compression and increased interstitial pressure, can increase both cell and tissue tension within the confined stroma, leading to the release, concentration and activation of various growth factors, ultimately assisting in tumor progression [40].

Not only cell generated forces but also external physical cues can alter the ECM and ultimately trigger mechanotransduction. For example, externally applied compression force can deform the ECM and decrease the interstitial space, which alters the transport and distribution of soluble factors within the ECM thereby modifying cell behavior [41]. Indirect effects of mechanical force on tissues include changes in levels and/or activity of various growth, differentiation and motility regulators, as well as ECM remodeling. The specificity of these force-induced effects can depend on the direction of the force (e.g. tension, compression and shear forces) as well as on its magnitude and duration. Tse *et al.* have shown that compressive stress stimulates migration of mammary carcinoma cells. The enhanced migration is accomplished by a subset of “leader cells” that extend filopodia at the leading edge of the cell sheet. Formation of these leader cells depends on cell micro-organization and is enhanced by compressive stress (**fig. 1.7**).

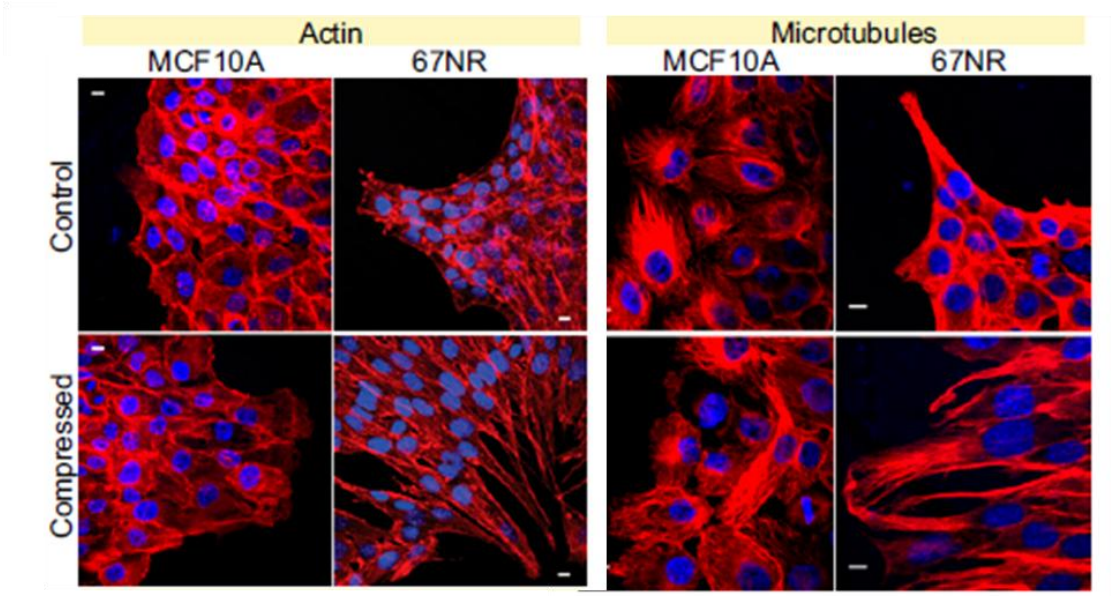

Figure 1.7. F-actin and tubulin staining of two lines of mammary carcinoma cells. The 67NR, but not MCF10A, cells demonstrated elongated actin filaments perpendicular to the cell denuded area and microtubule rearrangement in response to stress. (Scale bar 10 μm.) (Adapted from [20])

However, Helmlinger *et al* using multicellular tumor spheroids embedded in agarose gel demonstrated that solid stress (static compression exerted by changing the gel stiffness) inhibits tumor growth in vitro independently from host species, tissue of origin and differentiation state. [42]

Moreover, Lynch *et al* have studied that the effect of mechanical loading on the development and on the progression of metastatic breast cancer. They developed an *in vivo* model to investigate the role of skeletal mechanical stimuli on the development and osteolytic capability of secondary breast tumors. They have shown that applying compressive loading significantly reduces osteolysis, tumor formation and increased tibial cancellous mass due to trabecular thickening. [43]

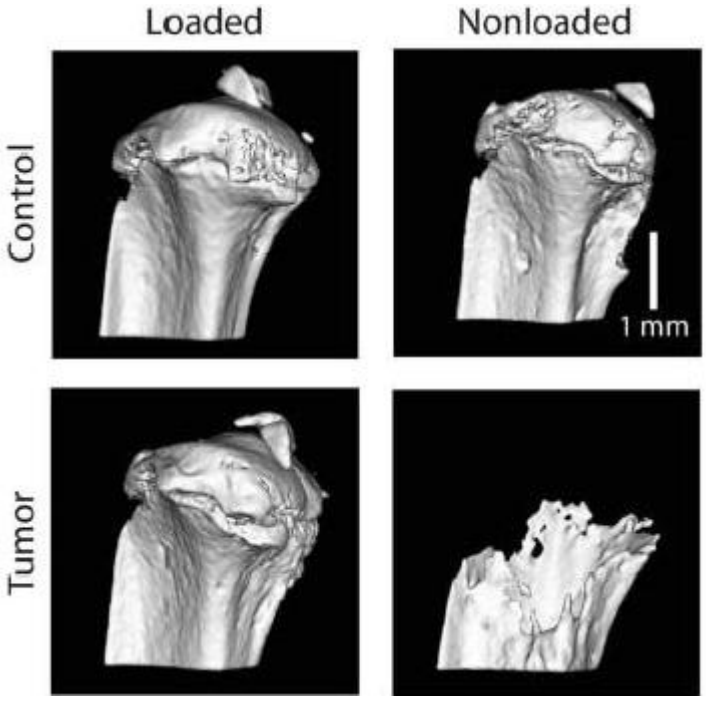

Figure 1.8. Indices of cancellous mass and architecture in sham-injected (Control) and tumor-injected (Tumor) animals via microCT. After two week bone volume fraction increased under loading condition (left) for both groups (tumor group significantly) and decreased dramatically in static condition for the tumor group. (Adapted from [43])

It still remains unclear whether mechanical stimuli inhibit or enhance tumor progression. Further investigation is needed to elucidate and understand the complex mechanism that links physical cues, mechanotransduction and tumor development. Bioreactors and 3D tissue engineered models might become, in the future, powerful tools to answer these unsolved questions.

1.2 Ewing's sarcoma family of tumors (ESFT)

Bone tumors include a wide variety of cellular entities originating from bone cells or their precursors, termed primary bone tumors, as well as originating from nonosseous origins, known as bone metastases that are common complications of several cancers (e.g., breast, prostate, and kidney). Of all of these tumors, some are purely osteolytic, such as giant cell tumors (benign entity), while specific subtypes lead to a new calcified matrix, as in the case of osteosarcoma or induce mixed osteolytic/osteoblastic lesions. The three main bone sarcomas include osteosarcoma, Ewing's sarcoma family tumors (ESFT) and chondrosarcoma. [44].

Ewing's sarcoma is the second most common bone malignancy in children and young adults, with a peak incidence between the ages of 14 and 20 years. Multi-disciplinary care incorporating advances in diagnosis, surgery, chemotherapy, and radiation has substantially improved the survival rate of patients with localized Ewing's sarcoma to nearly 70%. Unfortunately, those advances have not significantly changed the long-term outcome for those with metastatic or recurrent disease; 5-year survival remains less than 25%. This apparent therapeutic plateau exists despite extensive effort during the last four decades to optimize the efficacy of cytotoxic chemotherapy through combination of chemotherapies [45]. Therefore, it is clear that there is an urgent need to identify therapeutic molecular targets at the time of diagnosis, which in turn requires predictive experimental models.

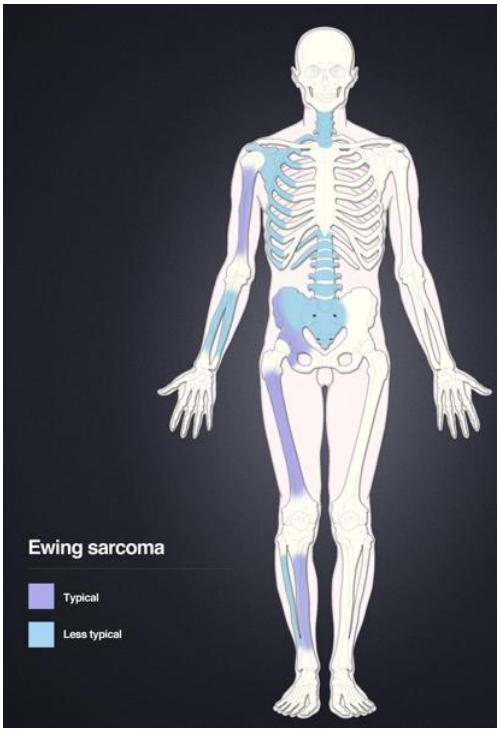

Figure 1.9. Distribution of Ewing's sarcoma. Most frequent locations are the large long bones and the pelvis.

1.2.1 Oncogenic mutation and cell of origin

Ewing's sarcoma family of tumors (ESFT) includes classical Ewing's sarcoma of bone and soft tissues, peripheral primitive neuroectodermal tumors (pPNET), Askin tumor (chest wall), and other less frequent variants.

More than 85% of Ewing's sarcoma family tumors (ESFT) are associated with the chromosomal translocation t (11; 22) (q24; q12) that generates the *EWS-FLI-1* fusion gene. The corresponding fusion protein is believed to behave as an aberrant transcription factor that transforms target cells by deregulating their gene expression program (**fig.10**). [46]

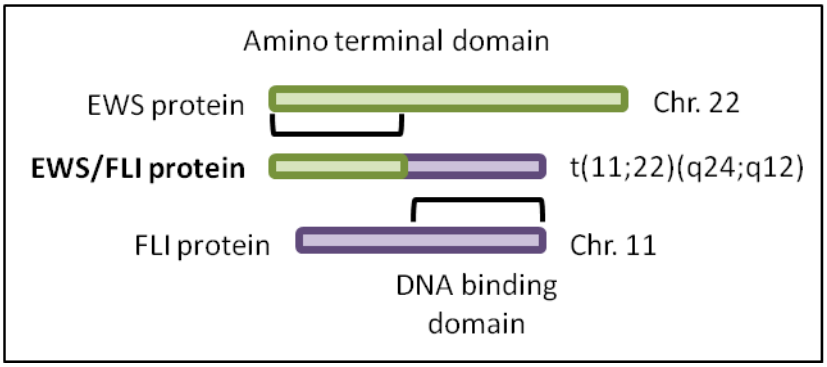

Figure 1.10. EWS-FLI fusion protein resulting from the chromosomal translocation t (11; 22) (q24; q12).

EWS-FLI-1 may participate in Ewing sarcoma pathogenesis by promoting at least two set of events that synergize in tumor development and progression: the cell proliferation and survival (inducing PDGFC, IGF1, MYC, CCND-1 and NKX2-2) and the escape from apoptosis and growth inhibition (repressing p21, TGFbRII and IGFBP3). In addition, EWS-FLI-1 appears to play a critical role in inducing the ESFT small round cell phenotype [47]. Recent analyses of molecular signatures suggest that ESFT originate from mesenchymal and/or neural crest cells. [46] [48]

1.2.2 Tumor development and phenotype

Morphologically, Ewing sarcoma is composed of sheets of small round cells (**fig 1.11**) with a high nuclear to cytoplasmic ratio and is often classified by pathologists into a group of small round blue cell tumors (e.g. neuroblastoma, alveolar rhabdomyosarcoma and lymphoblastic lymphoma). Immunohistochemical analysis has shown that, in more than 90% of cases, Ewing's sarcoma cells express the adhesion receptor CD99, commonly associated with lymphoid cells and believed to play a role in leukocyte transmigration of the endothelium. ESFT exhibit a tremendous potential to metastasize to lungs, bone and bone marrow. Metastases at diagnosis are detected in approximately 25% of patients [49]. Dismally, the prognosis of patients with metastasis at the time of diagnosis still remains poor and in most of the cases, is considered as a terminal event.

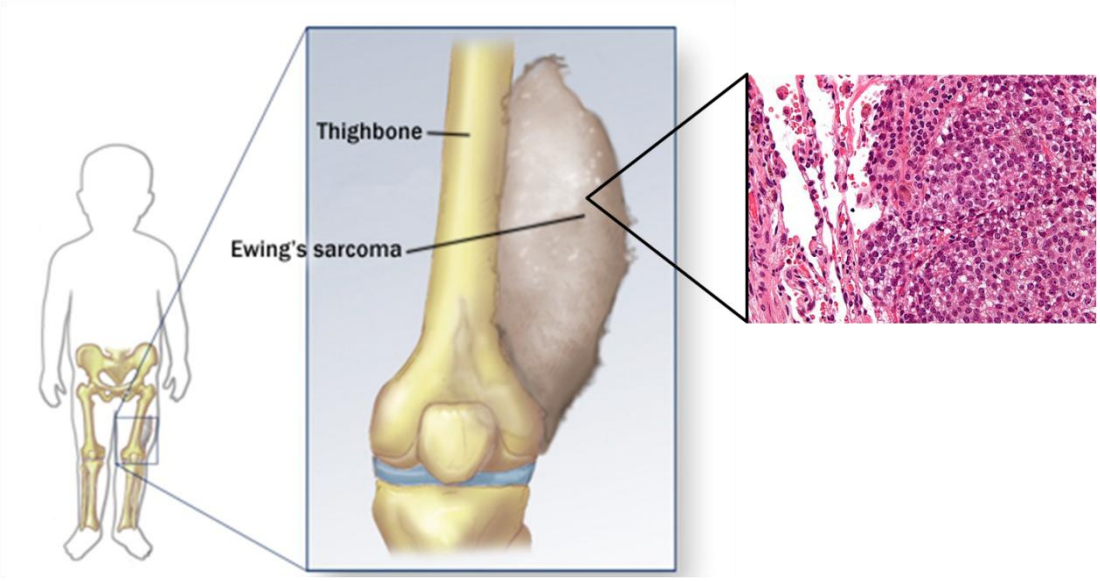

Figure 1.11. Ewing's sarcoma small round cells.

1.3 Cancer engineering

The main goal of Tissue Engineering, oppositely to the *in vivo* cell injection strategy, is the *in vitro* creation of artificial tissue having the ability to repair or simply replace lost or damaged tissue. Common tissue engineering strategies involve the extraction of cells from a small piece of tissue and their *in vitro* culture for later implantation using a carrier that allows the formation of new tissue (**fig.1.12**). [50]

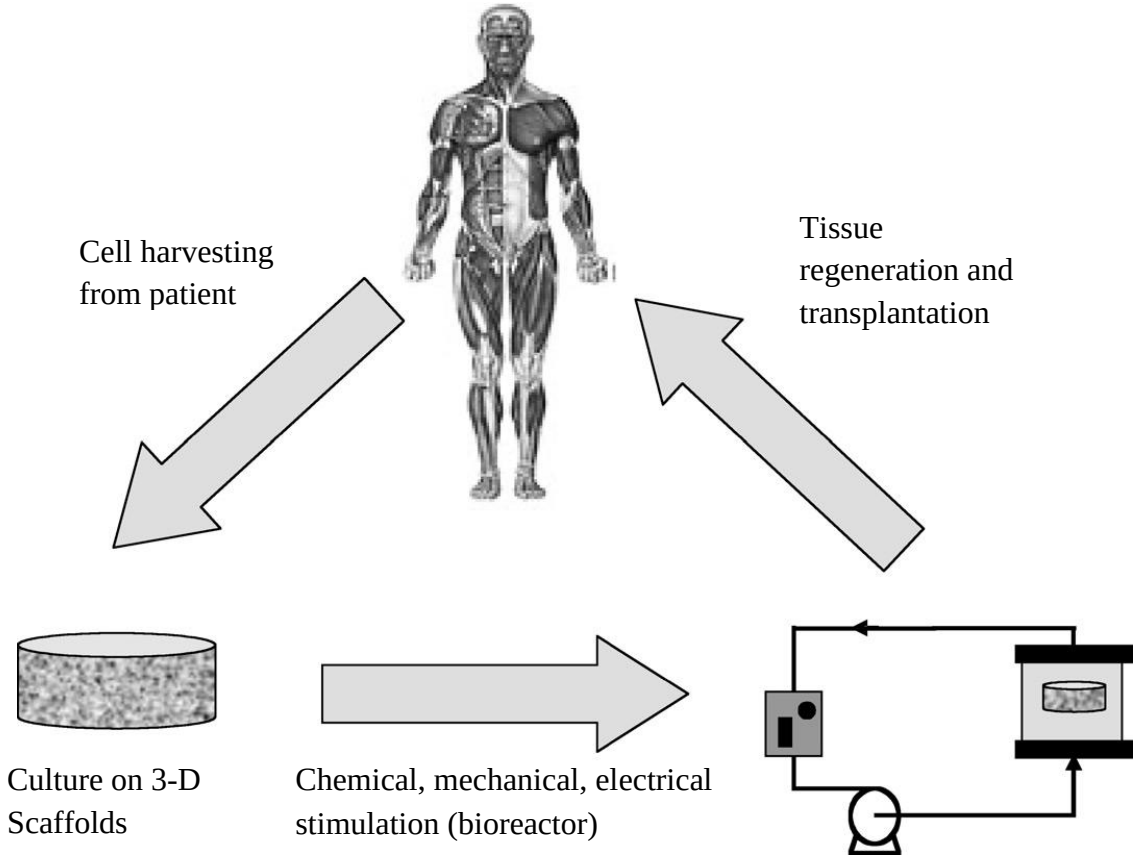

Figure 1.12. Basic steps in the process of Tissue Engineering.(Adapted from [50])

Most approaches in this field are based on common bioactive factors, consisting of cells (generally stem cells, or progenitor cells), a scaffolding material, and growth and differentiation factors [51]. Applying certain stimuli that can elicit specific responses to the cells can accelerate the *in vitro* creation of an efficient construct. Stimulation can be done in two major ways: chemically and electro/mechanically.

Chemical stimulation is carried out by using growth and differentiation factors (typically proteins or small molecules) specific for different responses. Growth factors play a major role in cell division, matrix synthesis, and tissue differentiation [52]. Examples of these proteins are: bone morphogenetic proteins (BMPs), which have been demonstrated to induce the differentiation of mesenchymal stem cells into an osteoblastic lineage (BMP-2 and BMP-7), and the vascular endothelial growth factor that greatly enhances angiogenesis [53] [54-56]. The need for *in vitro* mechanical/electrical stimulation in tissue engineering is drawn from the fact that most tissues function under specific biomechanical/bioelectrical

environments *in vivo*. These environments play a key role in tissue remodeling and regeneration. The stresses can be translated into different kinds of forces that range from load bearing or stretching to hydrodynamic forces due to fluid flow [57]. Thus, the mechanochemical/electrochemical microenvironment that progenitor cells grow into is expected to control the fate of these cells while undergoing differentiation toward different lineages. Specifically in the cardiac field, Tissue Engineering aims at overcoming the limitations of the cell therapies by generating clinically sized (1-5 mm thick) functional tissue grafts *in vitro* containing physiologically high density of viable cells. Another aim of TE is the creation of tissue for drug screening and disease models that would allow more in depth understanding of cancer development and its reaction to specific drugs and stimulations.

Throughout its brief history, the principal focus of Tissue Engineering has been to repair or replace damaged tissues using engineering principles and technologies. One popular approach has been to develop functional human tissues *ex vivo* for *in vivo* implantation. This strategy has seen some success in reconstructing simpler tissues, such as skin, bone, and cartilage, but clinically viable solutions for reconstructing more complex, vascularized tissues, such as the liver or the pancreas, remain elusive. For over a century our understanding of cancer processes and stages has been derived from detailed studies of the histopathology of tumors. In parallel with this approach, a vast collection of cell lines has been derived from different tumor tissues and stages. These cell lines are widely used in research because they are easy to maintain in culture, they represent important features of certain cancers and they are useful to unravel biochemical pathways. Despite these advantages, tumor-derived cell lines, often models of the parent histology, have different genetic profiles from those of the primary cells derived from patients. In addition, cell lines have limitations due to cross-contamination with other lines and in long-term cultures are prone to genetic drift. There is a natural convergence between Tissue Engineering and cancer biology that has already sparked collaborative efforts between experts in both fields [58]. At the other end of the experimental continuum, animal models frequently provide definitive tests of the importance of specific molecules and processes. However, animal models may not adequately reproduce features of, for example, human tumors, drug therapeutic responses, autoimmune diseases, and stem cell differentiation. [5].

A small yet growing number of cancer researchers, aware of the limitations of conventional 2D monolayer cell cultures, are moving towards the use of 3D cell culture systems as they begin to understand that the microenvironmental cues found in the ECM of the local cell niche, and that from other surrounding cells, are equally as important as the cell itself [59]. A tissue-engineered tumor model that recreates the 3D structure, the stromal environment and the signaling milieu present *in vivo*, could dramatically improve upon the current preclinical drug screening paradigm by providing valuable information about drug efficacy early in the drug development process. This is especially important for less common cancers, where limited patient numbers preclude widespread drug testing (e.g. Ewing's sarcoma) [60].

Each one of these aspects of the brand new field called Cancer Tissue Engineering will be discussed in the following paragraphs, with particular focus on some of the models most commonly used. Moreover, it will be resumed the state of the Art of the bioreactors used in TE, focusing in particular on Bone Tissue Engineering and highlighting the specific features of these devices that could lay the basis for innovative drug screening platforms in cancer research.

1.3.1 2D *in vitro* models

In vitro testing of anticancer drugs typically involves growing cancer cell lines in monolayers on tissue culture plastic and using high-throughput screening procedures to evaluate drugs efficacy. The studies on this component of cancer drug testing began in the late 1980s when the National Cancer Institute established a panel of 60 unique cancer cell lines to use in screening anti-neoplastic drug candidates. Since then, hundreds of other cancer cell lines have been used with similar intent. [58]

Fig.1.13. (Left) Typical monolayer culture in a polystyrene Petri dish; (right) light micrographs of MG-63 osteosarcoma cells grown in monolayer (Adapted from [61])

Despite these progresses, the monolayer culture has remained a poor predictor of whether a given drug will ultimately yield clinical benefit [62]. There are a number of well-known potential explanations for this, but the most dramatic alterations occur, however, because of the removal of the cells from their native microenvironment, including the extracellular matrix (ECM), soluble signals, 3D architecture, stromal cells, and irregular microvasculature that surround the tumor cells *in vivo*. [58]

It has been demonstrated that stromal elements affect many different aspects of cancer cell behavior, including the cell's proliferation rate and resistance to drug-induced apoptosis [63]. It is, therefore, no surprise that current *in vitro* drug-screening strategies, which specifically monitor changes in cell proliferation and cell death, often do not accurately forecast a tumor's *in vivo* response.

1.3.2 *In vivo* models

Human cancer is often studied within animal models to better replicate the biological complexity of human tumor growth. This provides tumor cells with many of the 3D microenvironmental cues that are missing during monolayer growth. In fact, numerous murine models have been developed to study human cancer. These models are used to

investigate the factors involved in malignant transformation, invasion and metastasis, as well as to examine response to therapy. One of the most widely used models is the human tumor xenograft. In this model, human tumor cells are transplanted, either under the skin or into the organ type (less frequent approach in bone cancer) in which the tumor originated, into immunocompromised mice that do not reject human cells. For example, the xenograft will be readily accepted by athymic nude mice, severely compromised immunodeficient (SCID) mice, or other immunocompromised mice [64]. Depending upon the number of cells injected, or the size of the tumor transplanted, the tumor will develop over 1–8 weeks (or in some instances 1–4 months, or longer), and the response to appropriate therapeutic regimes would be eventually studied *in vivo*. Another type of animal model for studying human cancer is the genetically engineered mouse (GEM) model. The genetic profile of these mice is altered so that one or several genes thought to be involved in transformation or malignancy are mutated, deleted or over-expressed; subsequently, the effect of altering these genes is studied over time and therapeutic responses to these tumors may be followed *in vivo*. Both athymic nude mice and mouse xenograft models that use human tumor cell lines have been adopted for decades to increase our understanding of factors affecting tumor growth; however, recent information regarding the key influence of the tumor microenvironment on tumor progression and growth has led to greater reliance on GEM tumor models using immunocompetent mice, as well as use of primary human tumor xenografts in humanized mouse models (**fig. 1.14**). [65]

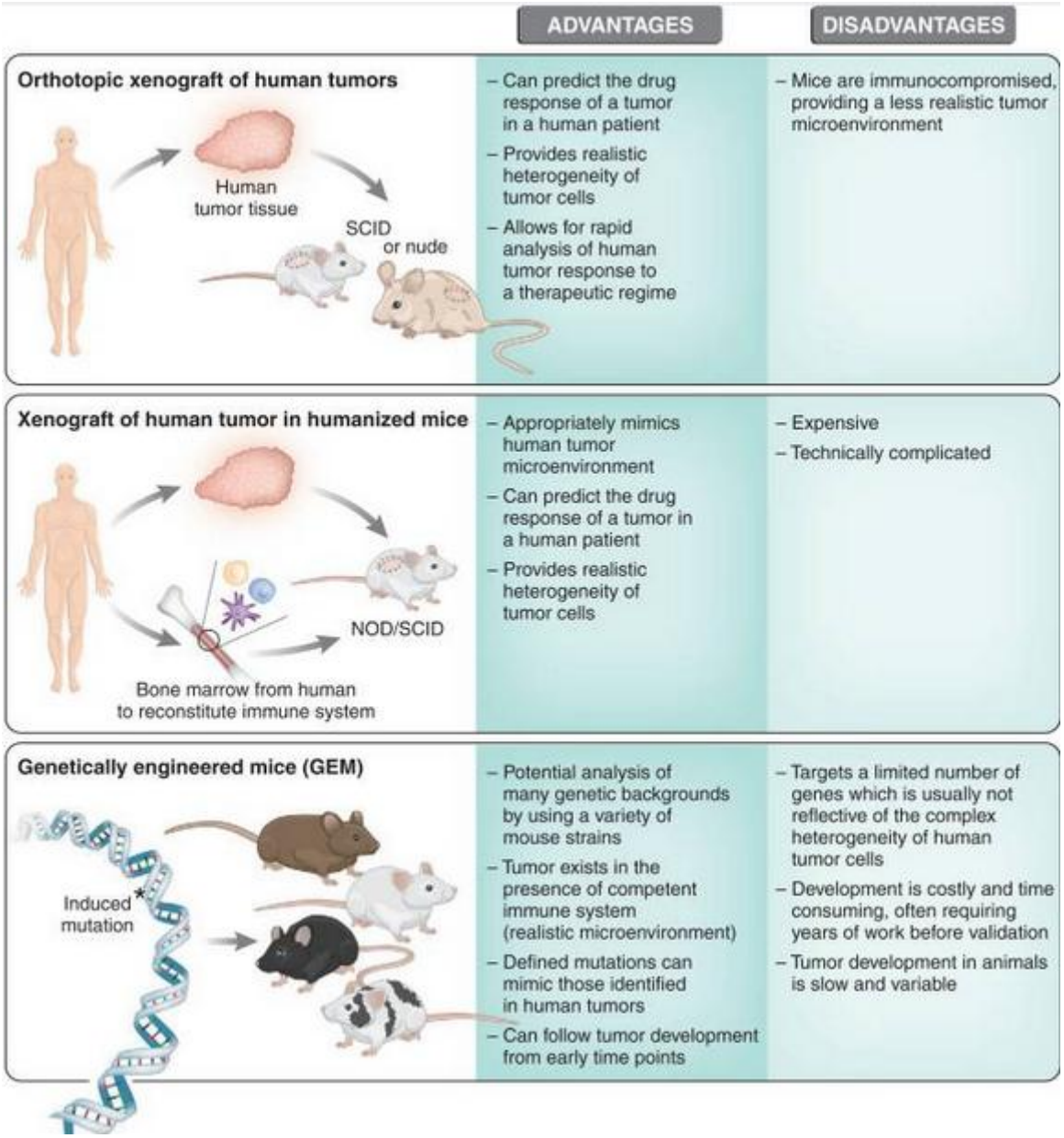

Figure 1.14. Types of murine model for studying human cancers. (Adapted from [65])

As with *in vitro* testing, several drugs are effective when tested on a xenograft but fail to succeed in phase II trials [66]. Not only the subcutaneous localization of the xenograft, but also the slight but important difference between a murine and human microenvironment, affects the outcome of the drug test. Several more sophisticated animal models are been developed but, even though they provide more biologically relevant data, the complexity

and difficulty of the experiments often precludes their widespread use. Moreover, they are not currently available for all cancer types and they still have limitations related to the foreign mouse physiology. [67]

1.3.3 Tissue engineered models

The most widely used 3D model is a small, tightly bound cellular aggregate that tends to form when transformed cells are maintained under non-adherent conditions called human tumor spheroid (**fig. 1.15**). These are cellular aggregates that, depending on the growth conditions and on the cell type, can range in size from 20 μm all the way up to 1 mm in diameter. The 3D architecture and extensive cell–cell contacts provided by spheroid growth appear to better mimic the *in vivo* cellular environment than two-dimensional (2D) monolayer cultures. Spheroids also exhibit many of the biological properties of solid tumors, including cell morphology, growth kinetics, gene expression, and drug response [68]. When grown within spheroids, compared to monolayer, cancer cells from a wide variety of tumor types consistently show greater resistance to anticancer drugs controls, being representative of what is often observed in the clinical setting [61]. This can be partially explained by the combination of several factors such as [69]:

- increased cell–cell contact,
- 3D cellular architecture,
- enhanced deposition of tumor-derived ECM within the spheroid, and,
- Lower overall cell proliferation rate.

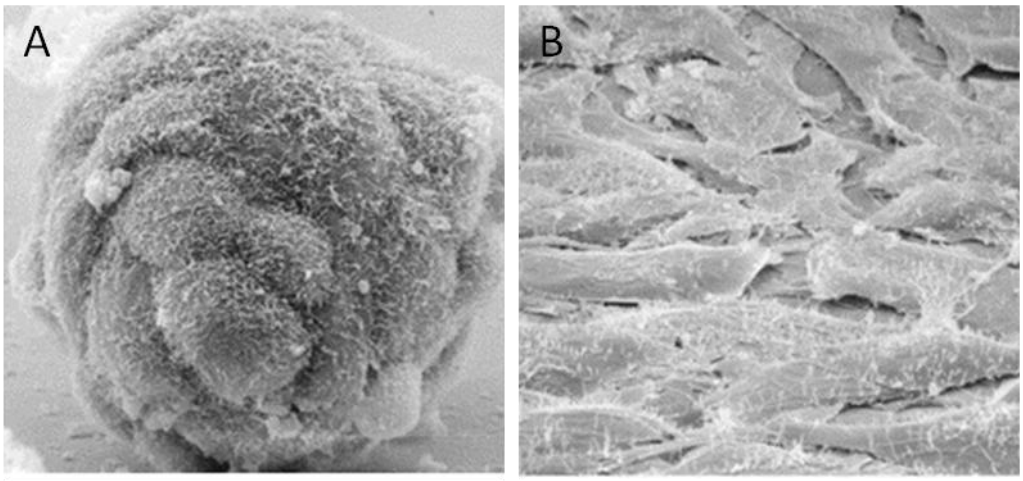

Figure 1.15. Scanning electron micrographs of MG-63 osteosarcoma cells grown as three-dimensional tumor spheroids (A) and in a monolayer (B) after 48 h of growth. (Adapted from [61])

Spheroids represent a great improvement in cancer research, but lately more sophisticated models have been developed using biological gels as a substrate for spheroid growth.

The earliest attempts to grow cancer cells within 3D substrates used small explants of cancer tissue within a natural gel. In the mid-1980s, Kleinman and Martin[70] were the first to demonstrate the value of reconstituted basement membrane from Engelbreth–Holm–Swarm mouse tumor extracts as a culture substrate, which allowed for the development of several products as a result of their pioneering work. Among these Matrigel^{TM}, which consists of mainly type IV collagen and laminin, was considered for many years to be the material of choice [71], based on crucial microenvironmental cues that are restored in 3D cultures of these laminin-rich extra cellular matrices (lrECMs). Even though all the different lrECMs represent well the micro- and nano-scale of the native ECM, their major drawback is that they often contain residual growth factors, undefined constituents or non-quantified substances, and moreover, their batch-to-batch variations make it difficult to compare and correlate work from different groups. [5, 72]

Because of its ubiquitous nature and relative ease of isolation, collagen was one of the earliest biomaterials to be widely used for 3D cell culture. Collagen gel embedding consists in the enclosing of small tumor explants (*ex vivo*) into a collagen matrix. This method was used to culture a wide variety of cancer types in a way that preserved the native tissue architecture and cell viability over several months [73]. Alginate gel has also

been widely used because it is a natural polymer brown seaweed) that solidifies (by a process called gelation) at room temperature in the presence of calcium ions. It has been possible to culture tumor aggregates embedded into alginate gel for more than a month and cell growth rates and tissue organization were similar to those of *in vivo* cancers. [74]

As a result of advances in the Tissue Engineering and biomaterials fields, a few researchers have moved beyond simple gel culture systems and have begun to use, as substrates for 3D cancer growth, polymer matrices, that are more representative of the *in vivo* architecture. The most used polymers are the poly(lactic acid) (PLA) [75] or poly(lactic-coglycolic acid) (PLGA) microparticles [76] (**fig1.16)**. These materials are biodegradable, cytocompatible polymers that are regulated by U.S. Food and Drug Administration [58]. PLGA and PLA polymers are commonly used polymers for tissue engineering applications (e.g. bone tissue generation and healing) because of their biocompatibility as well as high mechanical strength that maintains the matrix porous structure for cell migration and growth. However, since PLA/PLGA polymers are hydrophobic, matrixes formulated using these polymers are difficult to wet in cell culture medium, and hence have limited cell adhesion. Therefore, these matrixes are either treated with solvents (e.g., ethanol) and/or coated or blended with other hydrophilic polymers to promote cell adhesion. In fact, PLA/PLGA microparticles formulated with PVA in the internal matrix structure demonstrated better cell adhesion and cell growth than those formulated without it.

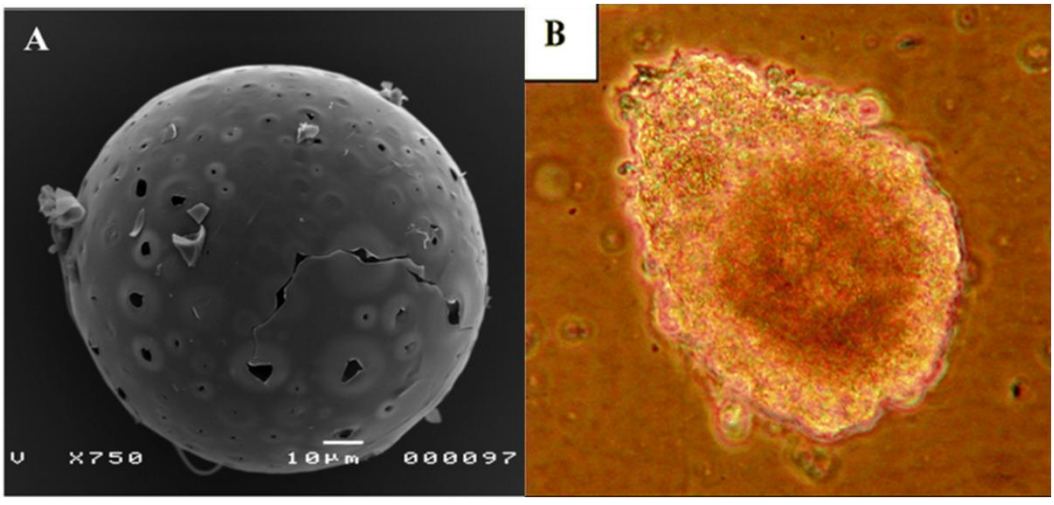

Figure 1.16. (A) Scanning electron micrograph of a typical PLA/PLGA microparticle. (B) Representative photographs of MCF-7 cells grown on PLA-PVA microparticles at 120 h (C) post-seeding. (Adapted from [75])

Fong *et al.* cultured a human Ewing's sarcoma cell line seeded onto electrospun polymeric scaffolds fabricated from poly (e-caprolactone) (PCL) for 20 days (**fig 1.17**). They showed that the cells were more resistant to traditional cytotoxic drugs than were cells in 2D monolayer culture and exhibited differences in the expression pattern of the insulin-like growth factor-1 receptor/mammalian target of rapamycin pathway [77].

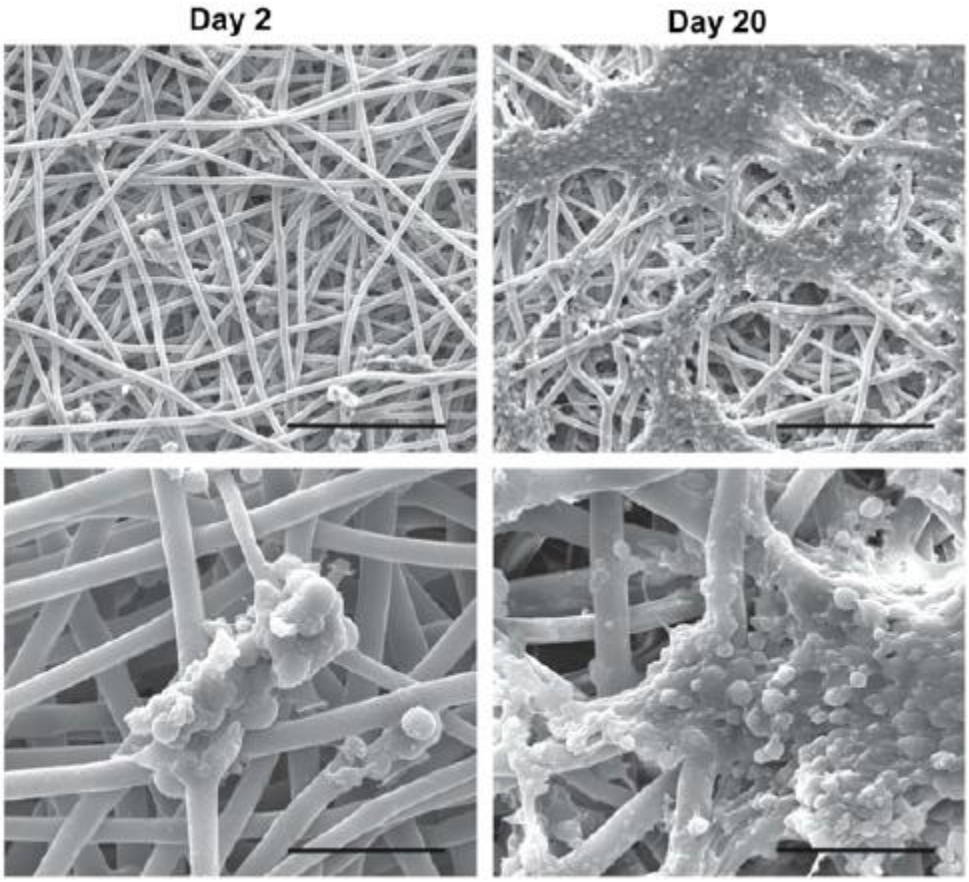

Figure 1.17. Morphological characterization of 3D EWS model. (A) Scanning electron micrographs of TC-71 cells seeded in electrospun 3D PCL scaffolds at low magnification (Upper; scale bar, 200 μm) and high magnification (Lower; scale bar, 50 μm). By the 20th day in culture, cells formed sheet-like clusters and exhibited small, round-cell morphology. (Adapted from [77])

These 3D *in vitro* models recapitulate several *in vivo* features such as three-dimensionality and tumor cell-tumor cell interaction, but they still present weaknesses and limitations. For

example, synthetic scaffolds are highly reproducible and tunable but cells sense mechanical and chemical cues that differ considerably from the **native ECM** (e.g. bone matrix). Moreover, the great majority of tumor models take in consideration the tumor cells alone, even though the *in vivo* stroma is characterized by a high number of cells, thus **co-culture** seems to be more a more realistic solution. Finally, very few tumor models recapitulate some of the most influencing cues that alter cells behavior and growth. For instance, it is well known that **mechanical stimuli** are fundamental for bone homeostasis and growth. In conclusion, it is interesting to study whether or not these cues may affect the tumor survival and proliferation.

Since cancer therapy requires targeting multiple pathways and cell types, preclinical drug testing done in **co-culture** and in **three dimensions** is likely to produce more meaningful results.

1.3.4 Bioreactors: state of the Art

Constructs are generally cultured *in vitro* because of the ability to have a high degree of control over the culture parameters by the use of bioreactors, which allows for more reproducible results and a better understanding of the mechanisms behind functional development of the tissue.

A bioreactor is generally defined as a device capable of creating the proper environment for the generation of a certain biological product [78]. Therefore, a bioreactor is described as a simulator, a device in which biological as well as biochemical processes can be carried out. In tissue engineering, bioreactors are used to impart certain forces that imitate different electromagnetic and mechanical stimuli occurring in the body. In **fig. 1.18** are resumed some of the most valuable bioreactors developed at Columbia University in the Laboratory for Stem Cells and Tissue Engineering and below their respective application are schematically resumed.

- First relevant bioreactor shown in the Figure is an incubator-based modular bioreactor with medium flow and compressive loading for tissue engineering of

cartilage [79] (**fig.1.18 a).**

- Altman *et al.* have developed a modular bench-top bioreactor with medium flow and mechanical loading (tension, torsion) for ligament tissue engineering (**fig.1.18 b, c)** [80] [11].
- Bioreactor chambers housing up to six tissue constructs, with direct perfusion through the cultured constructs and imaging capability, for the tissue engineering of the bone [12] (**Fig. 1.18 d).**
- Radisic *et al*. studied the effects of modular bioreactor with perfused culture chambers fitted with the pairs of electrodes for electrical stimulation, for cardiac tissue engineering [81, 82] (**Fig. 1.18 f).**
- A small-scale bioreactor system built by a combination of microfabrication and microprinting, for microarray cultures of cells in monolayers and thin gel settings [83] (**fig. 1.18 g).**
- A modular bench-top bioreactor with medium perfusion and computer driven environmental control developed for cell culture at the International Space Station [84] (**Fig. 1.18 h).**
- The first generation of the bioreactor shown in **fig. 1.18 d** with mechanical loading, for tissue engineering of cartilage [13, 85] (**fig.1.18 j).**
- The second generation of the bioreactor with medium perfusion and mechanical loading [unpublished] (**Fig. 1.18 k).**
- Bioreactor for tissue engineering of anatomically correct osteochondral grafts [12] (**Fig. 1.18 m, n, o).**

Figure 1.18. Representative Bioreactors developed at Columbia University in the Laboratory for Stem Cells and Tissue Engineering for cell culture and tissue engineering.

1.3.5 Applying mechanical stimulation with Bioreactors.

Mechanical stimuli represent major regulators of the development and function of many tissues, including musculoskeletal (cartilage, bone, ligament, tendon, and skeletal muscle) and cardiovascular (myocardium, heart valve, and blood vessels) tissues.

Mechanical forces regulate cell physiology under normal and pathological conditions, and modulate ECM synthesis and organization at various hierarchical levels; from molecules to whole tissues and organs. It is generally accepted that the structure and function of tissues and organs reflect the acting physical forces, with profound interactive effects. From the early days of Tissue Engineering, mechanical "conditioning" of cells cultured on biomaterial scaffolds was explored based on the premise that the same forces that govern

tissue development and remodeling *in vivo* would also enhance tissue development and function *in vitro*.

In several notable studies, stimulation protocols were designed to provide deformational loading of cartilage, mechanical tension of ligaments and muscle, and flow-induced stretch of blood vessels. The development of specialized bioreactors was a major contributing factor to these studies, which initially focused on the assembly of differentiated animal cells (e.g., bovine chondrocytes and rat cardiomyocytes) and recently have shifted toward human MSCs and ESCs.

In the human body, within the tissue, cells experience different types of mechanical stresses that have inspired many scientific groups. In fact, in the past fifty years a great number of groups have investigated how these different stimuli affect the tissue organization and architecture. In **fig. 1.19** are briefly listed physical cues commonly applied on TE construct, giving some examples of the effects that these stimuli can have on cell's phenotype and proliferation.

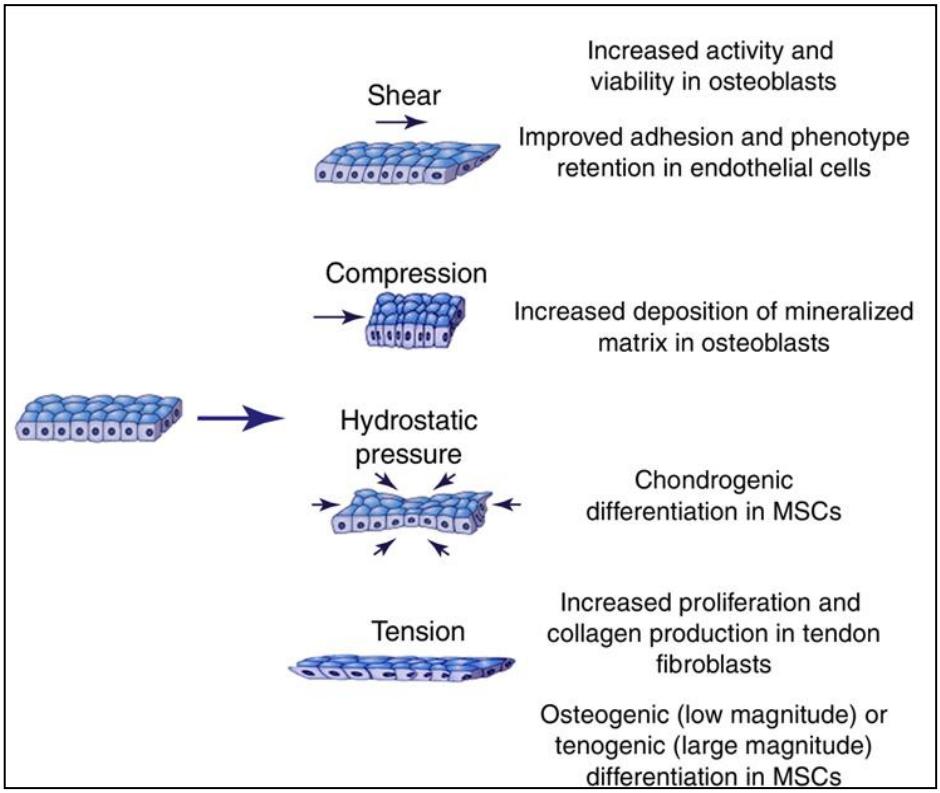

Figure 1.19. Examples of how mechanical forces have been applied in cell culture studies and tissue engineering strategies to affect stem cell fate, extracellular matrix (ECM) synthesis, and cell phenotype and proliferation. (Adapted from [86]).

In Cartilage Tissue Engineering it is well known that dynamic compression stimulates adult chondrocytes to secrete proteins such as collagen and glycosaminoglycans (GAG). This mechanical stimulus also leads to an architectural organization of the tissue that is of striking importance for a load bearing tissue such as cartilage.

Mauck *et al*. developed a bioreactor (**fig. 1.20**) capable of applying direct normal dynamic compression to agarose scaffold seeded with adult chondrocytes. They show how this physical stimulus, in concert with the scaffold features, enhances the mechanical properties of the tissue engineered cartilage [13].

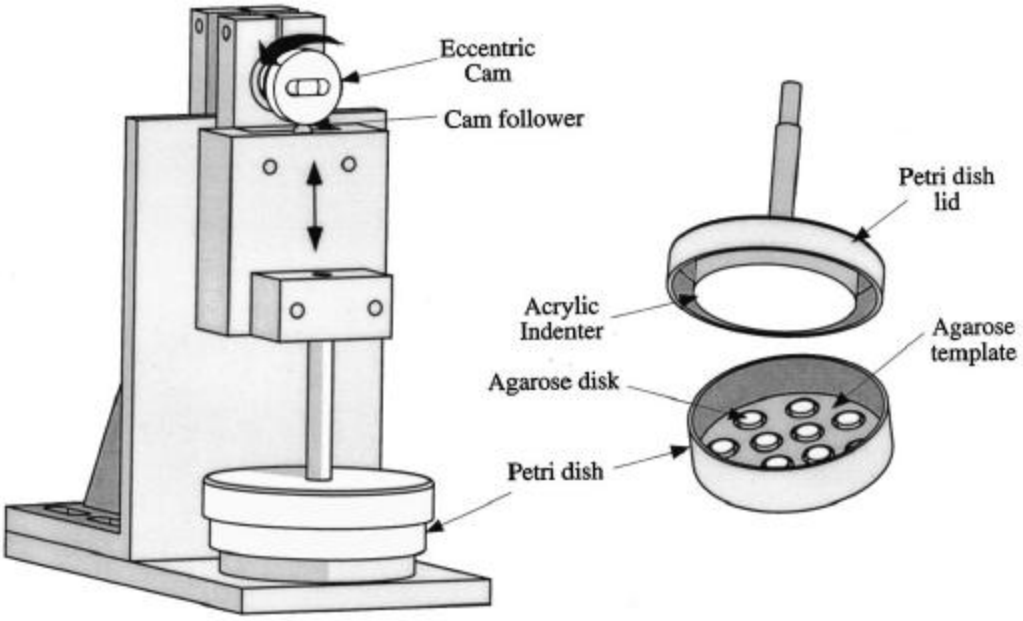

Figure 1.20. Schematic of the custom loading device. This bioreactor is capable of simultaneously deforming multiple chondrocyte-seeded agarose disks. A cam-follower system is used to impose the dynamic loading on unconfined samples. (Adapted from [13])

Nevertheless, Altman *et al*. designed a bioreactor that allowed the controlled application of ligament-like multidimensional mechanical strains (translational and rotational strain) to the undifferentiated cells embedded in a collagen gel. The application of mechanical stress over a period of 21 days up-regulated ligament fibroblast markers, including collagen types

I and III and tenascin-C, fostered statistically significant cell alignment and density and resulted in the formation of oriented collagen fibers – all features characteristic of ligament cells. They concluded that multidimensional mechanical stimulation, without the need of further growing factors can lead stem cells to differentiate towards a ligament cell line lineage (**fig 1.21)** [80].

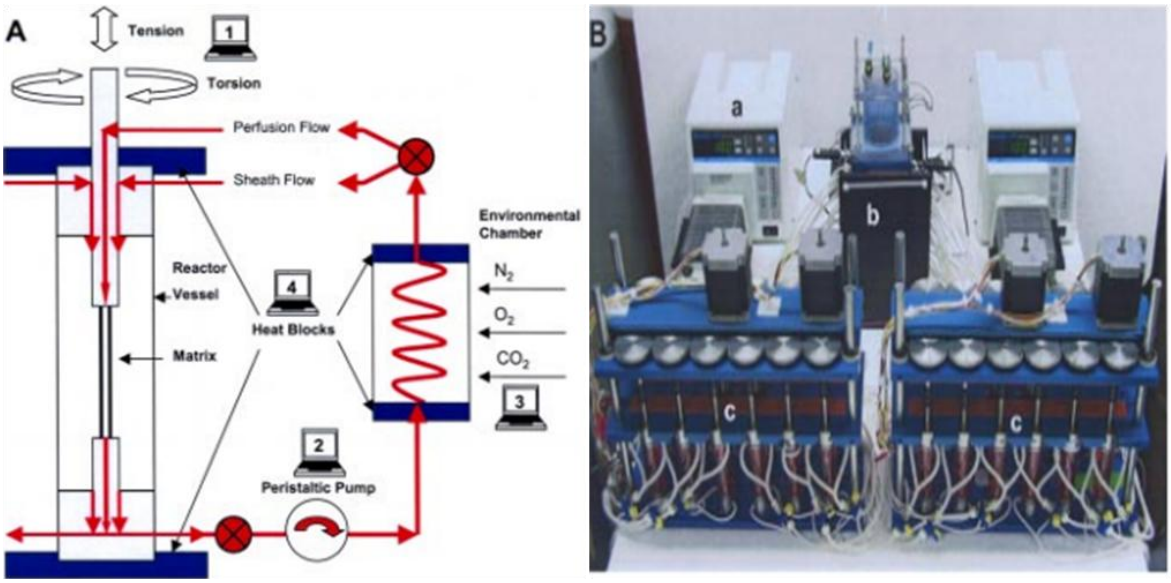

Figure 1.21. (A) Schematic illustrating the bioreactor system. (B) Functioning bioreactor system including: (a) peristaltic pump, (b) environmental gas chamber and (c) the two bioreactors containing 24 vessels. (Adapted from [80])

Some other studies have focus on the differentiation of adult stem cells towards osteogenic lineage. In particular, Jagodzinski *et al.* cultured human bone morrow stem cells (hBMSC) into bovine spongiosa and compared dynamical loading (normal compression) to perfusion alone and static condition, demonstrating that physical stimulus more than fluid flow can lead hBMSCs to differentiate into an osteogenic lineage [87] (**fig. 1.22 A**).

More recently Sittichokechaiwut *et al*. have shown that short bouts of dynamic loading are as effective as dexamethasone (widely to induce differentiation in hMSCs) at inducing matrix production by human bone marrow mesenchymal stem cells **(fig. 1.22 B)** [88].

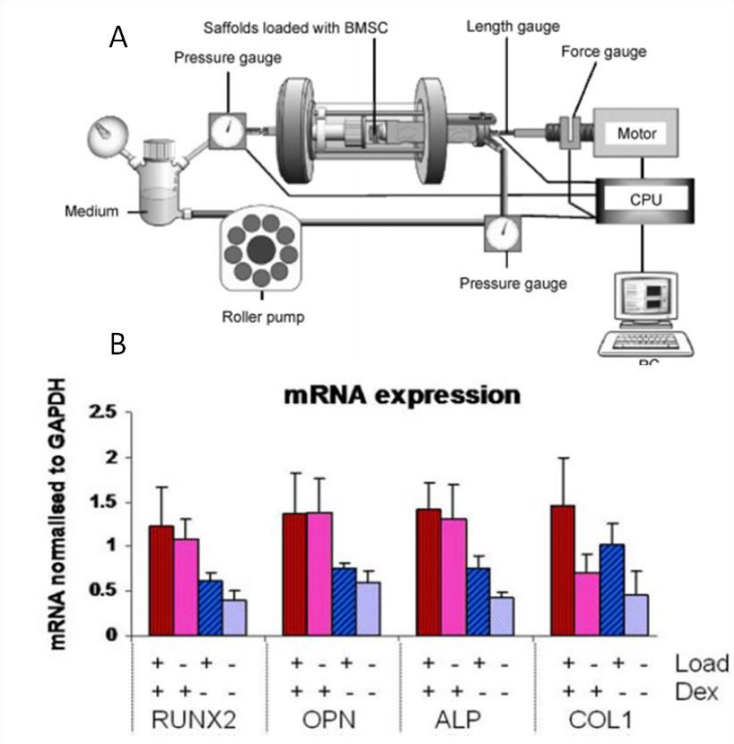

Figure 1.22. Bioreactor system used for the stimulation experiments: a linear servomotor was used for compression of the scaffolds. Continuous perfusion was performed by a roller pump. All parameters were entered and monitored by a PC (A). (Adapted from [87]); mRNA expression of RUNX2, OPN, ALP and COL1 12 h after a single bout of 2 h of loading. (B) (Adapted from [88])

As shown in the previous paragraphs, mechanical stimuli have been largely studied in various tissues within the musculoskeletal system and only more recently some researchers have focus their attentions also on their effect on Cardiac Tissue Engineering.

Shachar *et al*. have, in fact, studied the effect of mechanical loading and the fluid flow resulting from the compression of the construct and the movement of the plunger on neonatal rat cardiac cells seeded in an alginate scaffold (**fig. 1.23**). They had been able to demonstrate how short term stimulation increases the expression of connexin 43 and other important cardiac markers (a-actinin and N-cadherin) [89].

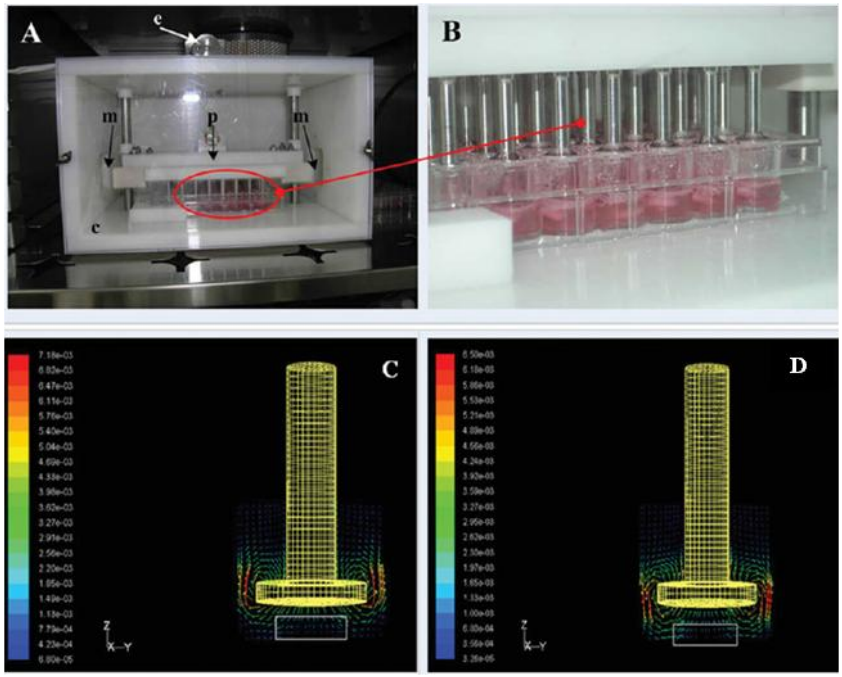

Figure 1.23. **The compression bioreactor and fluid dynamics**. (A) General view of the bioreactor, c bioreactor compartment; m silicone membrane; p compression platform. (B) The compression platform above the 48 well-plate containing the cell constructs. (C) The fluid flow velocity profile in an individual well while the piston is moving downwards (D) or upwards. (Adapted from [89])

In conclusion, it is possible to affirm that these devices were used to assess the effects of mechanical stimulation on healthy cells and, eventually, suggest that *in vitro* simulation of an *in vivo* stimulus – with or without the addition of specific growing factors – can lead to the formation of a more organized tissue. To our knowledge, bioreactors in cancer tissue engineering have yet not been employed. As previously explained, the evaluation of the effect of physical stimuli on cancer cells has been studied only by using cells embedded in a gel and changing its stiffness.

Thus, the design and the development of advanced devices that can simulate the microenvironmental stimuli sensed by tumor cells within the body remains an uncharted territory that still need to be explored. That is one of the aims of this thesis.

1.4 Objectives

In this chapter a general overview of the main arguments that all together represent the rationale for this work. In fact, tumors development proliferation and spreading was accurately resumed, focusing on a particular type of bone tumor: Ewing's sarcoma. This is known to be an aggressive soft tumor, characterized by small rounded cells, typically affecting young patients. Since there have been achieved poor results with the current treatments, the state of the Art regarding the cancer research approaches has been investigated. The lack of complexity of the 2D cell culture, not been representative of the tumor environment, has led to an increased use of mouse *in vivo* models. These models have allowed numerous scientific groups to determine a great set of therapeutic targets of cancer treatments. At the other hand, due to the slight yet important differences between human and mouse some of these targets have failed in clinical trials. **Aim 1** of this thesis is to develop a novel 3D Ewing's sarcoma model that could recapitulate several important tumor features, such as hypoxia, glycolytic phenotype and angiogenesis, lost in 2D cell culture, and that could serve in the future to identify new therapeutic targets. Moreover, in this chapter it was explained how several group have attempted to achieve viable tissue engineered constructs, by the mean of custom made devices, and commonly referred as bioreactors. In particular, in the field of bone tissue engineering, these devices have been designed to simulate significant physiological stimuli such as shear rate, compression and tension. Direct dynamic compression, resulting from the uni-directional motion of a piece in direct contact with the scaffold, has been used on cartilage, bone and osteochondral constructs. After promising results, it seems unlikely that in the near future it will be possible to achieve an implantable viable tissue engineered construct resulting in a shift of attention of many researchers towards different solutions. In this thesis, a novel application for compression bioreactors will be proposed. In fact, it is here hypothesized that dynamic compression, may help simulate the physical cues sensed by tumor cells and that through the mechanotransduction machinery may reactivate the expression of clusters of genes related for example to focal adhesion, in the tissue engineered model of Ewing's sarcoma. Thus, after analyzing the advantages and the drawbacks of the existing devices, **aim 2** of this work is to design a novel compression bioreactor that allows the user to culture a statistically significant number of samples (n=24), easy to assemble, with a user friendly

interface and suitable for drug studies. After a multi-step validation of the tumor model and the bioreactor, respectively in **aim 1** and in **aim 2,** in **aim 3** these tools come together in the pilot study. As previously described, the objective of the pilot study is to support further insight on the effects of mechanical loading on tumor's behavior and to understand whether or not physiological-like stimuli lead to a more aggressive phenotype.

The three main goals of this thesis can be resumed as follows:

- **Aim 1:** development, validation and characterization of a novel 3D Ewing's sarcoma model that *(i)* re-express focal adhesion and cancer related genes, (*ii*) recapitulates the original hypoxic and glycolytic tumor phenotypes and (*iii*) acquire angiogenic capacity and vasculogenic mimicry that favor tumor initiation and adaptation.
- **Aim 2:** design and validation of a compression bioreactor that allows operating with a statistically significant number of independent samples, easy to assemble, with a user-friendly interface and suitable for drug studies.
- **Aim 3:** study the effects of physiological mechanical stimuli on tumor cells behavior, applying dynamic compression to the tissue engineered Ewing's sarcoma (TE-ES) via the compression bioreactor.

In the next chapters the developmental process will be thoroughly explained describing the materials and methods employed, integrating some validation results of the fundamental elements composing the TE-ES. Finally, after an accurate characterization the results of the three aims will be discussed.

Chapter 2 - Materials and Methods

One of the two main goals of this project was the generation, validation and characterization of a novel tissue engineered tumor model. In the introduction has been analyzed the current State of the Art regarding Cancer Tissue Engineering, targeting as an uncharted territory advanced 3D models. In fact, it has been demonstrated that there is an urgent need for more complexes models that can mimic more closely the tumor environment. The second goal of this work is, somehow, an innovative approach in cancer research. As explained in **Chapter 1**, nobody until now has ever employed a bioreactor to apply direct dynamic compression to a 3D tumor model. Since this kind of mechanical stimuli are typically sensed by cells within a tissue (for example, bone tissue), it seems very attractive to have a better understanding on how they affect tumor's fate.

For the tissue-engineered model of Ewing's sarcoma (TE-ES) every single component of the model will be described, explaining how they have been validated. Then, will be enunciated all the techniques that allowed to characterize it.

In the second part of this chapter, will be pointed out the work flow adopted in the design and development of the compression bioreactor. Moreover, every single piece that composes the device will be illustrated in detail, including the controlling system and how it has been validated. Finally, the two main goals converge into a pilot study that will give interesting insights on the effects of physical cues, provided by the compression bioreactor, on the TE-ES.

2.1 Tissue-engineered model of Ewing's sarcoma: generation

The Ewing's sarcoma model is generated starting from fundamental components such as: native ECM, osteoblast-like cells and, finally, tumor spheroids. In this section, will be explained the methodology and techniques needed to build a tissue engineered Ewing's sarcoma.

The generation of the model starts with the decellularization of a bovine trabecular bone plug and the seeding of hMSCs onto it. Hence, after differentiating the stem cells into osteoblast-like cells the Ewing's sarcoma cell lines in form of spheroids has to be added.

2.1.1 Decellularized bone scaffolds

The decellularized bone scaffolds are prepared following a well published protocol from previous studies performed at Columbia University's Laboratory for Stem Cells and Tissue *Engineering* [14] [15]. Briefly, cylindrical trabecular bone grafts (4 mm in diameter) were cored from the subchondral region of carpometacarpal joints of 2-week- to 4-month-old cows. The plugs were washed with a high-velocity stream of water to remove the marrow from the pore spaces and then for 1 hour in phosphate buffered saline (PBS) with 0.1% ethylene-diamine-tetra-acetic acid (EDTA) at room temperature. This step was followed by sequential washes in hypotonic buffer (10 mM Tris, 0.1% EDTA, overnight at 4°C), detergent (10 mM Tris, 0.5% sodium dodecyl sulfate (SDS), for 24 hours at room temperature) and enzymatic solution (50 U/mL DNAse, 1 U/mL RNAse, 10 mM Tris, for 3–6 hours at 37°C) to remove any remaining cellular material. After each step, the scaffolds were rinsed with PBS for 1 hour. After SDS treatment, several washes (≥7) were performed until no more bubbles indicating the presence of detergent were seen in the PBS during washing. At the end of the process, decellularized bone plugs were rinsed in PBS, freeze-dried, and cut to 4-mm-long cylinders. Scaffolds were sterilized in 70% ethanol for 1 h and incubated in culture medium overnight before seeding cells.

2.1.2 ES cell lines, hMSCs culture and spheroid formation

Ewing's sarcoma cell lines SK-N-MC (HTB-10) and RD-ES (HTB-166) were purchased from the American Type Culture Collection (ATCC) and cultured according to the

manufacturer's specifications. Briefly, RD-ES cells were cultured in ATCC-formulated RPMI-1640 Medium (RPMI) and SK-N-MC cells were cultured in ATCC-formulated Eagle's Minimum Essential Medium (EMEM). Both media were supplemented with 10% (v/v) Hyclone FBS and 1% penicillin/streptomycin. In order to generate *in vitro* an ES cell line (EW-GFP cell line), a lentiviral plasmid containing the EWS/FLI mutation was introduced into hMSCs (kindly provided by Dr. Elizabeth R. Lawlor, University of Michigan, Ann Arbor (MI), USA). EWS-GFP cells were cultured in DMEM supplemented with 10% (v/v) Hyclone FBS and 1% penicillin/streptomycin. U2OS osteosarcoma cell line and HEK293T cell line were cultured in Dulbecco's Modified Eagle Medium (DMEM) supplemented with 10% (v/v) Hyclone FBS and 1% penicillin/streptomycin.

The cultivation, seeding and osteogenic differentiation of Human Mesenchymal Stem Cells (hMSC) were performed as described in previous studies [14] [15]. Briefly, hMSC were cultured in basic medium (DMEM supplemented with 10% (v/v) Hyclone FBS and 1% penicillin/streptomycin) for maintenance and expansion, followed by osteogenic medium (basic medium supplemented with 1 μM dexamethasone, 10 mM β-glycerophosphate, and 50 μM ascorbic acid-2-phosphate) for osteogenic differentiation. Due to the highly osteogenic properties of the mineralized bone scaffolds used to culture the cells, the supplementation of BMP-2 was not necessary. To form tumor cell spheroids, 0.3 x106 Ewing's sarcoma cells were centrifuged in 15 mL Falcon tubes, 5 minutes at 1200 rpm, with 4mL of medium and cultured for one week at 37°C in a humidified incubator at 5% CO_2.

2.1.3 Model assembly

Cell culture scaffolds (4 mm diameter x 4 mm high plugs) were prepared from fully decellularized bone as in previous studies [14] [15]. The scaffolds were seeded with 1.5 x106 hMSCs (passage 3) and cultured in 6 mL of osteogenic medium for 4 weeks. Medium was changed twice a week. After 4 weeks, the scaffolds were bisected; one half was seeded with Ewing's sarcoma cells (3 spheroids per scaffold) (TE-ES) and the other half was used as a control (TE-bone).

Three tumor models were formed using the three tumor cell lines. For each tumor, TE-bone was used as a control. TE-RD models (and their counterpart TE-bone controls) were cultured in RPMI medium. TE-SK-N-MC models (and their counterpart TE-bone controls) were cultured in EMEM. TE-EWS-GFP models (and their counterpart TE-bone controls) were cultured in DMEM.

All culture media were supplemented with 10% (v/v) Hyclone FBS and 1% penicillin/streptomycin. TE-ES and TE-bone models were cultured at 37°C in a humidified incubator at 5% CO_2 for 2 and 4 weeks.

2.2 Tissue-engineered model of Ewing's sarcoma: validation

When generating a novel model, it is crucial to validate the components used to build it. In order to do so, numerous analysis techniques – such as immunohistochemistry (IHC), quantitative real-time PCR and cytometry – have been adopted.

Firstly, will be explained the qualitatively evaluation of the TE-bone by using IHC. Then, by the mean of qRT-PCR, specific bone markers that are commonly expressed in osteoblast cells have been analyzed.

In the second part of this paragraph, will be described how the tumor cell lines have been validated by using FACS analysis of negative and positive surface markers in Ewing's sarcoma cells.

2.2.1 Tissue engineered bone (TE-bone)

It has been previously shown that hMSCs differentiate into osteoblastic lineage and form viable, functional human bone when cultured on 3D scaffolds made of decellularized bone in osteogenic-differentiation medium [90] [17]. This approach was used to engineer a bone niche (TE-bone) for the tumor model. First, the osteogenic potential of hMSC (passage 3)

after three weeks of monolayer culture in osteogenic medium was tested. Positive Alkaline phosphatase and Von Kossa stainings (**Fig. 2.1 a, b**) demonstrated bone differentiation capacity of hMSCs.

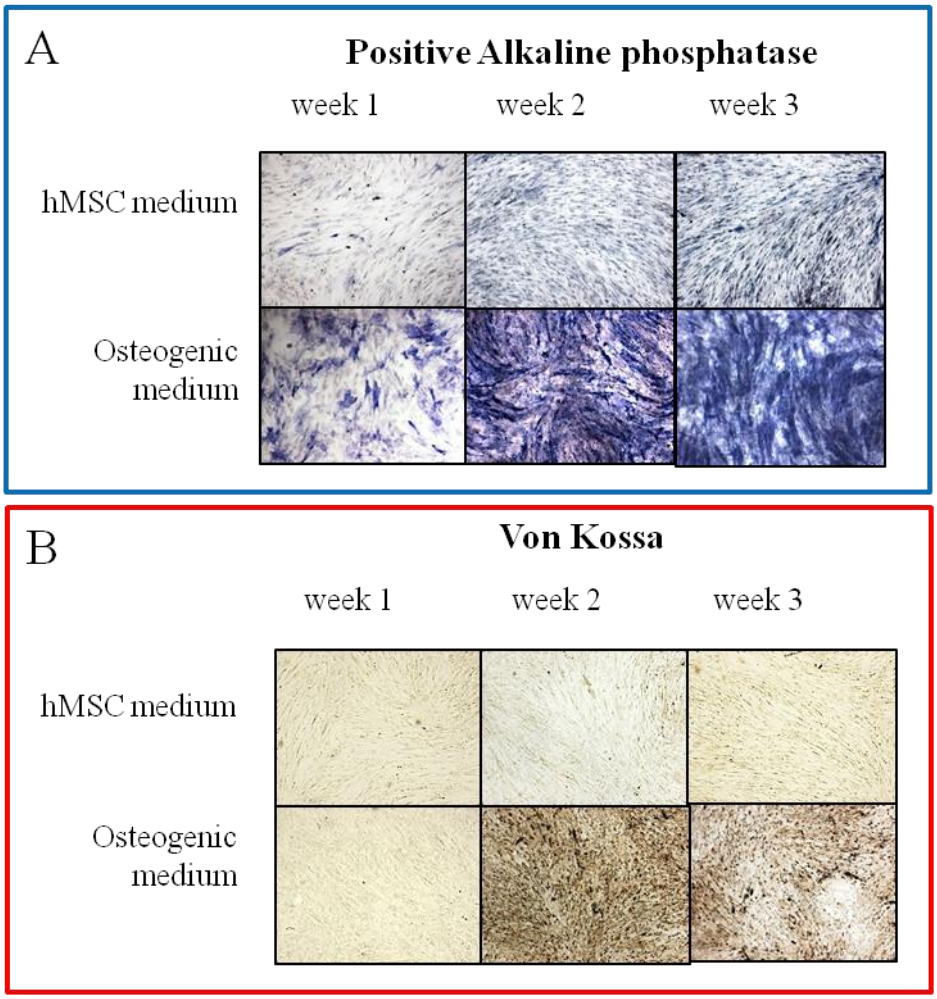

Figure 2.1. Bone marker staining in 2D cell culture. (A) Osteogenic differentiation evaluation by alkaline phosphatase staining of three samples. **(B)** Mineral deposition analysis by the von Kossa method. Images are representative of a total analysis

Moreover the expression of typical bone markers was analyzed by qRT-PCR (**fig. 2.2**). In particular, mRNA levels of Osteopontin (OPN), Bone Sialoprotein (BSP), and Osteocalcin (OCN) in hMSC cultured in monolayer in hMSC medium or osteogenic differentiation medium overtime were assessed demonstrating induction and bone differentiation.

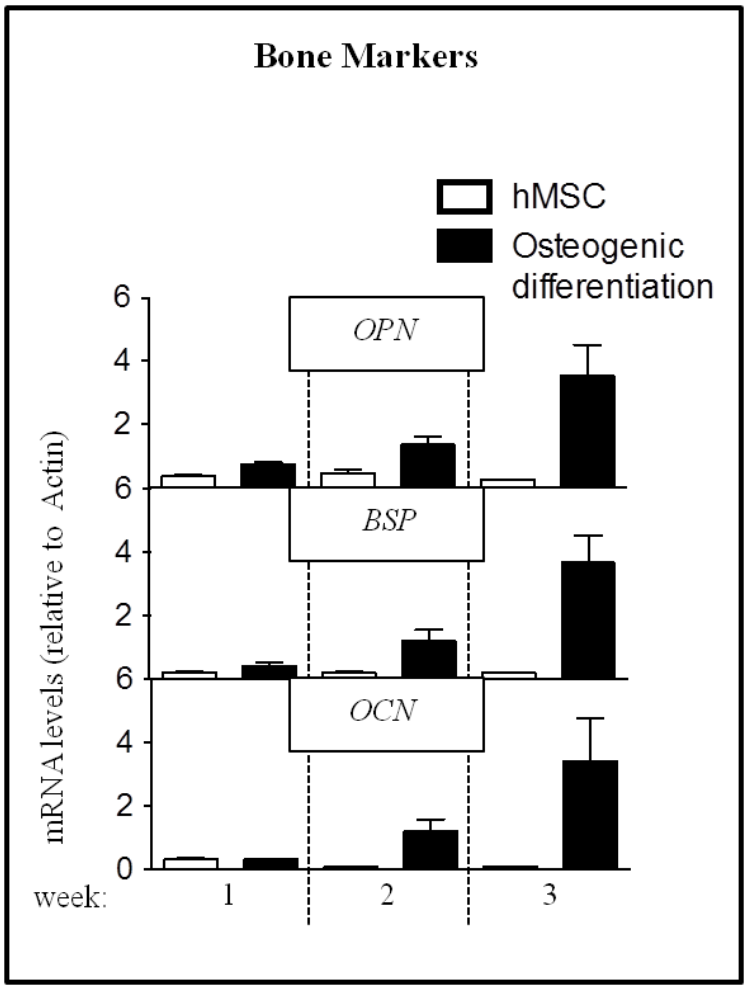

Figure 2.2. qRT-PCR analysis of bone genes during osteogenic differentiation in monolayer. All data represent mean +SD (n=3)

In parallel, 1.5x106 hMSC (passage 3) were cultured in 4x4mm cylindrical decellularized bone scaffolds for 6 and 8 weeks, in osteogenic differentiation medium, and observed elevated expression levels of bone related markers (OPN, BSP and OCN) as compared to the differentiation of same cells in monolayer cultures (**fig. 2.3 A**).

It has been further confirmed bone-related protein expression by IHC suggesting that TE-bone was properly generated (**fig. 2.3 B**).

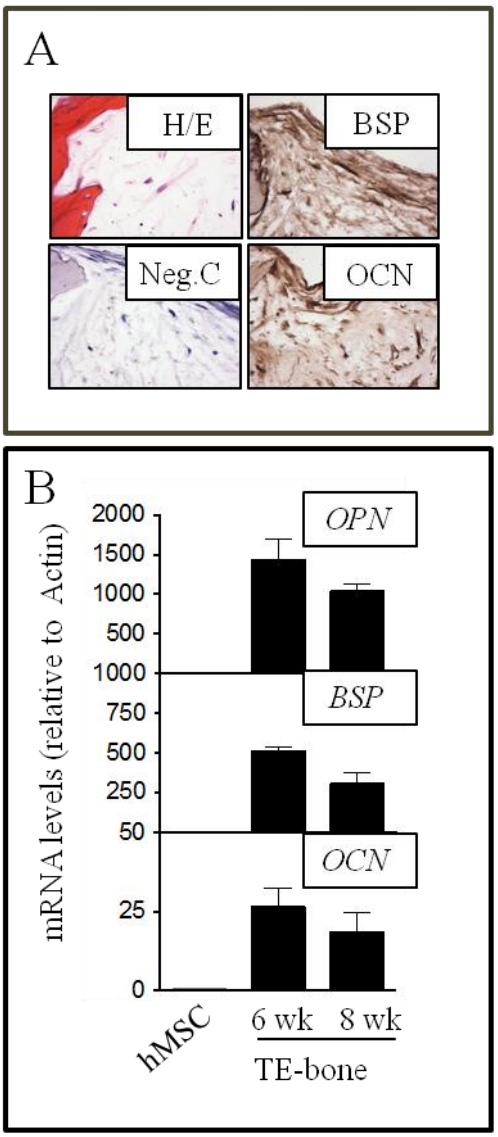

Figure 2.3. TE-bone osteogenic differentiation. (A) Bone-related protein expression analysis by IHC in TE-bone at week 8. Counterstaining was performed with hematoxylin QS (blue). Representative images, n=3; H/E, Hematoxylin and Eosin. (B) qRT-PCR analysis of bone genes during osteogenic differentiation in scaffold. mRNA levels of Osteopontin (OPN), Bone Sialoprotein (BSP), and Osteocalcin (OCN) in hMSC cultured in a bone scaffold during 6 and 8 weeks in osteogenic differentiation medium were assessed and compared to hMSC at t=0.

Because it is well know that hypoxia is a pivotal microenvironmental factor for tumor development [91]**,** hypoxia in the middle of the TE-bone was confirmed by tissue immunofluorescence of pimonidazole-binding cells (**fig. 2.4**).

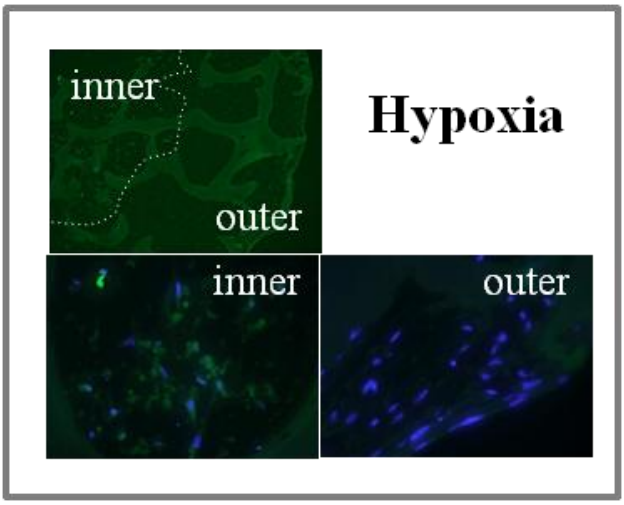

Figure 2.4. Hypoxia analysis in TE-bone by tissue immunofluorescence of pimonidazole-binding cells (green). Inner = inner part of the scaffold. Outer= outer part of the scaffold. Nuclei were stained with DAPI. Representative images, n=3

2.2.2 Ewing's sarcoma cell lines

Two Ewing's sarcoma cell lines expressing GFP, RD-ES (primary bone tumor cell line) and SK-N-MC (primary cells originated from an Askin's tumor and metastasizing in the supraorbital area) were used to develop the tumor models (**fig. 2.5 A**). Surface markers (characterized by FACS) were, as expected, CD13, CD44 and CD73 negative and CD90, CD105 and CD99 positive (**figs. 2.5 B**).

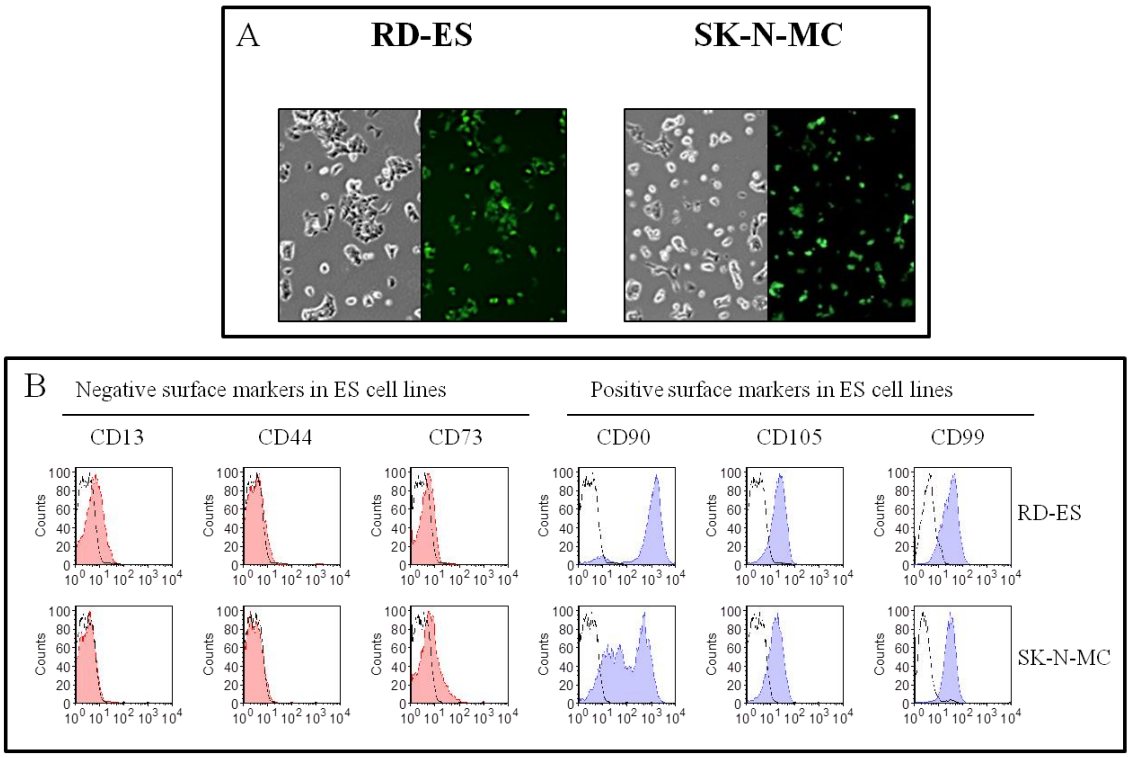

Figure 2.5. RD-ES and SK-N-MC validation. Morphology of two ES cell lines, RD-ES and SK-N-MC. Left panel: brightfield images showing typical small round cell ES morphology. Right panel: GFP expression images by fluorescence microscopy. RD-ES and SK-N-MC were stably transduced with pBabe-GFP retroviral vector as described in **appendix A1** (b) FACS analysis of negative and positive surface markers in Ewing's sarcoma cells (protocol in **appendix A2**).

In order to generate *in vitro* an ES cell line (EW-GFP cell line), a lentiviral plasmid containing the EWS/FLI mutation was introduced into hMSCs (kindly provided by Dr. Elizabeth R. Lawlor, University of Michigan, Ann Arbor (MI), USA) (**fig. 2.6 A**). Surface proteins expression in EW-GFP cell line (by FACS) was compared to hMSCs, exhibiting high levels of the ES-related marker CD99 and losing CD13, CD44 and CD73 hMSC-specific markers (**Fig. 2.6 B**).

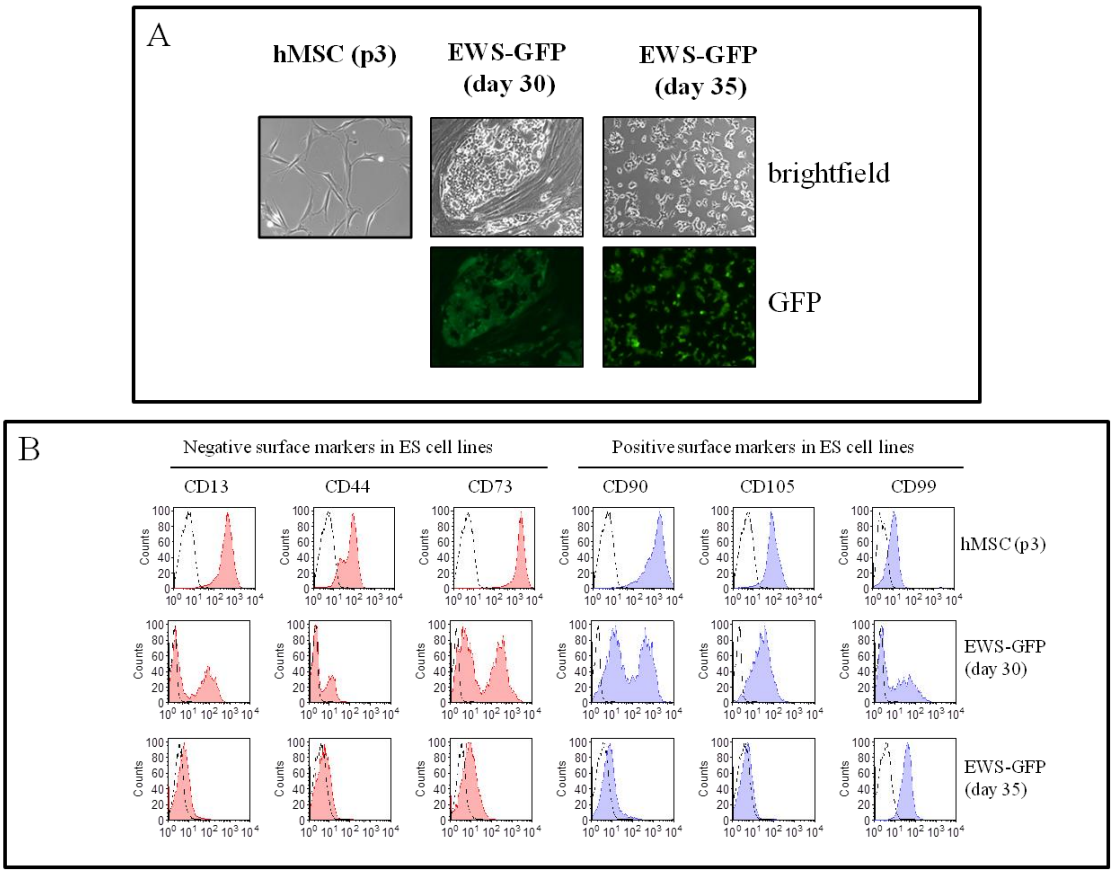

Figure 2.6. EWS-GFP cell line validation. (A) Top panels: Brightfield images of hMSC (passage 3, p3) and transduced with EWS-GFP vector at day 30 (without passage) and day 35 (passage 2). Low panels: GFP expression images at day 30 and 35 post-transduction. (B) Analysis of hMSC and ES surface markers in EW-GFP cell line. hMSC were CD13, CD44, CD90 and CD105 positive and expressed low levels of CD99 specific ES marker. EWS-GFP at day 35 lost hMSC surface proteins acquiring a similar ES surface markers profile and expressing high CD99 levels.

2.3 Tissue engineered Ewing's sarcoma: model characterization.

In this section will be briefly described the techniques used to characterize the TE-ES model. In particular, the aim will be to study in depth the re-expression of focal adhesion genes, often differentially expressed in 2D cell lines, compared to real tumor. For this purpose, a high throughput Micro-array analysis, comparing tumor cells lines (cultured in a monolayer) to tumor tissue harvested from patients, has been used. Moreover, the

glycolytic phenotype using IHC, TUNEL assay and qRT-PCR will be studied. Finally, it is well known that primary tumors express and eventually secrete angiogenesis related factors to induce the formation of novel blood vessels. ELISA assay has been used, coupled with IHC and qRT-PCR, to characterize angiogenesis in the model. The detailed explanation and the interpretation of the results are postponed to **Chapter 3.**

2.3.1 Micro-Array data analysis

Expression of genes in native Ewing's sarcoma tumors and cell lines was studied in 11 cell lines and 44 tumors by applying the barcode method to the Affymetrix Human Genome U1332 Plus 2 gene expression data of Savola *et al.* [92]. A probe set was considered expressed in cell lines/tumors only if detected in all cell lines/tumors. Where a gene had multiple probe sets, the gene was only counted once. Genes expressed in cell lines, but not tumors, or in tumors, but not cell lines, were identified from the asymmetric difference of both sets.

2.3.2 Quantitative real-time PCR (qRT-PCR)

Total RNA was obtained using Trizol (Life Technologies) following the manufacturer's instructions (see details in **appendix A3**). RNA preparations (2 μg) were treated with "Ready-to-go you-prime firststrand beads" (GE Healthcare) to generate cDNA. Quantitative real-time PCR was performed using DNA Master SYBR Green I mix (Applied Biosystems). mRNA expression levels were quantified applying the ΔCt method, ΔCt = (Ct of gene of interest - Ct of Actin).

GFP primers were selected as previously reported [93]. Other qRT-PCR primer sequences were obtained from the PrimerBank data base (http://pga.mgh.harvard.edu/primerbank/) (for the complete list of primer sequences see **appendix A4**)

2.3.3 Histology and Immunohistochemistry (IHC)

TE-ES and TE-bone models were fixed in 10% formalin, embedded in paraffin, sectioned at 4 μm and stained with hematoxylin and eosin (H/E). The sections were then stained for CD99 (dilution 1:500; Signet antibodies, SIG-3620) and GLUT1 (dilution 1:500; Abcam, ab652) as previously described [17], and counterstained with Hematoxylin QS (Vector Labs). For PAS staining, periodic acid-Schiff (PAS) (from Sigma-Aldrich) was used according to the manufacturer's instructions. hMSC (passage 3) were plated in 24 well plates (1 × 104 cells/cm2) and cultured for 3 weeks in either basic medium or osteogenic medium. At weeks 1, 2 and 3 osteogenic differentiation was analyzed by alkaline phosphatase activity (Sigma–Aldrich, St Louis, MO, USA), following the manufacturer's instructions and by von Kossa staining. Sections were incubated with 1% AgNO3 solution in water and exposed to a 60 W light for 1 h. Hypoxyprobe^{TM}-1 (pimonidazole) Kit for the Detection of Tissue Hypoxia (Chemicon International, Inc., Temecula, CA, USA) was used to detect hypoxia in TE-bone according to the manufacturer's instructions. Preparations were mounted with vectashield and *nuclei* were counterstained with DAPI (Vector Labs, H-1200).

2.3.4 TUNEL assay

Apoptotic cells were detected by an *in situ* cell death detection kit, TMR red (Roche Applied Science, Mannheim, Germany), according to the manufacturer's instructions (for detailed protocol see **appendix A5**). The assay measures DNA fragmentation by immunofluorescence using TUNEL (terminal deoxy-nucleotidyl transferase-mediated dUTP nick end-labeling) method at the single cell level. One hundred cells per field (n=3) in the center of the TE-ES model (n=3) were counted to quantify the percentage of apoptotic cells. Nuclei were stained with Hoechst 33342 (Molecular probes).

2.3.5 Enzyme-Linked Immunoabsorbent Assay (ELISA)

24-hour supernatants from TE-ES and TE-bone controls were analyzed to detect angiogenic proteins, using a Proteome Profiler Human Angiogenesis Array Kit (R&D Systems, ARY007) according to the manufacturer's instructions (for detailed protocol see **appendix A6**).

2.3.6 Native tumors

Ewing's sarcoma tumors were obtained from the Columbia University Tissue Bank. The samples were fully de-identified. Three different frozen tissue samples were cut in sets of 6 contiguous 10 μm-thick sections and homogenized in Trizol (Life technologies) for RNA extraction and subsequent gene expression analysis.

2.4 Compression Bioreactor: system specifications

The first phase in designing a new device is defining the general specifications. In the particular case of bioreactors, devices conceived to culture and stimulate cell constructs, the first important requirement is the compatibility with the good laboratory practice (GLP). Therefore the bioreactor has to guarantee the complete absence of any contamination during the whole culture period by isolating the culture environment from the external environment. In other words, the whole process has to be sterile. For this reason, the choice of the materials to use is critical, especially for the components in contact with medium and cells that should be biocompatible and easy to sterilize (possibly in the autoclave that represents the gold standard method for sterilization). Moreover, the parts in direct contact with the cells should be disposable or, at least, used a limited number of times.

The culture of the constructs can vary from short (a few days) to long (a few weeks) periods of time. It is then very important that the materials used are resistant to the aggressive and corrosive fluids and do not release any degradation products that can be toxic to the cells or alter the outcome of the experiment.

The compatibility with the good laboratory practice does not only affect the choice of the materials but also requires reducing the number of steps that could jeopardize sterility in every procedure. Therefore, it is important to reduce and simplify the number of steps necessary to insert the samples in the system. Moreover, these procedures have to be performed in a sterile biological hood. Here every procedure has to be executed slowly and carefully to avoid contamination. Thus, simplifying and lowering the number of steps to perform greatly lowers the risk to a mistake that leads to contamination. Simplifying the assembly of the device is also important because most of the times the user is not an engineer or an expert but more often is a biologist or a laboratory technician that is only familiar with the standard static culture devices such as Petri dishes, multi-wells and flasks.

Another aspect for a device that could potentially be commercialized in the future is the cost of both the materials and the production. The materials should be easy and inexpensive to obtain and machine. Also the electronic components needed to control the system can make the price go conspicuously high, thus a trade-off between cutting-edge technology and costs should be found.

The device should also have a reduced volume to fit in a standard cell culture incubator necessary to control the environmental parameters (temperature, pH and humidity) that is usually designed to house Petri dishes and flasks and not big and complex bioreactors.

In addition to all the characteristics already listed, it is also often desirable to have culture chambers in the bioreactor that are transparent, allowing a thrilled monitoring of the culture without manipulating or stopping the device, enhancing the risk of contamination.

A proper bioreactor should indeed be able to deliver some relevant biophysical stimuli, such as the mechanical one, making it then suitable for several fields in which Tissue Engineering is applied (e.g., bone, cartilage, cardiac and cancer). Nevertheless, a well projected device should be flexible regarding the range of stimulation parameters available, it should integrate a proper system for oxygenation of the 3D cell cultures it hosts; and, eventually, should also be able to deliver the same type of stimuli while housing constructs of different dimensions.

The last, but not least, characteristic that must possess a bioreactor that operates in the Tissue Engineering field, is the one that allows to culture multiple samples (at least four) in parallel. If this is respected, it would then be possible to perform statistical analysis of the results and verify their consistency, leading to a more precise and reliable study.

In the following sections will be presented the description of how, after a solid rationale, has been conceived the system object of this project, along with an accurate study of the bibliography.

2.5 Compression Bioreactor: design and development

The first challenge that occurred during the design of the bioreactor was finding a way to improve those developed so far by different scientific groups and laboratories, in order to transform it in a completely novel platform.

The aim was, specifically, to develop an innovative platform that could support different sizes of constructs, several types of cells, and that could, simultaneously, allow to an operator to vary multiple parameters without affecting any outcome. After a thrilled analysis of the state of the art, it seemed even more important to overcome some of the main limitations of those devices that require highly skilled operators, but also extremely expensive. For these reasons the first step has been to develop a system that could easily be assembled in a sterile environment and that could provide a proper mechanical compression to the scaffolds and the tumor cells.

After the identification, in the existent bioreactors, of all the aspects that needed an improvement, it has been possible to define the three main modules that should compose an innovative device:

- The culture module that includes the main platform with the culture chambers that provides the mechanical stimuli.
- The compression module that comprises the stepper motor and the linear actuator.
- The control module and user interface that involves the microcontroller through

which all the culture and the stimulation parameters can be inserted and adjusted.

For the first two modules, the culture and the compression ones, the preliminary design has initially been finalized thanks to the realization of the technical drawings of the main parts with SolidWorks®, a 3D parametric drawing software (Dassault Systemes SolidWorks® Corp.). All the simulations have then been realized using COMSOL® Multiphysics (COMSOL ltd.) to identify the critical components of the design, thus giving a strong rationale for the choice of the materials. These have to be at the same time biocompatible with the cultures and possess the proper mechanical properties. In fact, when it comes to bioreactors and cell culture the range of materials that meet the stringent characteristics' requirements, such as biocompatibility, is less wide than for any other type of device. Therefore, this strongly affects not only the fabrication process of the pieces, but also, and more importantly, the overall geometry.
For the control module, the third one identified, an Arduino microcontroller (ATMega and Mini, Sparkfun Electronics) has been chosen to control the hardware components of the device. Those components already include the stepper motor and will, in the future, allow controlling also the sensors responsible of giving feedback on the displacement.

In conclusion, it has been demonstrated how the design of a bioreactor goes through a multi-step process that starts with a strong rationale and an accurate in-depth study of the state of the art of the bioreactor field, and that ends with the choice of the most suitable materials and geometries. Those will then allow more accurate and repeatable experiments, characterized by a low degree of assembly complexity and errors in the analysis of contingent scientific results.

In the next parts of this work will be analyzed in detail each module that composes the innovative bioreactor developed in the framework of this project.

2.5.1 Culture module

For the reasons explained in the previous paragraph, a standard cell culture 24-well-plate (Falcon, BD Biosciences) has been used as the main platform that hosts the culture chambers. This allowed to have room for a consistent number of samples (n>4) ensuring statistical significance (**fig.2.7)** of the tests.

Figure 2.7. 24-well cell culture.

The 24-well plate is a multi-well cell culture device made of treated (or untreated), clear polystyrene, commonly used in laboratories. Each well has a diameter of 1.5*cm* and is 1.85*cm* deep, while the whole plate is 12.8*cm* long and 8.5*cm* wide. The use of this platform brings several benefits, such as:

- Cost: the 24 well plates are much less expensive than any custom made chamber that should be machined from raw materials.
- Availability: it's part of any lab's standard equipment.
- Sterility: it comes packaged individually and sterile and it is also disposable.
- Transparency: it's made of clear polystyrene, which makes it transparent and imaging compatible.
- Simplicity: it's a basic lab instrument that any biologist or technician is familiar with.

The more relevant downside of this plate is that it can't be altered, so it is always the stimulation system that has to be adapted to the fixed geometry, and not the other way around. For this reason, the culture chambers developed for this system are composed of custom-made inserts that can match the geometry of the wells, as shown in the drawing in **fig. 2.8** below**.**

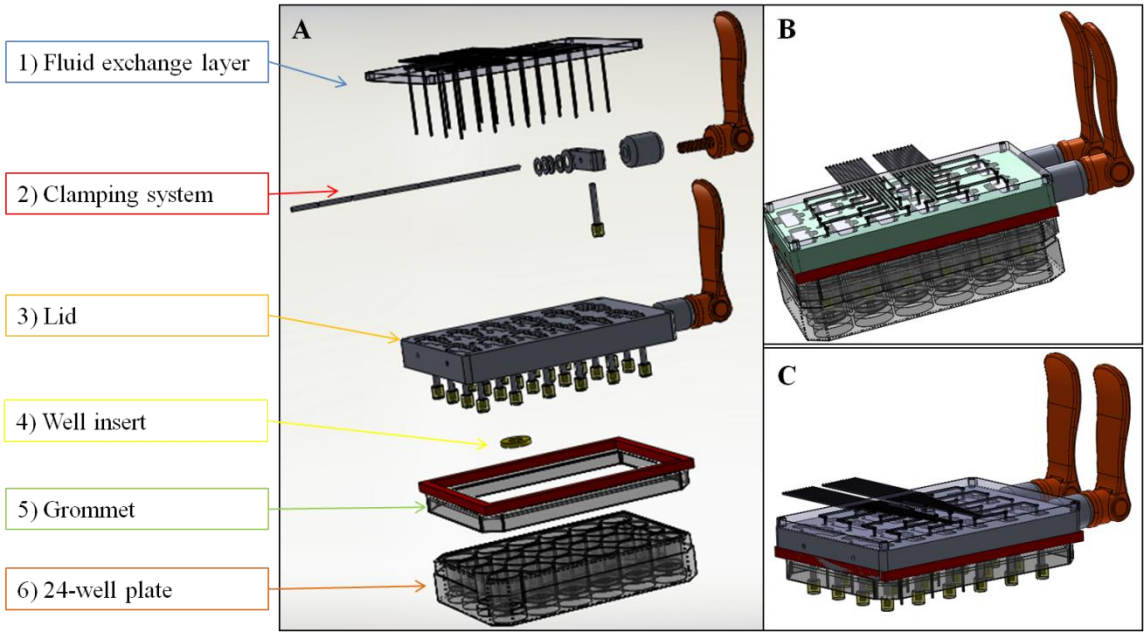

Figure 2.8. SolidWorks® overview of the culture module. Exploded view of the main components in the culture module (A). Assembled view of the culture module (B). Isometric view of the assembled lid that, with a vertical motion, provides compression to the constructs.

In the figure, from top to bottom, these are the elements shown:

7) *The fluid exchange layer*: this component is needed to add and remove independently the medium from each culture well. By this mean, it is also possible to add growing factors or drugs to each sample, individually.
8) *The Clamping system*: here it is shown how, with a combination of special springs called Belleville springs and cam levers, the plunger can easily be clamped and released. Without the clamping force, the plungers will then fall freely upon the scaffold giving a precise "zero" positioning.

9) *The Lid*: this is the supporting part for the *Clamping system* and the *fluid-exchange layer*.
10) *The Well insert*: this component sits at the bottom of each well and is meant to hold the scaffold in the correct position.
11) *The Grommet*: this is a boundary of soft silicone that is meant to seal the chambers and to bear the loading that derives from the vertical motion. It is attached to a modified version of a 24-well plate cover.
12) The 24-well plate: this component represents the base of the bioreactor, providing 24 independent culture wells.

Here below will be explained in detail each single component of the bioreactor, in order to allow a more deep comprehension of the complete bioreactor developed in the aim of this project.

1) The fluid exchange layer

One of the primary drawbacks identified in the existing devices is that, in order to change the culture medium, it is always necessary to open the culture chamber. Whereas, the design of this innovative system allows the operator to change the medium, to add growing factors or even drugs and so on, directly from the sterility hood. Thus, there is no need to move the bioreactor from the incubator and to open it, making possible and repeatable long and more elaborated experiments.

The *fluid-exchange layer* is made with stereolitography technique casting liquid PDMS (polydimethylsiloxane) mixture inserted into a custom-designed mold (**fig. 2.9**).

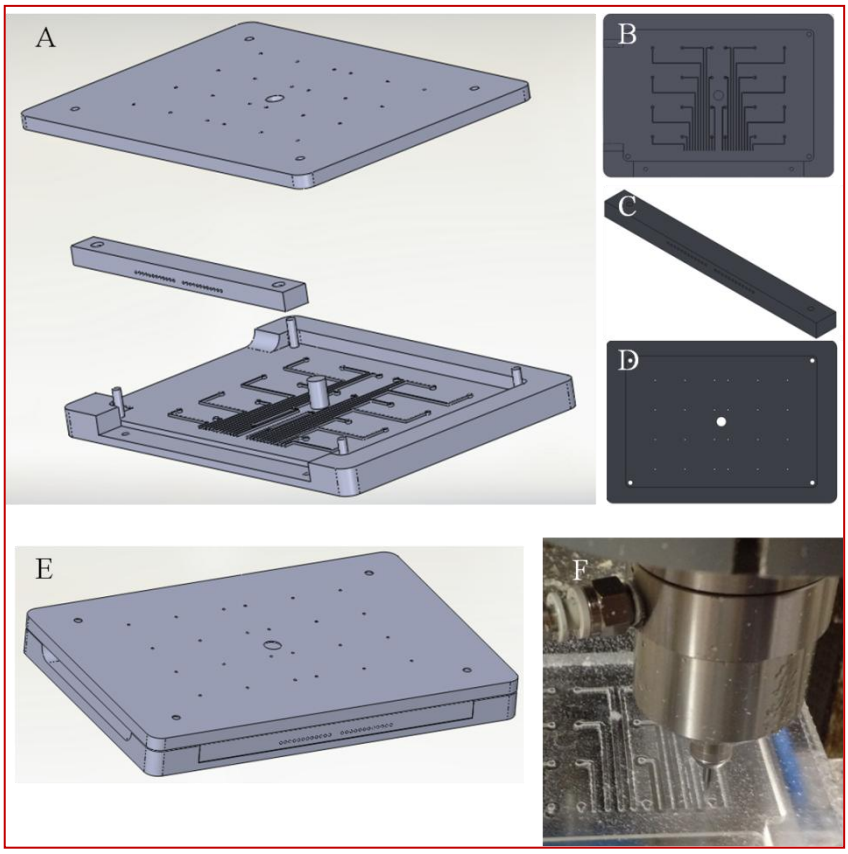

Figure 2.9. Modular mold for PDMS casting. Exploded view of the modular mold (A). Bottom pieces with thin features (B). Side part with 1 mm holes (n=24) (C). Cover piece that seals the mold (D). Assembled isometric view of the mold (E). Cutting process of the piece by the CNC milling machine (F).

The mold is composed of three modular parts: the bottom, the cover and a side piece. The bottom piece (**fig.2.9 B**) is characterized by very thin features (width 0.5x1 mm high, n=24) resulting as groves on the hardened PDMS. It also has a lateral hole that allows the pouring of the liquid PDMS.

The side piece (**fig 2.9 C**) allows the integration of stainless (SS) tubes (precision miniature stainless steel tubing 316, 19.5g, 0.039" outer diameter, 0.027" internal diameter, 0.006" wall, n=24) into the casted PDMS. Each one of these tubes, running along the side of the component, has been be coupled with a PTFE (polytetrafluoroethylene) tube (PTFE lightweight wall tubing 19 awg, internal diameter 0.038") ending in the sterility hood.

Finally, the cover piece (**fig.2.9 D**), that not only serves as the sealing lid of the mold, but that also possess holes that allow the integration of additional SS tubes – that run into the

PDMS from the top of the component. These tubes, afterwards, stick out of the PDMS layer and run into each of the 24 wells on the plate.

All the pieces just described are made of optical clear polycarbonate (McMaster-Carr) and machined with a CNC (computer numerical control) milling machine (**fig.2.9 E**).

Nevertheless, the process to obtain the PDMS piece from the mold follows a standard Stereolithography technique. Briefly, the liquid PDMS base (Sylgard 184 Silicone base, Dow Corning) is mixed with the curing agent (Sylgard 184 Silicone curing agent, Dow Corning) with a ratio of 10:1 respectively. The mixture, stirred until a uniform consistency, is then reached and placed in vacuum for debubbling. When ready, the liquid PDMS mix is casted into the assembled mold and debubbled again. The mold is then placed in a 55 ^{o}C oven overnight. After this hardening period, the three pieces are carefully detached, starting from the cover piece. Once also the side piece is removed, it is finally possible to detach the hardened PDMS layer from the fine-finished surface of the mold.

The PDMS base obtained with such methods (**fig. 2.10**) is then sealed with a commercially available, biocompatible adhesive-back silicone sheet (thickness 1 mm). This solution ensures sealing even after several sterilizations in the autoclave at high temperatures and pressure, and is therefore optimal for long and elaborated experiments. The final piece has 24 independent channels that allow the medium to flow from the sterility hood, through the PTFE tubing, into each well. On the contrary, medium flows out of the well through the SS tube coming out perpendicularly from the piece, running again in the channel and ending in the sterility hood through the PTFE tubes.

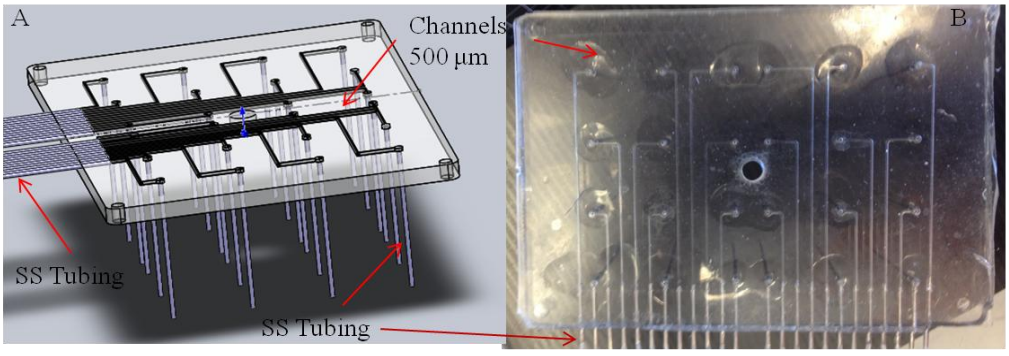

Figure 2.10. Piece resulting from the PDMS casting in modular mold. SolidWorks® model of the final product of the stereolitography (isometric view) (A). Picture of the actual *fluid-exchange layer* after PDMS casting (B).

As already pointed out early in this paragraph, maintaining sterility during long term experiments is imperative and for this reason a simple, yet efficient, way to keep sealed the PTFE tubes sitting in the sterility hood has been adopted (not assumed sterile all the time). Injection adaptors (SMITHS MEDICAL injection adaptor, length 2.2cm, priming volume 0.1ml), commercially available, have been employed since they can be reused several times without the risk of compromising sterility. The injection adapters (**fig. 2.11 A**) are provided with a male luer-lock that allows an easy coupling with off-shelf needles with female luer-lock (**fig. 2.11 B**) (standard equipment in common laboratories). The gauge size of the needles (stainless steel blunt needle with 19 gauge luer polypropylene hub, 1-1/2" length) has been chosen to fit tightly the PTFE tubes. Finally, the length of the PTFE tubes can be easily adjusted depending on the distance between the incubator (where the bioreactor is located) and the sterility hood (where the culture medium can be added/removed).

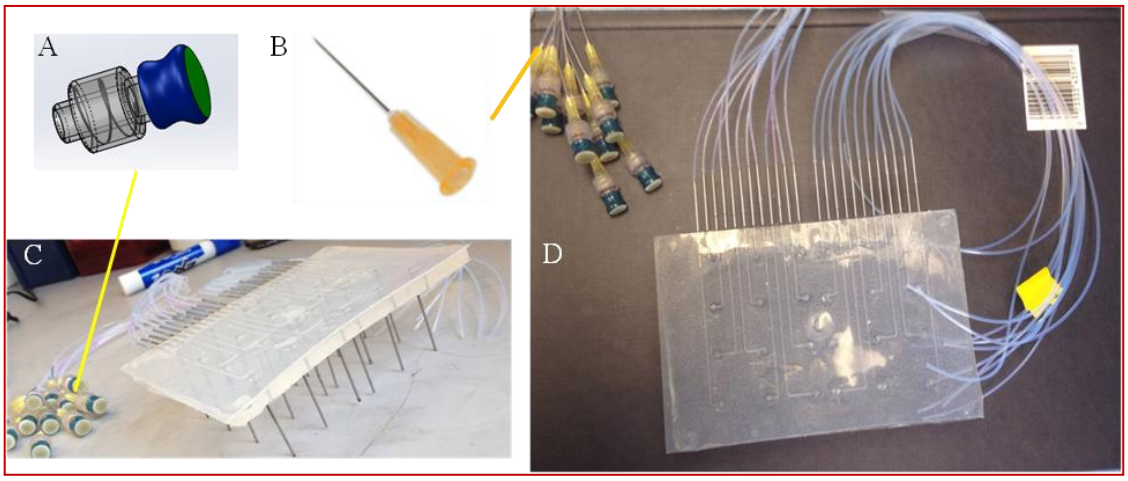

Figure 2.11. Final assembly of the fluid-exchange layer. SolidWorks® model of the disposable injection adapter (A). Stainless steel blunt needle (B). Overview of the final piece with injection adapters coupled with needles (C). Top view of the final assembly (D).

2) The Clamping system.

Several devices providing direct dynamic compression have been designed and developed in the past 20 years, but almost all of them have a great limitation: the imprecise

positioning of the plunger (the piece in direct contact with the scaffold that transmits compression to the cells).

The geometry of a scaffold, even if it can sometimes be highly reproducible, presents variations in its dimensions e.g. do to the cutting process. To avoid experimental error, it has been chosen to design a system that would allow a precise and repeatable zero positioning. In fact, the plunger is initially forced between two SS pieces (one fixed and one movable) by a clamping mechanism, consisting in a combination of springs and cam-levers. When the camlever releases the plunger from the clamping force provided by the springs (pushing the moving part away from the fixed part), it falls freely upon the scaffold in virtue of the gravity force.

Since the bioreactor object of this work has been designed to house up to 24 samples, it would have been time consuming adjusting one-by-one the plungers – for example, by the mean of micrometer set screws. That is why it has been designed with this particular "zero positioning" characteristic. In **fig. 2.12,** an exploded view of the clamping mechanism is depicted.

Figure 2.12. SolidWorks® representation of the clamping system. (A) Zoomed top view of two plungers clamped between the moving part (A1) and the fixed part (A2). (B) Trimetric view of the bioreactor's lid. (C) Exploded view of all the pieces composing the clamping system: 1) cam-lever, 2) standoff, 3) threaded nut, 4) moving part, 5) plunger, 6) Belleville spring, 7) Belleville washer, 8) threaded rod.

The clamping system hereby explained, is comprehensive of eight pieces:

1) Cam-levers: They allow quick fastening and unfastening without the use of any tool. They also permit to the user to tighten by threading like a traditional fastener; however, for final tightening the cam lever is pushed downward. To unfasten, the cam lever is pulled up releasing the clamping force and allowing the fastener to be unthreaded. They are ideal for quick change operations, where parts only have to be loosened and not completely unassembled. In this particular application, the cam-

lever when pulled up releases the plungers from the clamping force deriving from the springs (McMaster-Carr, quick-positioning cam handles, Type 303 Stainless Steel, 1/4"-20 Thread x 13/16" Thread Length).

2) Standoffs: they serve as pulling surface for the cam-lever and help to space from the lid (McMaster-Carr, metric 18-8 SS unthreaded standoff 13mm od, 16mm length, m6 screw size).
3) A Nut: when it is threaded to the long rod, it engages the moving part when the cam-lever moves upwards (McMaster-Carr, undersized machine screw hex nut, 10-24 thread size, 5/16" width, 7/64" height).
4) A Moving part: it is a custom-made piece shaped to house two plungers. It has two holes that allow the tubes to come out perpendicularly from the Medium-exchanging layer to go precisely into each well (**fig. 2.13**).

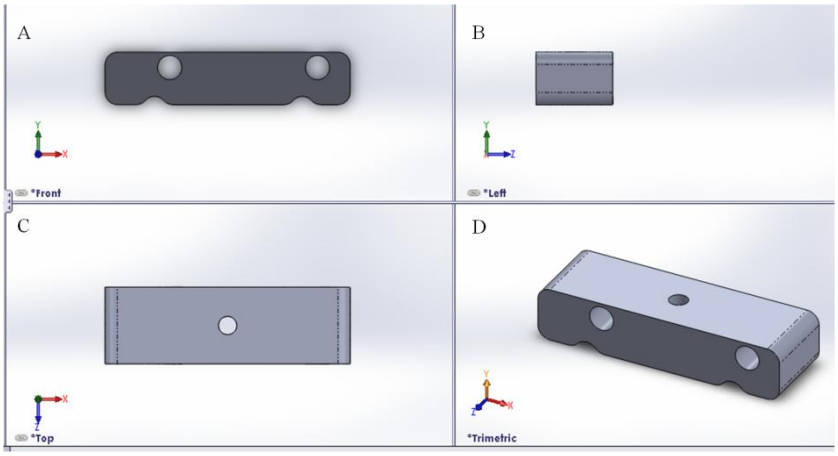

Figure 2.13. SolidWorks® model of the moving part. (A) Top view of the piece with the holes that allow the tubes sticking out of the *fluid-exchange layer* to go all the way through the lid and to end in the culture well. (B) Lateral view of the piece. (C) Front view of the piece with central hole for the threaded rod to go through. (D) Trimetric view of the piece.

5) A Plunger: it is the part in direct contact with the scaffold and it is secured to the lid. This part is composed by a SS 316 cylinder (diameter 3.17 mm, height 30 mm) press fitted into a ULTEM® cylinder (diameter 6 mm, height 6.35 mm).
6) Belleville springs: they are conical springs that can hold large loads in small spaces. They are designed to fit over rods, and it is possible to use them singly, or stacked

as shown to increase load and deflection (the distance the spring compresses). In a nested stack, the load is increased by the number of springs used. In an inverted stack, the deflection is increased by the number of springs in the stack, while retaining the load of only one of them across the span of the stack. In a nested and an inverted stack, both the load and the deflection are increased (**fig. 2.14**).

In this device, an alternation of nested and inverted stack that result in a balance between load and deflection has been used.

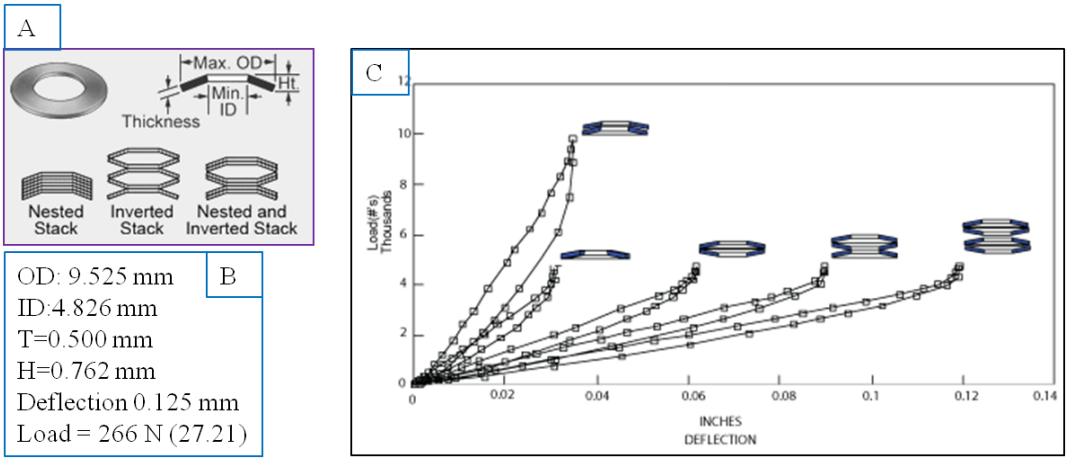

Figure 2.14. Belleville springs. (A) Overview of a Belleville spring (McMaster-Carr) with main dimensions and stacking configurations. (B) Dimensions of the springs used in the bioreactor. (C) Qualitative example of the effect of the stacking (load vs. deflection).

7) Belleville washers: they are also known as "conical washers" and have a slightly cupped shape that gives them a spring-like flexibility to resist loosening, due to heat and vibration. In combination with the Belleville springs, they allow to adjust the clamping force as desired (McMaster-Carr, stainless steel Belleville washer .190" id, .375" od, .030" thick).
8) A Threaded rod: going through the lid, it transmits the clamping forces and connects all the pieces together.

In conclusion, the cam-levers are a handy loosing system that allows the operator to easily release the plungers, that otherwise would be tightly clamped to the lid, thanks to flat but

powerful springs. All the pieces are made of 316 stainless still and, thus, not only they ensure consistence and longevity, but they can also be completely sterilized reducing the risk of contamination.

3) The Lid

The lid is the central part, were all the pieces come together. It is milled out of a raw rectangular bar made of stainless steel 316. The design is thought to maximize consistency, minimizing the material needed. It allows an easy assembly with the *fluid exchange layer* and it has a threaded hole at its center. This is because it is in the center that will be coupled the motor and the lid by using a particular system that will be explained later in this chapter.

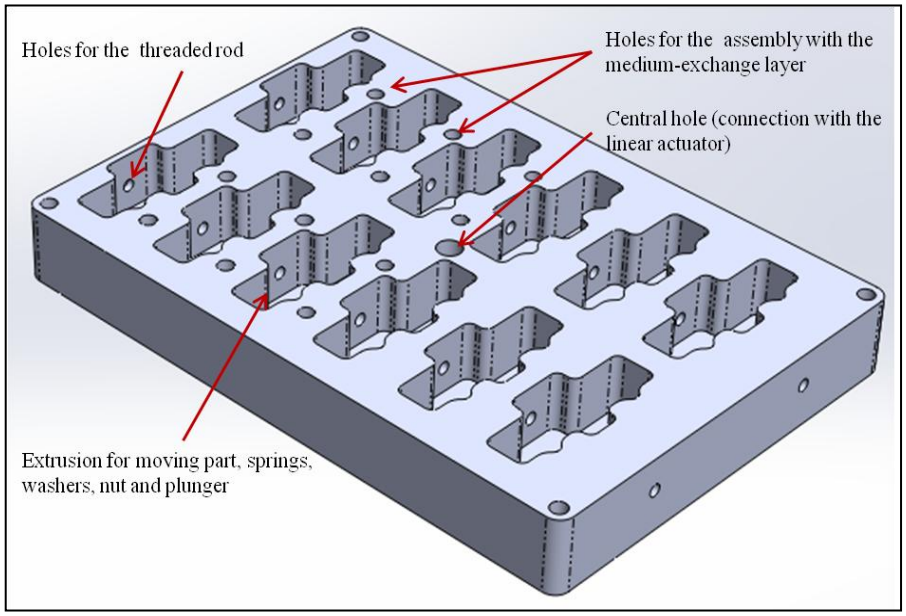

Figure 2.15. SolidWorks® model of the lid.

4) The Well insert.

The well insert is a custom-made disc that fits exactly the well in a standard 24-plate. It has a central offset (diameter 6 mm) that allows the exact placement of the scaffold in the center of each well and, thus, in correspondence with the plunger. It also has a dumping effect; in fact, it reduces the load on the polystyrene plastic that has not a high compressive

modulus. At the contrary, the well insert are made of a very resistant polymer – often employed in aeronautic application – called ULTEM®. Also known as Polyetherimide (PEI), it is an amorphous, amber-to-transparent thermoplastic with characteristics similar to the related plastic PEEK. Relative to PEEK, PEI is cheaper and lower in impact strength, but has a higher use temperature. In **fig. 2.16** a typical plunger- scaffold-well insert configuration is shown and the dimensions of the well insert and the main properties of its material are resumed.

A

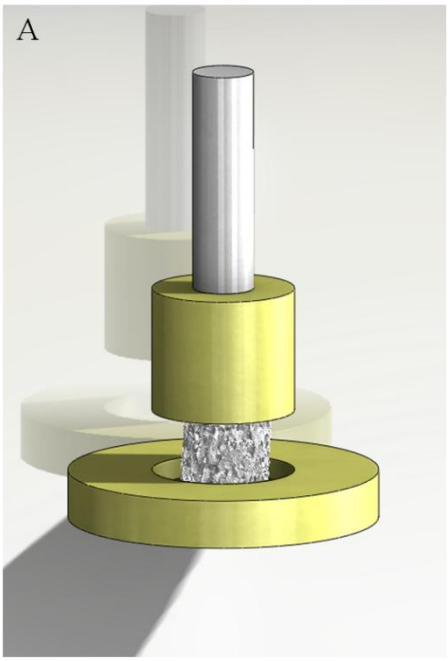

B

Mechanical Properties	Metric	Test
Hardness, Rockwell M	114	ISO 2039/2
Hardness, H358/30	165 MPa	ISO 2039/1
Tensile Strength, Ultimate	160 MPa	ASTM D 638
Elongation at Break	2.00%	5 mm/min; ISO 527
Tensile Modulus	9.00 GPa	DIN 53457
Flexural Strength	225 MPa	2 mm/min; ISO 178
Flexural Modulus	8.10 GPa	DIN 53457
Ultimate Compressive Strength	175 MPa	ASTM D 695
Compressive Modulus	7.50 GPa	DIN 53454
Poissons Ratio	0.38	ASTM D 638
Shear Strength	100 MPa	ASTM D 732
Thermal Properties		
Thermal Conductivity	0.290 W/m-K	ISO 8302
Deflection Temperature at 0.46 MPa (66 psi)	212 °C	ASTM D 648

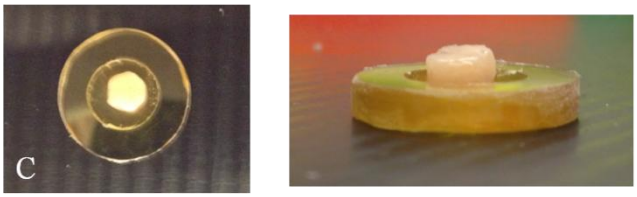

Figure 2.16. Well insert. (A) Plunger-scaffold- well insert configuration. (B) Principal mechanical and thermal properties of ULTEM®. (C) Top view and side view of a real well insert housing the TE-ES.

5) The Grommet.

The grommet and the modified 24-well plate cover are the pieces that allow keeping sterility throughout the entire experiment. Standard culture plates have a cover that is designed to provide an even oxygen diffusion without compromising sterility. This is achieved thanks to the cover's features that match, with a loose fit, the features of the plate underneath it. Thus, in order to keep this advantage the cover has been modified, cutting out the central part and leaving intact the burdens. This solution allows keeping the advantage previously described. On the other hand, the grommet is made out of Super-Soft

Silicone Rubber (McMaster, tensile strength 1.4 MPa). Like other silicone, this rubber stays flexible over a wide temperature range, but its softness gives it better conformability than other rubber. Furthermore, it absorbs the vertical motion of the lid that pushes against it without detaching from it avoiding contaminations.

6) The 24-well plate.

As previously anticipated, the base of the culture module is a standard 24-well plate commercially available and commonly used in most of Tissue Engineering laboratories around the world.

It has the advantages of being relatively cheap (compared to custom made pieces), to be disposable and to allow a simultaneous work with up to 24 samples. This last aspect appears to be crucial in terms of reducing the experimental error and maximizing the reproducibility and the consistency of the experiment.

2.5.2 Compression module

The compression load is the result of a straight vertical motion provided by a Haydon Kerk integrated stepper motor/linear actuator. A stepper motor is a brushless, synchronous, electric motor that converts digital pulses into mechanical shaft rotation. Every revolution of the stepper motor is divided into a discrete number of steps, often 200 steps, and the motor must be sent a separate pulse for each step. The stepper motor can only take one step at a time, and each step is the same size. Since each pulse causes the motor to rotate with a precise angle, typically 1.8°, the motor's position can be controlled without any feedback mechanism. As the digital pulses increase in frequency, the step movement changes into continuous rotation, with the speed of rotation directly proportional to the frequency of the pulses. Stepper motors incorporate a permanent magnet rotor, coil windings and magnetically conductive stators. Energizing a coil winding creates an electromagnetic field with a north and south pole. It is the stator that carries the magnetic field. The magnetic field itself can be altered by sequentially energizing or "stepping" the stator coils, which generates rotary motion. The diagram below (**fig. 2.17 A**) illustrates a typical step sequence

for a two phase motor. In Step 1, phase A of a two phase stator is energized. This magnetically locks the rotor in the position shown, since unlike poles attract, then phase A is turned off and phase B is turned on, the rotor rotates 90° clockwise. In step 3, phase B is turned on but with the polarity reversed from Step 1, this causes another 90° rotation. In Step 4, phase A is turned off and phase B is turned on, with polarity reversed from Step 2. Repeating this sequence causes the rotor to rotate clockwise in 90° steps.

Stepper motor "step modes" include full, half and micro-step. The type of step mode output of any stepper motor is dependent on the design of the driver (explained in more detail in the next paragraph). For this application microstepping has been object of interest, which is a relatively new stepper motor technology that controls the current in the motor winding to a degree that further subdivides the number of positions between poles. Some microstepping drives are capable of dividing a full step (1.8°) into 256 micro-steps, resulting in 51,200 steps per revolution (0.007°/step). It is typically used in applications that require accurate positioning and smoother motion over a wide range of speeds. On the other hand, like the half-step mode, microstepping provides approximately 30% less torque than full-step mode. Finally, step motors are used every day in both industrial and commercial applications because of their low cost, their high reliability, their high torque at low speeds and their simple, rugged, construction that operates in almost any environment.

Then the rotary motion of a stepper motor can be converted to linear motion using a lead screw/worm gear drive system. The lead, or pitch, of the lead screw is the linear distance traveled for one revolution of the screw. If the lead is equal to one inch per revolution, and there are 200 full steps per revolution, then the resolution of the lead screw system is 0.005 inches per step. As already explained before, even finer resolution is possible by using the step motor/drive system in microstepping mode. In this case will be used a linear actuator (HaydonKerk 5700 series, size 23), that provides a stepping range between 4 - 50 μm with a maximum thrust value of 880 N (**fig. 2.17 B**). It is possible to find all the specifications and the technical drawings in **appendix A7** and **A8.**

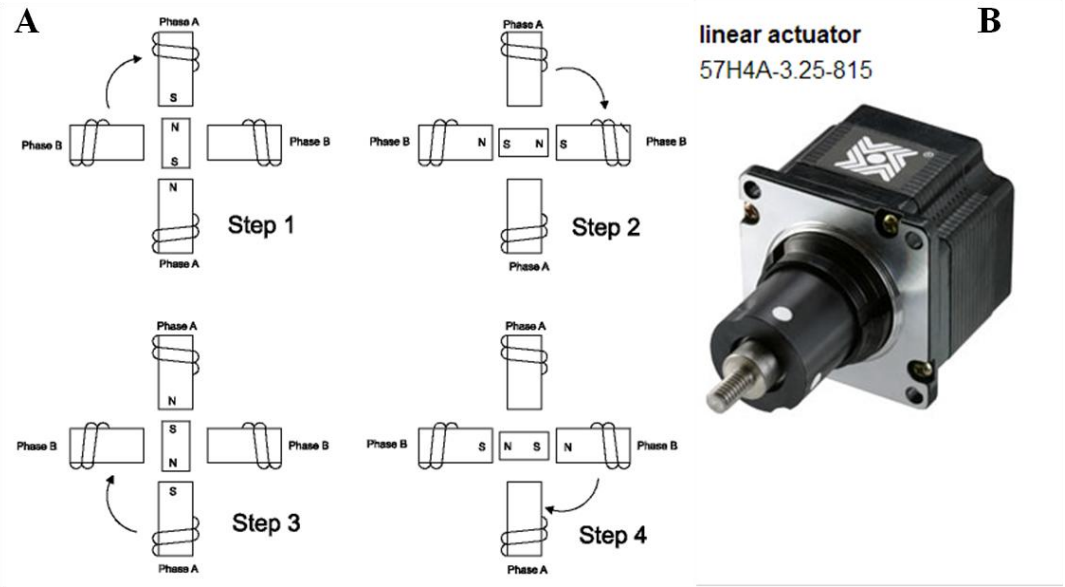

Figure 2.17. Stepper motor and stepping. (A) Diagram of a stepping sequence. (B) Image of the Stepper motor coupled with the linear actuator employed in the system.

The linear actuator and *Lid* are connected by a rigid shaft coupling. Specifically, a rigid coupling is a unit of hardware used to join two shafts within a motor or mechanical system. In fact, by precisely aligning two shafts and holding them firmly in place, they help to maximize performance and reduce shock. In particular, the shaft coupling connects the linear actuator's rod with a thumb screw that is stably screwed into the lid. Thus, this solution allows the operator to fasten the two pieces (the linear actuator and the *Lid*) using the shaft coupling and also makes it possible to adjust the four set screws to ensure a tight coupling (**fig. 2.18**).

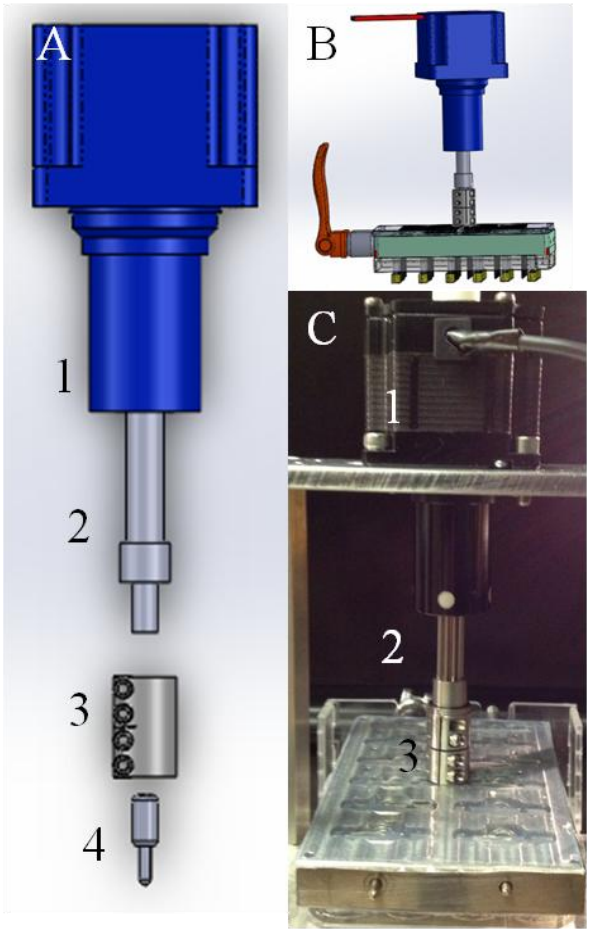

Figure 2.18. Overview of the motor-lid coupling mechanism. (A) SolidWorks® exploded view with the linear actuator (1), loader rod (2), shaft coupling with the four set screws (3), and thumb screw (4). (B) SolidWorks® side view of the motor and the lid connected. (C) Actual view of the linear actuator (1) and its rod (2) connected to the lid with the shaft coupling (3).

2.5.3 Control module and user interface

As previously described, the device chosen to apply loading was an integrated stepper motor/linear actuator. Although the device's motion is linear, it is the same as a typical bipolar stepper motor in the way it is controlled and in the discrete form of its motion. The loader control system consists of an Arduino Pro Mini and an A4988 stepper motor driver IC. The A4988 allows the Arduino to control the motion of the actuator with just two microcontroller digital output pins. One pin sets the direction of motion and the other causes the actuator to take one step every time that it is pulsed. In addition, four other

digital output pins are used to send a four-bit binary number to the stepper driver indicating the desired micro-stepping resolution (**fig 2.19**).

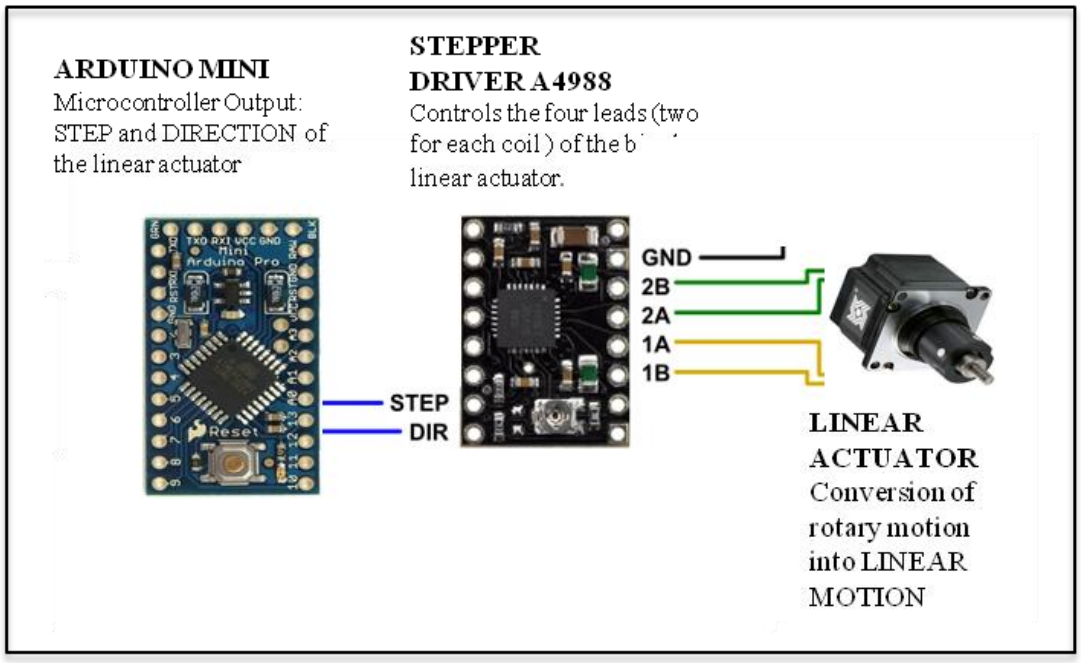

Figure 2.19. Microcontroller and stepper actuator. Communication between stepper driver and linear actuator controlled by the Arduino mini.

The way in which the control system can produce various loading profiles is as follows. Within a user friendly graphical user interface (**fig 2.20**), the operator selects a governing waveform for the loading. The options are: triangular, sinusoidal, and trapezoidal waveforms. Then, the operator specifies the frequency, amplitude, and resolution of the motion. In addition, for a trapezoidal profile, also the duty cycle is selected. The software restricts the operator from selecting parameters that exceed the capabilities of the system (for more detail on the system capabilities see **appendix A9**). After the parameters are finalized and the operator clicks the update button, the computer serially transmits several bytes of data to the Arduino that characterize the chosen profile. After all of this is accomplished, the operator no longer plays a role and all actuator control is executed by the Arduino.

Every 2 milliseconds, the Arduino runs an algorithm to determine whether or not it should command the actuator to take a step. The basis for this determination are two variables:

one that tracks how many 2 ms time increments have passed and one that tracks how many steps have been taken. From the number of time increments that occurred and from the characteristics of the loading profile, the Arduino calculates how many steps *should have been taken* by the current instance. If this number exceeds the number of steps that *have been taken*, a step is taken and both variables are incremented. Otherwise, no step is taken and only the time tracking variable is incremented. Once the loader has moved through one half-period of the loading profile, the variables are set back to zero and the direction of motion is reversed. This is because the motion of the actuator is identical in each half-period, the direction simply switches each time.

For triangular and trapezoidal waveforms, the number of steps that should have been taken by the current instance is calculated from a linear x = mt equation, where x is the expected displacement, t is time, and m is the slope as determined by the parameters of the loading profile. For sinusoidal waveforms, the calculations comes from a x = Acos (ωt) equation, where A and ω are determined by the parameters of the loading profile (detailed code in **appendix A10)**.

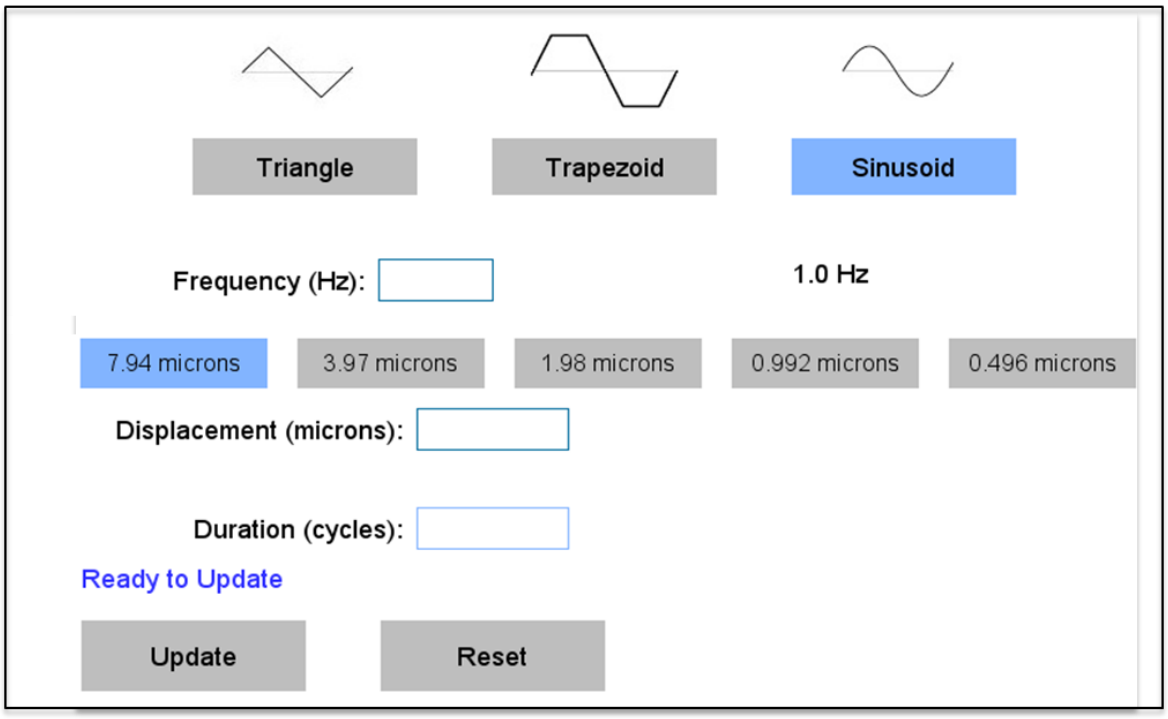

Figure 2.20. GUI: general user interface. First the operator has to choose the desired wave form, then the frequency, resolution and amplitude of the displacement. Finally the number of cycles has to be tipped in.

Thus, the user interfaces just with the intuitive GUI and selects the parameters needed with no further operation needed. A personal computer will be connected through a common USB cable to an enclosure (**fig.2.21**) that contains the Arduino Mini with the stepper driver, power supply and a fan to avoid excessive heating for high duty cycles. The enclosure connected to the stepper motor, is placed outside the incubator, ensuring that the circuits are not in contact with its humidified ambient and thus preventing any damage. Finally, the enclosure has an ON/OFF button on the back, an UP and DOWN button to control manually the stepper actuator and a RESET button that resets the Arduino to zero (see **appendix11** for circuit schematic).

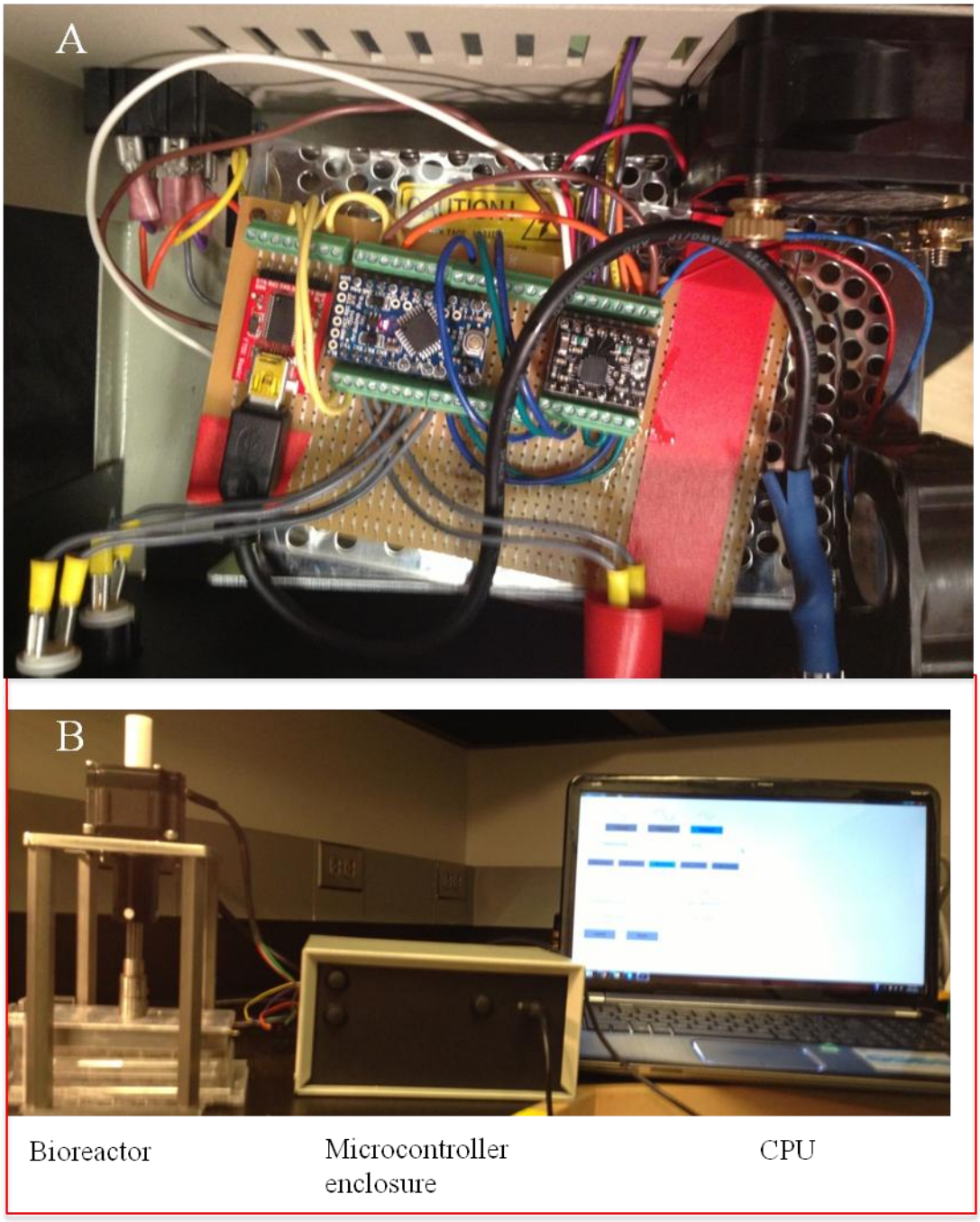

Figure 2.21. General overview of the Control module. Inside view of the enclosure where the Arduino, stepper driver, fan, power supply and additional circuitry are (A). The operator controls the bioreactor from a personal computer connected to an enclosure containing the controlling system.

2.5.4 Discussion, critical analysis and final prototype specifications

After an extensive review of the state of the Art regarding bioreactors, focusing in particular on a specific type of mechanical stimulus, it has been decided to design and develop a device that provides dynamic compression to twenty-four independent samples. The choice to employ a standard 24-wells plate has been taken since the device has been built with the aim to be easy-to-use and with most of the pieces commercially available. All the pieces in contact with any biological tissue are autoclavable and, therefore, ensure the sterility during the final assembly. The *fluid exchange layer*, not only allows the replacement of the culture medium, but it also consent the operator to administer growing factors or other chemical compounds to each well individually. Hence, it can be said that this device would be very suitable for drug screenings. Moreover, the GUI represents one of the numerous user friendly features that this bioreactor can provide. In fact, the operator interacts with the microcontroller just by typing a few basic parameters such as frequency, amplitude and resolution. Last but not least, it is possible to simulate significant biological processes by selecting three different wave forms: triangle, trapezoid and sinusoid.

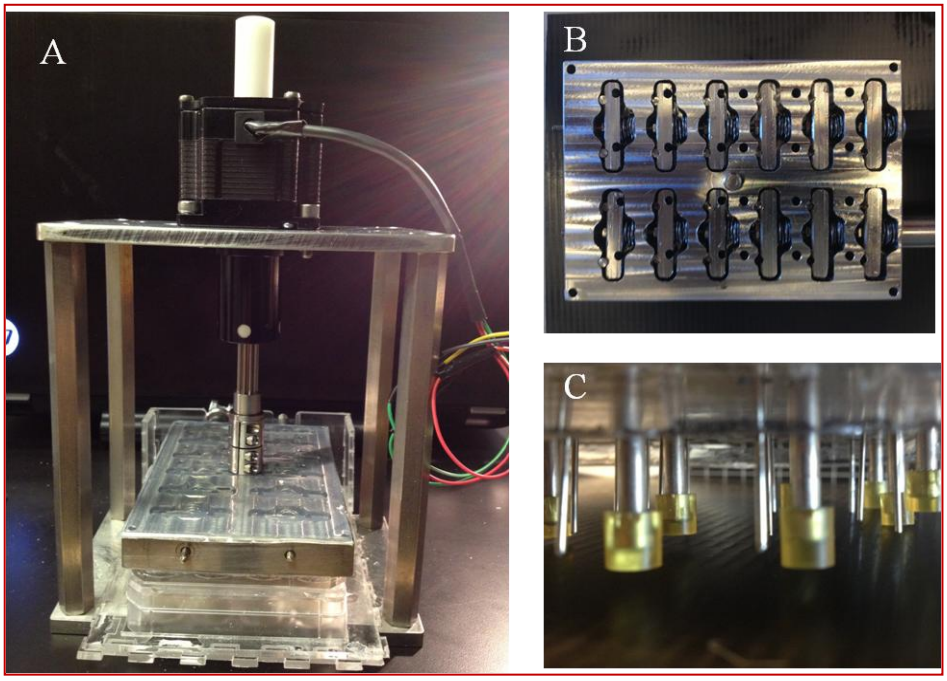

Figure 2.22. Final assembly of the bioreactor. (A) Assembled bioreactor. (B) Top view of the lid. (C) Zoomed view of the plungers and the SS tubes.

2.6 Compression Bioreactor: testing and characterization

In this section will explained how it has been decided to test and characterize the bioreactor to prove its reliability. First, by keeping constant the frequency value and measuring different magnitudes of displacement for the three different waveforms the accuracy of the motor has been measured. Secondly, a simulation on COMSOL® Multiphysics 4.2a of a basic experimental setup to evaluate the stress field within the culture chamber has been operated. Finally, the bioreactor has been tested biologically on a TE-EWS, trying to evaluate the effect of mechanical compression on Ewing's sarcoma (pilot study).

2.6.1 Technical validation

The efficacy of the device is determined by how accurately the load is transmitted to the constructs, which in turn requires accuracy of platen movement in response to the system controller. Validation was carried out to confirm the spatial and temporal accuracy of platen movement in the absence of actual cell-seeded specimen to determine whether or not it was maintained over the operating period of the system. These are necessary steps to ensure the reliability and reproducibility of the device.

Practically, the accuracy of platen displacement was assessed by comparing expected results with those obtained. To monitor the displacement of the lid an electronic dial indicator (Mitutoyo Electronic Indicators, resolution ±3μm) mounted on the bioreactor was used. Different magnitudes of displacement in millimeters were configured for the individual application of compressive loading for the three different waveforms (triangular, trapezoid and sinusoidal). Frequency was held constant first at 0.1 Hz and then at 1 Hz . The applied displacements were then plotted against the measured displacements to assess the correlation between these variables.

2.6.2 Finite element analysis of stress field resulting from mechanical stimulation of trabecular bone

To characterize and predict the behavior of the bioreactor a simulation in the software COMSOL® Multiphysics 4.2a has been implemented. In particular, it was important to identify what was the stress field generated by a dynamic compression in a physiological range on the TE-ES object of the experiment. It was critical to predict the magnitude of the stress to assess whether or not the materials and the motor would be suitable for this application.

First of all, a decision had to be taken on what would be the best stimulation value in terms of stress. After studying the bibliography and taking as reference the review written by Ozcivici *et al.* [94], the decision has been to simulate a 0.7 % strain with a sine wave form at 1 Hz.

Using such a low strain value, according to Keaveny *et al*., it could be assumed that the trabecular bone behaves as a linear elastic material [16] (**fig 2.23**).

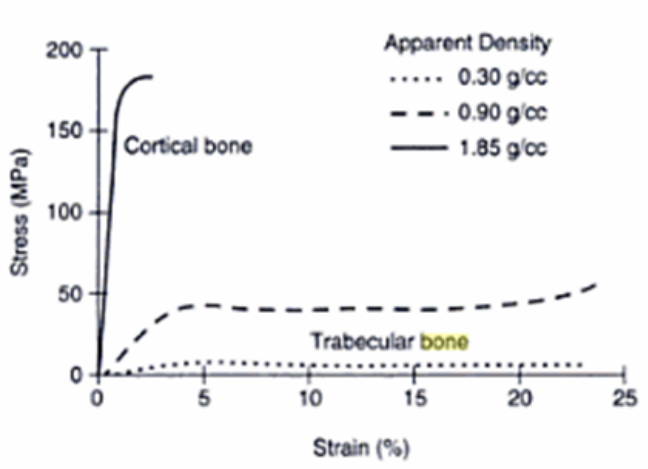

Figure 2.23. Linear elastic behavior of trabecular bone.

Finally, Young Modulus (50 MPa), density (434 kg/m^3) and Poisson ratio (0.3) were used according to the paper published by Marcos-Campos *et al.* [17].

In the software the 3D *Structural mechanics module* was chosen because it allows the user to study displacements, stresses, and strains in a 3D body given applied loads and constraints. A *Quasi-static analysis* that solves a time-dependent problem, assuming the

structural mechanics part being static was performed. At first, all the constant parameters (Young modulus, density and Poisson ratio) were inserted, then the exact geometry has been recreated as a 3D version of the culture chamber, including the plunger, the well insert and a 4x2 mm cylindrical scaffold. Finally, Von Mises's tensor has been solved to evaluate the stress field generated in culture chamber.

2.6.3 Pilot study

After the technical validation, where the reliability and the consistence of the system have been evaluated, it has been decided to use the compression bioreactor in a pilot study. In particular, as explained in the introduction, since nobody had previously studied the effects of dynamic compression on tumors behavior it seemed appropriate to use the compression bioreactor to mechanically stimulate the TE-ES. The main goal was to understand whether or not physical cues such as compression, kept in a physiological range, could influence tumor's behavior by enhancing or inhibiting its development and spreading.

2.6.3.1 Cell seeding, culture and stimulation protocol

The TE-ES was generated by using the established protocol described previously and the samples were stimulated using the compression of the bioreactor (**fig 2.23**). Briefly, hMSCs was seeded onto a decellularized bovine bone cylinder (4x2 mm) and cultured for four weeks in osteogenic medium, where they differentiate in osteoblast-like cells. Then, the Ewing's sarcoma spheroids, generated starting from the SK-N-MC cell line, were added to the TE-bone and they have been cultured statically for two weeks.

In parallel, the TE-bone that will serve as control in the stimulation experiment was cultured as well. After 6 weeks in culture, the TE-ES (n=3) were transferred in the compression bioreactor for stimulation. The compression protocol consisted in twenty-four hours of culture in the bioreactor with three loading inputs. The first application consisted of 0.7% of strain (for a 2 mm thick scaffold it equals 14 μm of displacement amplitude), applied using a sinusoidal wave form for the vertical motion at 1 Hz frequency for 1800

loading cycles (equivalent of 30 minutes of stimulation). In particular, the samples were stimulated right after the relocation into the bioreactor and after an overnight rest they were stimulated again, both in the morning and in the afternoon. The same stimulation protocol was applied to TE-bone constructs that served as control samples. Finally, the samples were harvested for analysis.

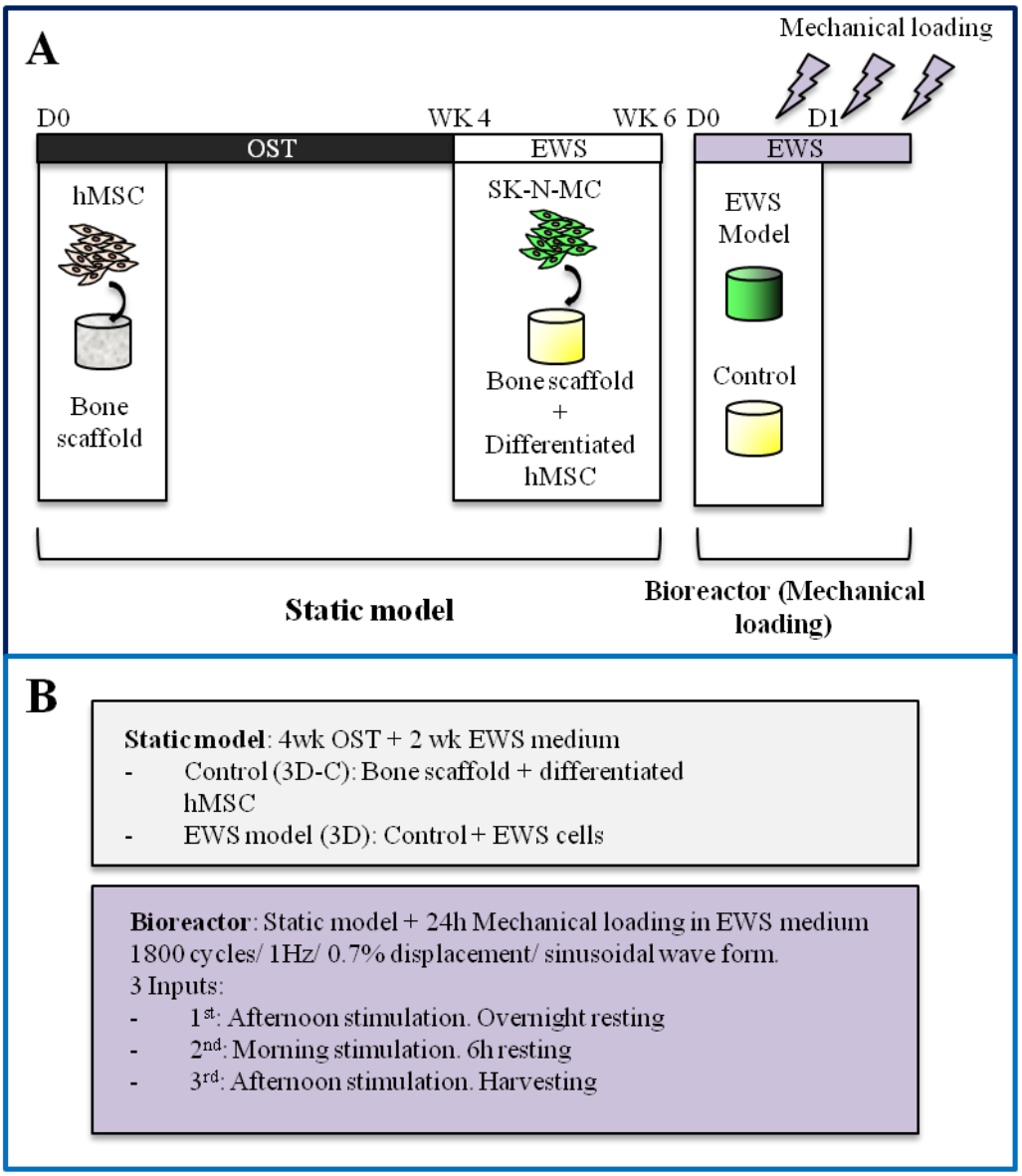

Figure 2.23. Model generation and stimulation protocol. (A) TE-ES and TE-bone were generated in a static culture with the application of 3 cycles of mechanical loading. (B) Schematic resume of the stimulation protocol.

2.6.3.2 Re-expression of focal adhesion genes in TE-ES

The initial stages of cell adhesion and focal-complex formation are associated with activation of RAC1 and CDC42, which stimulate lamellipodia and filopodia, respectively. These processes enable membrane protrusion and cell polarization in the direction of forward movement, whereas subsequent assembly of tension inducing actin stress fibers and mature focal adhesions are controlled by RHOA and activation of downstream effectors such as DIA1/2 or RHO-associated kinase (ROCK). Thus, tumor cells can move through a three-dimensional matrix either with a rounded morphology, characterized by RHO–ROCK dependence, or an elongated morphology, more related to CDC42 activation. It is also well known that Rho and Cdc42 are closely related small GTP-binding proteins that are implicated in mediating cellular responses to mechanical stimuli [95]. Taking together, these concepts led to the study of whether or not dynamic compression would lead to a re-expression of focal adhesion genes. Briefly, analysis of RHOA and CDC42 (by qRT-PCR, detailed protocol in **appendix A3**) in stimulated TE-ES SK-N-MC models compared to SK-N-MC cells cultured in 2D, ES tumor samples from patients (T) and TE-ES SK-N-MC non-stimulated models.

2.6.3.3 4 F-actin immuno-staining

Cells sense the stiffness of their environment by generating forces from within the cell that pull against the extracellular matrix. These contractile forces are largely based on actin–myosin interactions, because inhibition of actin or myosin activity abolishes the ability of epithelial cells to contract 3D matrices and to undergo tubulogenesis [96]. Moreover, focal adhesions (FAs) are sites of integrin clustering that form a physical link between the actin cytoskeleton and the ECM to transduce force between the cell and its microenvironment [97]. Therefore, it is evident that FAs and f-actin are linked together in the mechanism of mechanotransduction. For this reason, stimulated TE-ES SK-N-MC models are compared to the non-stimulated TE-ES SK-N-MC after f-actin immuno-staining (detailed protocol in **appendix A12**).

Chapter 3 – Results and Discussion

In the previous chapter have been outlined and validated all the components that comprise the TE-ES model. Moreover, the bioreactor has been disassembled and every piece has been thoroughly described. Hence, it has been explained how the device was tested and how a stimulation experiment was simulated using COMSOL® Multiphysics.
Finally, the two aims of this project were reunited in the pilot study, where the TE-ES have been stimulated with the compression bioreactor. Additionally, in this chapter have also been explained all the outcomes of the previously described experiments, giving an exhaustive and complete overview of the results.

3.1 Tissue engineered model of Ewing's sarcoma

After an accurate validation process, providing solid bases for the assembly of this model, in this section will be described how it was characterized.
In the first part, will be outlined the temporal work flow and protocol followed to build the TE-ES model. Hence, using CD99 staining and analyzing the gene expression of *GFP*, *EWS-FLI* and *NKX2.2* by qRT-PCR, the tumor viability was studied at weeks 2 and 4. Moreover, after a Micro-array analysis, a set of genes that were differentially expressed in real tumors compared to cell lines was detected. From this list a set of genes related to focal adhesion and tumorigenesis was selected and their expression was measured; it resulted that half of these genes were up-regulated compared to cell lines proving that the 3D environment together with a co-culture might foster the re-expression of important genes for tumor survival.
Furthermore, hypoxia is a common feature in fast growing tumors such as Ewing's sarcoma. Hypoxic conditions in the center core of the neoplasia, where necrotic areas are visible (studied with TUNEL staining), can often force tumors to adapt. This adaptation leads to a glycolytic phenotype that results in a consumption of glucose instead of oxygen. To assess if in this model the tumor feature is present, the gene expression of *HIF1-α* has

been studied along with the expression of GLUT1. Additionally, tumor cells react to hypoxic conditions and fast proliferation, expressing and secreting factors that are related to angiogenesis. To study this mechanism, was analyzed the expression of *VEGFA*, that is a gene playing a central role in the formation of new blood vessels. Lastly, an important feature of tumor cells – trying to adapt to a harsh environment – was highlighted. Vasculogenic mimicry is in fact an attempt of "struggling" cells to form new blood vessels by assuming a particular shape that mimics the vessel's lumen.

3.1.1 Generation

To form the tumor model, Ewing's sarcoma (ES) spheroids (providing a 3D context for local interactions of cancer cells) were introduced into a human bone niche generated by tissue-engineering technology (TE-bone) (**fig. 3.1**).

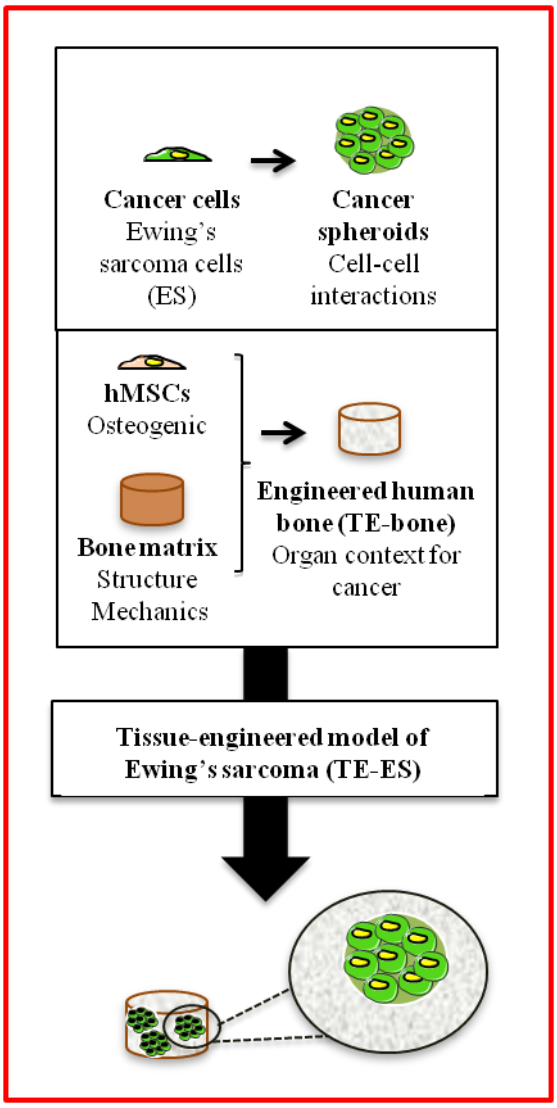

Figure 3.1. Methodology used to develop bioengineered models of Ewing's sarcoma tumor.

TE-bone plugs were cultured for 4 weeks in osteogenic differentiation medium as in previous studies [17]**.** Simultaneously, tumor spheroids were cultured in ES medium for one week. TE-bone plugs were bisected through the center, and 3 ES spheroids were introduced into one half of the construct, generating the Tissue engineered Ewing's sarcoma (TE-ES) model; the other half of each TE-bone plug served as control. TE-ES models and their control counterparts were cultured for an additional 2 or 4 weeks in ES medium (**fig. 3.2**).

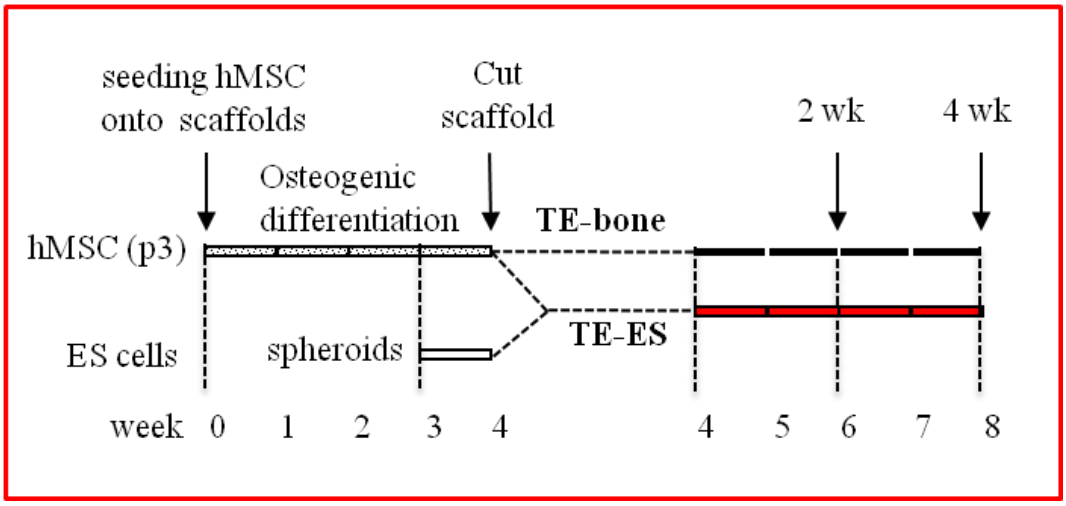

Figure 3.2. TE-ES generation: temporal work flow.

Three different TE-ES models were generated, using two existing ES cell lines (TE-RD-ES and TE-SK-N-MC) and a new developed line (TE-EW-GFP). In **figure 3.3** can be seen Hematoxylin and Eosin images of TE-bone controls and TE-ES models (TE-RD-ES, TE-SK-N-MC, TE-EW-GFP) at week 2 and 4, after introducing tumor spheroids. In these pictures is evident how ES cells assume their characteristic small rounded shape, commonly seen in patients affected by Ewing's sarcoma.

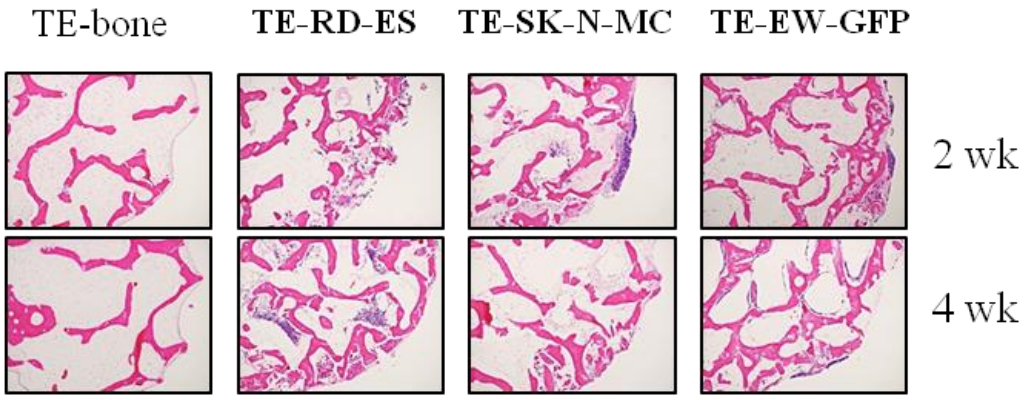

Figure 3.3. Qualitative representation of the TE-ES compared to TE-Bone.

3.1.2 Re-expression of focal adhesion and cancer-related genes

In order to validate the TE-ES model, histological sections were analyzed by hematoxylin-eosin staining, allowing the detection of large areas with small-round cells that were CD99 positive and surrounded by bone cells and ECM (**Fig. 3.4**). Hence, the tumor cells are in contact with both the osteoblast-like cells and the bone ECM. In TE-bone was noticeable the characteristic spatial disposition of osteogenic differentiate hMSCs.

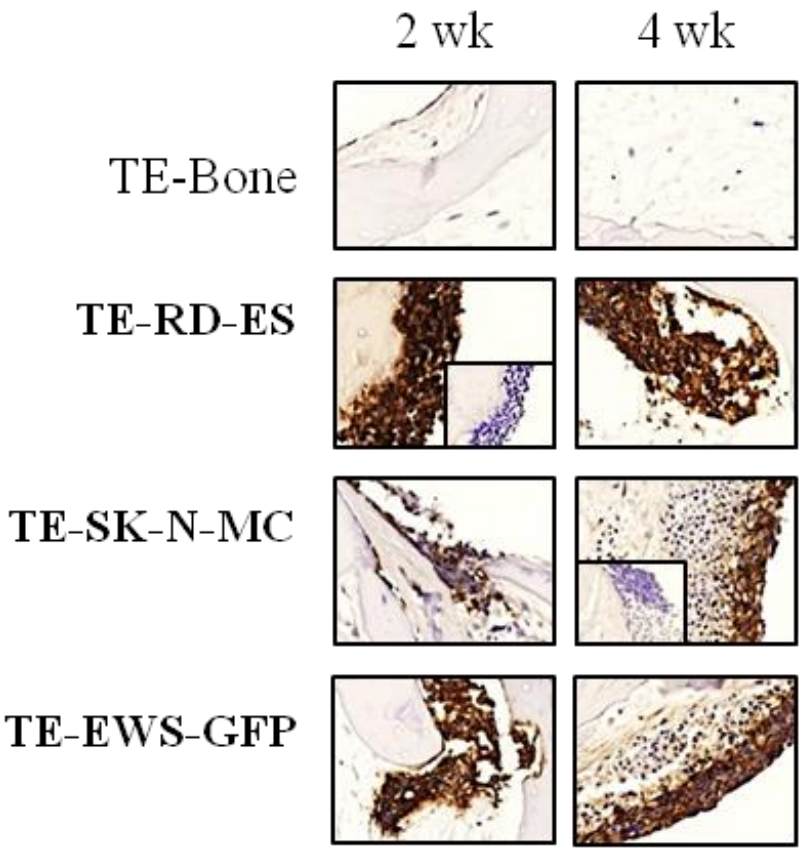

Figure 3.4. Immunohistochemical staining of TE-bone and TE-ES models for Ewing's sarcoma marker CD99 at weeks 2 and 4. Insets represent negative controls without primary antibody. Representative images are shown (n=3 per condition). Counterstaining was performed with Hematoxylin QS (blue)

GFP levels in TE-ES models and their cell line counterparts cultured in monolayers (by qRT-PCR) confirmed expression in both cultures (**fig. 3.5**), demonstrating ES tissue formation and the presence of ES cells in the bone context. *EWS-FLI* mRNA and the well-

known EWS-FLI target *NKX2.2* were expressed at low levels in ES cell monolayers as compared to native ES tumors from patients (**fig. 3.5**). Notably, both genes were up-regulated in all three TE-ES models, for all three cell lines studied, suggesting a clear effect of the microenvironment in regulating ES gene profile (**fig. 3.5**).

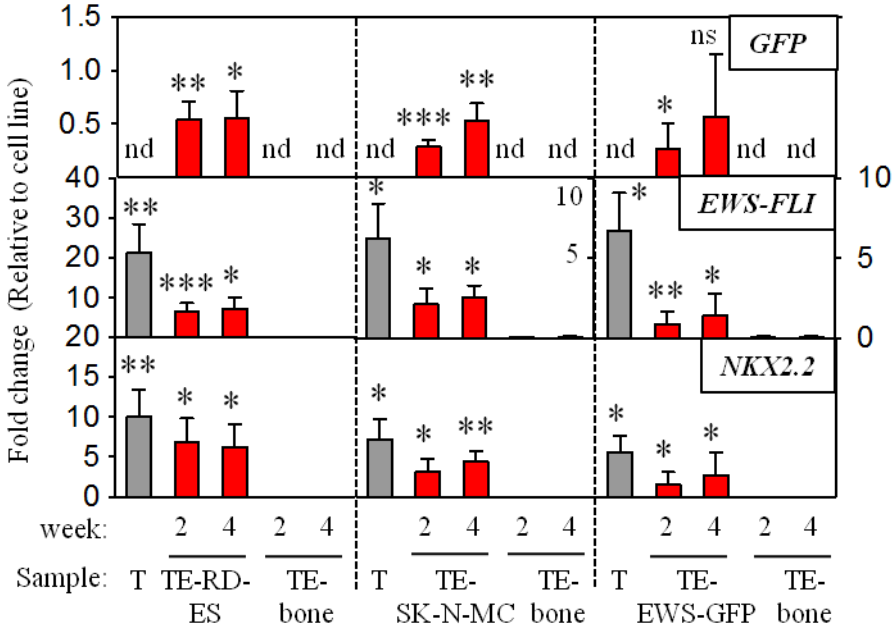

Figure 3.5. qRT-PCR analysis of GFP, EWS-FLI and NKX2.2. Fold change was calculated by first normalizing to actin levels in the individual samples and then to the corresponding levels in cells cultured in 2D. Data are shown as Average ± SD n=3-5). Two-tailed Student´s t-test was used to determine statistical significance. *p < 0.05; **p < 0.01, ***p < 0.001; nd, not determined; ns, not significant; T, Ewing's sarcoma tumors.

A number of studies have shown significant differences in gene expression between tumors from patients and cells cultured in monolayers, due to the flat, unnatural plastic environment [2]**.** The presence or absence of expression of genes in 44 tumors from patients and 11 cell lines, were analyzed by applying the barcode method to the Affymetrix Human Genome U1332 Plus 2 gene expression data of Savola *et al.* [92]: 599 genes were identified expressed in tumors, but not in cell lines (**Table 3.1**). Comparing mRNA expression between the two cell lines (RD-ES and SK-N-MC) and 3 ES tumors by qRT-PCR, the up-regulation of 24 genes in ES tumors was observed.

Condition	Number of genes
Genes expressed in cell-lines	2977
Genes expressed in tumors	2430
Genes expressed in cell-lines but not tumors	1312
Genes expressed in tumors not cell-lines	599

Table 3.1. Number of genes expressed in ESFT and in cell lines

Importantly, all these genes were related to focal adhesion and pathways in cancer (Table 3.2).

Focal adhesion:	ACTN4,CCND2,COL1A2,COL3A1,COL6A1,COL6A2, COL6A3,FLNB,MYLK,PDPK1,PPP1R12A,IGF1,VCL
Pathways in cancer:	CDKN1B,CTBP1,CTBP2,ETS1,KRAS,PIAS1,RXRA, STAT3,TP53
Both:	CDC42,COL4A1,COL4A2,CTNNB1,FN1,JUN,LAMA4, LAMB1,LAMBC1,PIK3R1,PTEN

Table 3.2. Focal adhesion genes and genes related to pathways in cancer. Genes expressed in ESFT but not in cell lines.

By analyzing these 24 genes in the TE-RD-ES and TE-SK-N-MC models relatively to their monolayer counterparts, strong re-expression (fold change >3) for 12 genes was confirmed (**fig. 3.6**). In the graph it can be seen the expression of the TE-ES compared to the TE-bone, all normalized to the ubiquitous actin expression and then to the expression in cells culture.

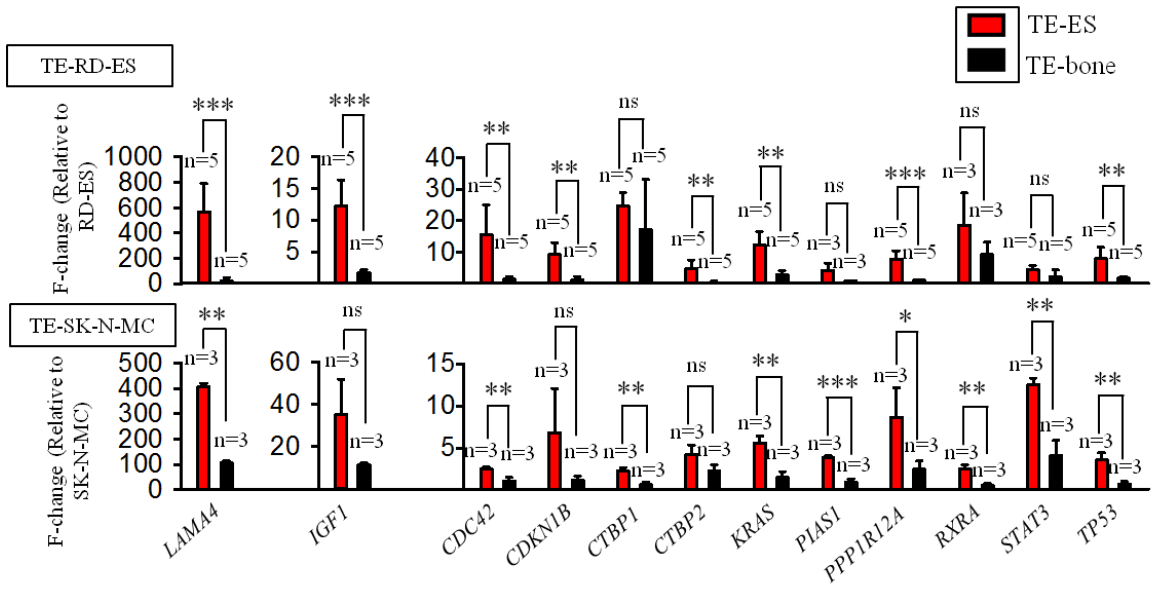

Figure 3.6. qRTPCR analysis of the ES genes expressed in tumors and not in cell lines cultured in 2D. Fold change was calculated by first normalizing to actin levels in the individual samples and then to the corresponding levels in cells cultured in 2D. Data are shown as Average ± SD (n=3-5). Two-tailed Student´s t-test was used to determine statistical significance. *p < 0.05; **p < 0.01, ***p < 0.001; nd, not determined; ns, not significant; T, Ewing's sarcoma tumors.

Noteworthy, IGF1 was one of the targets found and validated (12.2 ± 4.11 fold change in TE-RD-ES relative to RD-ES cell monolayers; 35.08 ± 16.84 fold change in TE-SKN- MC relative to SK-N-MC monolayers). IGF signal transduction pathway is thought to play a key role in ESFT development and proliferation [98] and a number of preclinical and clinical trials inhibiting IGF-1R have been undertaken [99]**.** The results support the importance of tumor microenvironment for gene expression and suggest that TE-ES models recapitulate, at least in part, ES gene expression signatures.

3.1.3 Recapitulating hypoxic and glycolytic phenotypes

At early stages of cancer, tumors are avascular masses where oxygen and nutrients delivery are supplied by diffusion and, therefore, growing in central areas is compromised [100]. To

maintain energy production, tumor cells respond and adapt to the hypoxic environment by increasing the amount of glycolytic enzymes and glucose transporters, such as GLUT1 and GLUT3, via the hypoxia-inducible factor-1 (HIF1α) [100]. These processes were exhaustively studied, using tumor spheroids and tumor micro-regions *in vivo*, observing an outer viable tumor (with proliferating cells), an inner hypoxic area (with quiescent adapted viable cells) and a central necrotic core where oxygen and glucose levels are critically low [101] [102]. The tumor model provides a native-like niche that mimics tumor heterogeneity in terms of oxygen and nutrients supply, as demonstrated by hypoxia in the center of the tissue constructs, but not in the outer areas (previously showed in **Chapter 2 fig. 2.4**). In order to evaluate whether TE-ES models recapitulate the initial steps of tumor generation, necrotic areas in the core of the tumor models have been analyzed and the levels of HIF1α and GLUT1 to those in cell monolayers and TE-bone controls have been then compared. First, the focus has been the construct interiors where were found necrotic areas similar to those observed in native tumors (**fig. 3.7**).

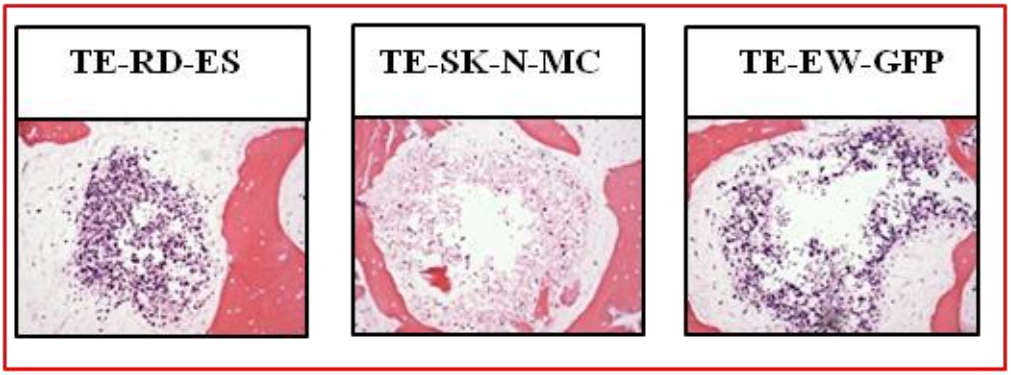

Figure 3.7. Necrotic areas in the inner part of TE-ES models. Hematoxylin and Eosin staining of TE-RDES, TE-SK-N-MC and TE-EW- GFP at week 2. Representative images are shown (n=3 per condition)**.**

TUNEL assays after 4 weeks of cultivation revealed higher cell death in the middle of the TE- SK-N-MC tumor model (73 ± 36%) relatively to TE-RD-ES (29± 3%) and/or TE-EW-GFP(16± 2%) (**fig. 3.8**).

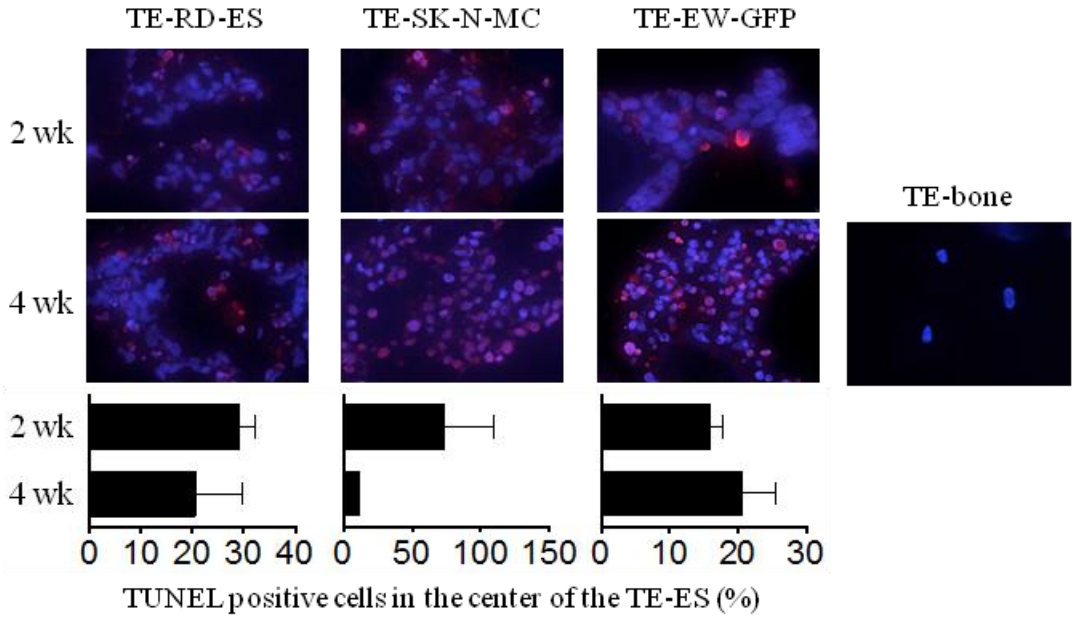

Figure 3.8. TUNEL immunofluorescent staining of TE-ES and TE-bone in the center of the models. Upper panel: representative pictures of TUNEL-stained inner areas. Apoptotic cells stain red; cell nuclei were stained by Hoechst 33342. Lower panel: Quantification of TUNEL-positive cells in the inner part of the indicated TE-ES models.

These results suggest that RD-ES and EW-GFP cell lines may be better adapted than SK-N-MC cell line to restrictive conditions at the centers of the constructs. In response to hypoxia (at week 2), transcription levels of HIF1α were 40 times higher in the TE-RD-ES tumor model relatively to the RD-ES cell monolayers, and 30 times higher relatively to TE-bone. Interestingly, HIF1α expression decreased with time in culture, reaching at week 4 levels similar to those in TE-bone (**fig. 3.9**).

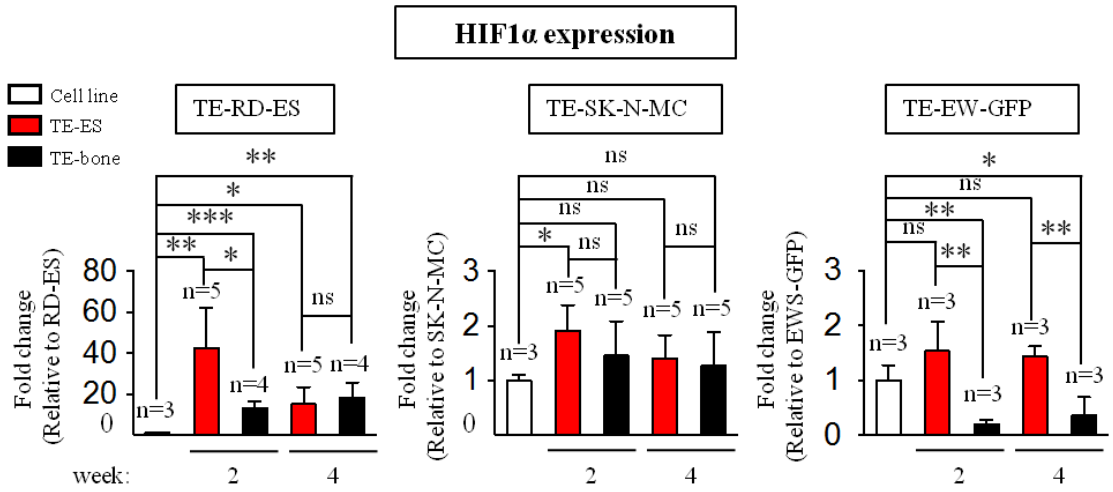

Figure 3.9. HIF1α mRNA levels in TE-ES models. Fold change was calculated by first normalizing to actin levels in the individual samples and then to the corresponding levels in cells cultured in 2D. Data are shown as Average ± SD (n=3-5). Statistical significance was determined by the two- tailed Student's t test. *p < 0.05; **p < 0.01, ***p < 0.001; ns, not significant.

Surprisingly, it was found that transcriptional expression of HIF1α was not significantly increased by hypoxia in TE-SK-N-MC and TE-EW-GFP models as compared to cell lines (**fig. 3.9**). Also, the SK-N-MC and EW-GFP cell lines expressed higher levels of HIF1α than the RD-ES line, and the expression levels in the SK-N-MC cells were comparable to those in TE-bone. These data suggest that tumor cells, that have low transcriptional levels of HIF1α (RD-ES line), increase expression in order to adapt to hypoxic environment. In contrast, cell lines expressing high levels of HIF1a (SK-N-MC and EW-GFP) seem to be insensitive to hypoxia, at least at the transcriptional levels. HIF1α thus appear to play a protective role in the adaptation of tumor cells to hypoxia.

To assess the role of hypoxia in the induction of glycolytic response, were examined the levels of GLUT1 protein in TE-bone and TE-ES models. As expected, very high levels of GLUT1 were observed, favoring glucose uptake and tumor survival in inner areas where oxygen and medium supply are compromised (**fig. 3.10**).

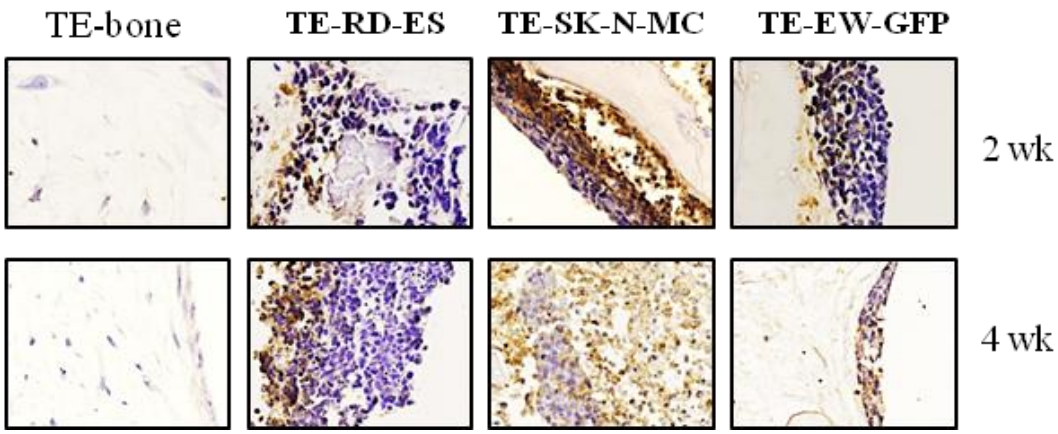

Figure 3.10. Immunohistochemical staining of GLUT-1 in TE models over time. Counterstain: Hematoxylin QS (blue). Representative images are shown (n=3 per condition).

Noteworthy, GLUT1 was expressed in necrotic areas in the TE-SK-N-MC model.

Taken together, these data demonstrate that the RD-ES cells expressing high levels of HIF1α adapt to hypoxia in the TE bone environment by recapitulating some aspects of hypoxic and glycolytic tumor phenotype, and mimicking inner-necrotic and outer-survival signatures. In comparison, the SK-N-MC and EW-GFP cells expressing low levels of HIF1α showed less ability to adapt to hypoxic microenvironment.

3.1.4 Recapitulation of angiogenic ability and vasculogenesis mimicry

Tumor cells respond to oxygen and nutrient deprivation by promoting vascularization that maintains tumor growth and survival [18]**.** Induction of vascular endothelial growth factor (VEGFA) is an essential feature of tumor angiogenesis that is driven by hypoxia and mediated by HIF1α [103]**.** To address whether hypoxia modulates angiogenic ability of the tumor, VEGFA transcriptional levels in TE-ES models were analyzed. High induction of VEGFA in TE-RD-ES was found at week 2 compared to the RD-ES cell line and TE-bone (**fig. 3.11**).

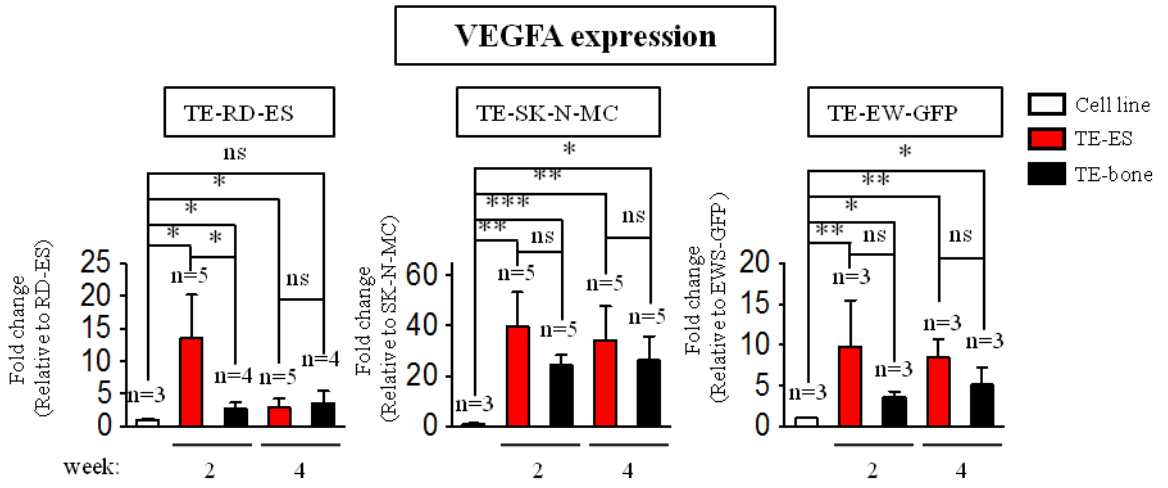

Figure 3.11. VEGFA mRNA levels in TE-ES models. Fold change was calculated by first normalizing to actin levels in the individual samples and then to the corresponding levels in cells cultured in 2D. Data are shown as Average ± SD (n=3-5). Two-tailed Student´s t-test was used to determine statistical significance. *p < 0.05; **p < 0.01, ***p < 0.001; ns, not significant.

Notably, levels decreased by week 4, as observed for HIF1- α. In further support of the adaptive advantage of RD-ES cells cultured in TE-bone, VEGFA mRNA levels were not significant increased in TE-SK-N-MC and TE-EW-GFP tumor models as compared to TE-bone controls (**fig. 3.12**). Then, it has been attempted to identify angiogenic proteins secreted by TE-ES tumors. By ELISA analysis of 24-hr supernatants, 56 human angiogenesis-related proteins were analyzed at week 2. Due to the differences in growth of different cell lines, it was not possible to directly compare secretion rates. However, these analyses clearly demonstrated that 8 proteins (Angiopoietin, CXCL16, Endothelin-1, FGF-7, IGFBP1-1, PIGF, TGF- β1 and TIMP4) were highly expressed in TE-RD-ES and TE-EW-GFP tumor models compared to TE-bone (fold change >3). In contrast, none of these proteins was detected in the TE-SK-N-MC tumor model. These results confirm that the SK-N-MC cells failed to induce essential adaptive elements to survive and proliferate in TE-bone (**fig. 3.12**).

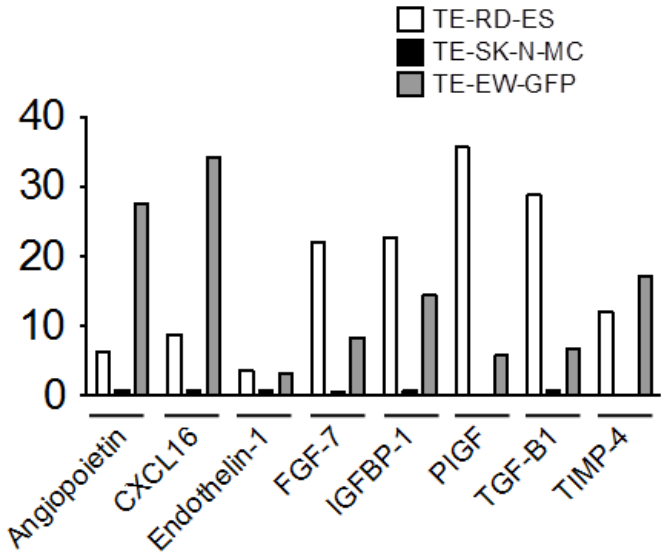

Figure 3.12. Angiogenesis-related proteins detection in TE-ES culture media. Expression levels of the indicated proteins were assessed by ELISA and compared with expression levels in the TE-bone counterparts.

Interestingly, Endothelin-1 is implicated in ES proliferation and invasion, while IGFBP1-1 prolongs the half-life of IGF-1, a well-known target gene of EWS-FLI and TGF-β1. These observations are consistent with previous studies, validating the system object of this work.

Finally, an evaluation of vasculogenic mimicry (VM) in TE-ES models was made. Native ES is featured by the presence of blood lakes and PAS positive cells expressing endothelium-associated genes [19]. This property is known as VM and is stimulated by hypoxia [104]**.** Thus, VM can provide functional perfusion channels composed only of tumor cells. The endothelium associated genes (LAMC2, TFPI1 and EPHA2) were highly expressed in the TE-RDES at weeks 2 and 4 (**fig. 3.13**), confirming VM in the TE-RD-ES model.

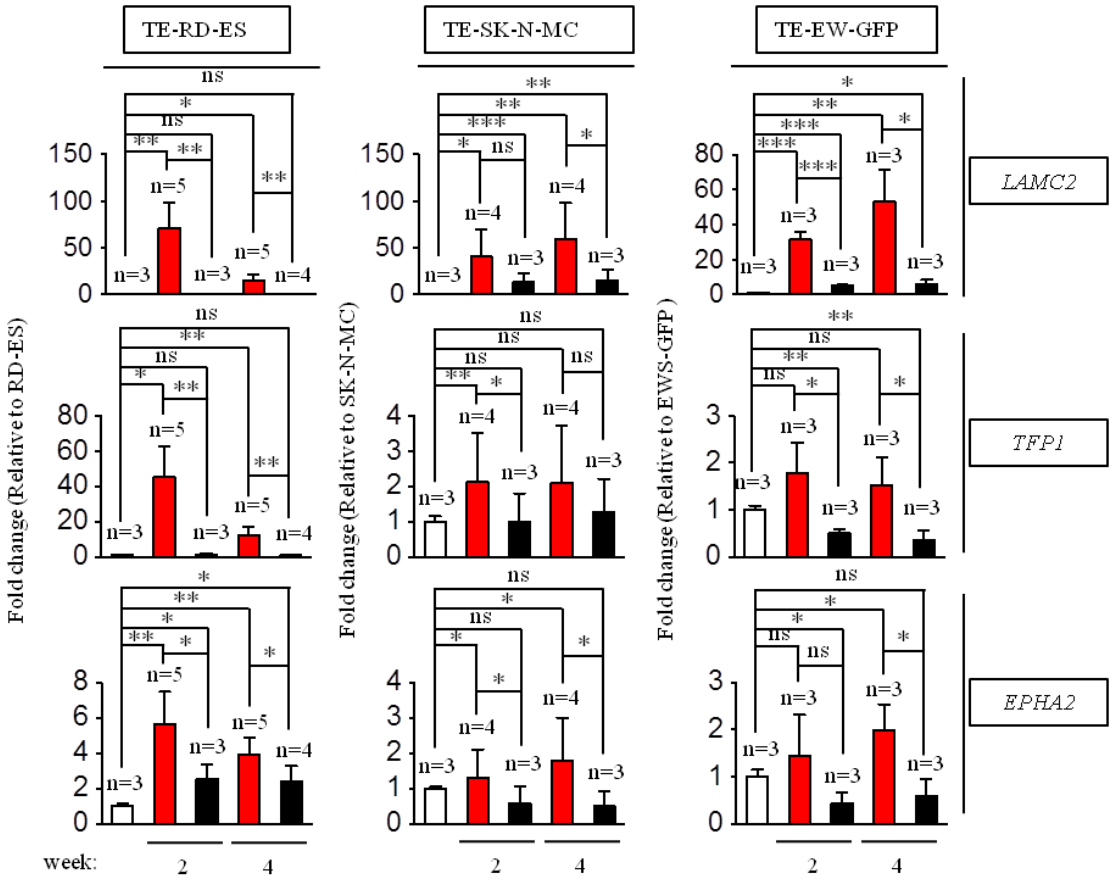

Figure 3.13. qRT-PCR analysis of vasculogenic mimicry markers. Relative endogenous expression of each gene was normalized to actin and the fold change was obtained normalizing to the levels in corresponding cell lines cultured in 2D. Data are shown as Average ± SD (n=3-5). Statistical significance was determined by the two- tailed Student's t test. *p < 0.05; **p < 0.01, ***p < 0.001; ns, not significant.

Consistent with all other data, cells in the SK-N-MC model re-expressed VM genes as levels lower than those measured for the TE-RD-ES model. However, these expression levels were significantly up-regulated at week 2 for TFP1 ($p<0.01$) and EPHA2 ($p< 0.05$) and at week 4 for LAMC2 ($p<0.01$) and EPHA2 ($p< 0.05$) as compared to SK-N-MC and TE-bone (**fig. 3.12**). Moreover, the TE-EW-GFP model expressed high levels of LAMC2, TFPI1 and EPHA2 at week 2 and 4 as compared to TE-bone (**fig. 3.12**).

Tissue sections stained with PAS revealed positive areas in all the TE-ES models (except in TE-EW-GFP at week 2), as compared to negative-PAS TE-bone (**fig. 3.14**). Taken together, these results confirm that RD-ES cell line has higher capability to adapt to TE-bone than the SK-N-MC line.

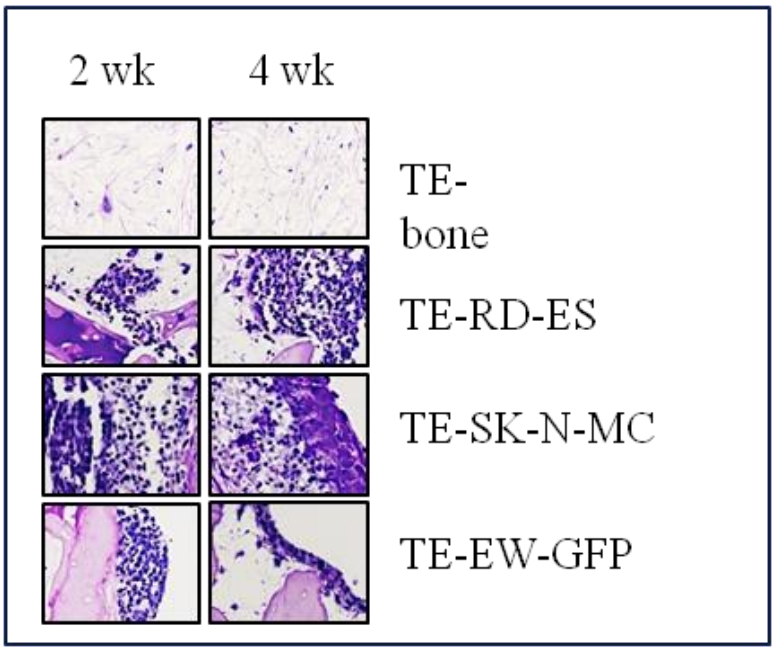

Figure 3.14. Representative images of PAS-stained sections from TE-bone and TE-ES models at week 2 and 4. Representative images are shown. n=3 per condition.

3.2 Bioreactor: final assembly and validation

In **Chapter 2** all the pieces that form the compression bioreactor were illustrated and described individually. In this Chapter, a complete overview of the system – focusing in particular on its features – will be given. Additionally, the results of the COMSOL® simulation that provided a good anticipation of what were the stresses that arose in the TE-ES during compression will be hereby discussed. To conclude, the data set resulting from the technical validation will be shown and analyzed.

3.2.1 Compression Bioreactor: overview and features

The design of a new compression system starts from an accurate study of the advantages and drawbacks of the existing devices. Afterwards by the mean of a 3D CAD (computer-aided design) software, the first virtual prototype is made. This represents an important step because it highlights the assembly and the functional process, hence allowing the optimization of the design. Most of the pieces are commercially available, consistently reducing the production costs. The remaining the pieces are shaped using different fabrication techniques, such as CNC milling processes. After assembling the bioreactor, it is possible to distinguish four main modules:

- **The Culture module**: that comprehends the pieces that are in direct contact with the cells and the scaffold.
- **The Compression module**: that includes the linear actuator coupled with the stepper motor, and the hardware needed for the connection to the *Culture module*.
- **The Control module**: that incorporates the Arduino microcontroller, which communicates with the Stepper driver, and the additional circuitry (e.g. power supply, fan).
- **The General User Interface (GUI):** that is meant to be an intuitive and user-friendly interface, where the operator can type in the different parameters of the compression cycle.

In **figure 3.15** all the modules just cited can be found. Briefly, the system is designed around a standard 24-well plate that not only is disposable, but that also allows the user to culture a statistically significant number of independent samples. Moreover, a *Lid* (**fig.3.15 A**), that could perfectly seal the culture plate, was designed using a modified 24-well plate cover. Attached to the cover and interfacing the *Lid,* it can be found a Super-Soft Silicone rubber that works as a grommet, bearing the loading resulting from the vertical motion.

One of the biggest drawbacks of existing devices is primarily the plunger positioning, being either inexact or requiring complex operations to be adjusted. The mechanism proposed in this device uses a combination of Cam-Lever and springs that ensures the quick and precise positioning of the plungers. In fact, when the Cam-Levers are pulled up, engaging the springs, they release the plungers from the clamping force, leaving them free

to fall upon the scaffold. On the other hand, when the Lever-Cams are loosened, the springs apply a great load on the *moving part* – that clamps then tightly the plungers.

The *Lid* is a custom-made piece that has specific holes matching the SS tubes coming out of the *fluids-exchange layer*. This piece, fabricated by PDMS casting, allows the renewal of the culture medium and, as each channel is autonomous, also the contingent addition of growing factors or drugs. Finally, a disc with a central off-set is placed at the bottom of each culture well, as also called *well insert,* which allows the exact positioning of the scaffold at the center of the well. A shaft coupling connects the linear actuator's rod to a thumb screw in the middle of the *Lid.* Hence, by the mean of two set screws on the shaft coupling, it is possible to fasten tightly the *Lid* to the motor.

The Compression module (**fig. 3.15 B**) comprises a linear actuator (rotary motion of a threaded screw transformed into linear motion) coupled with a stepper motor. This mechanism allows some very fine motions of the *Lid,* having a stepping resolution in the order of microns. The micro-stepping is achievable thanks to the serial communication between an Arduino Mini and a Stepper driver (**fig. 3.15 C**). These two components are controlled by an operator that commands the motion by interfacing with a user-friendly and intuitive GUI. First, the program asks to choose between one of the three different wave forms (trapezoid, triangular and sinusoidal), then the user has to type in the displacement's resolution, the amplitude and the frequency needed. After setting also the number of cycles, selecting the upload button makes the system start (**fig. 3.15 D**).

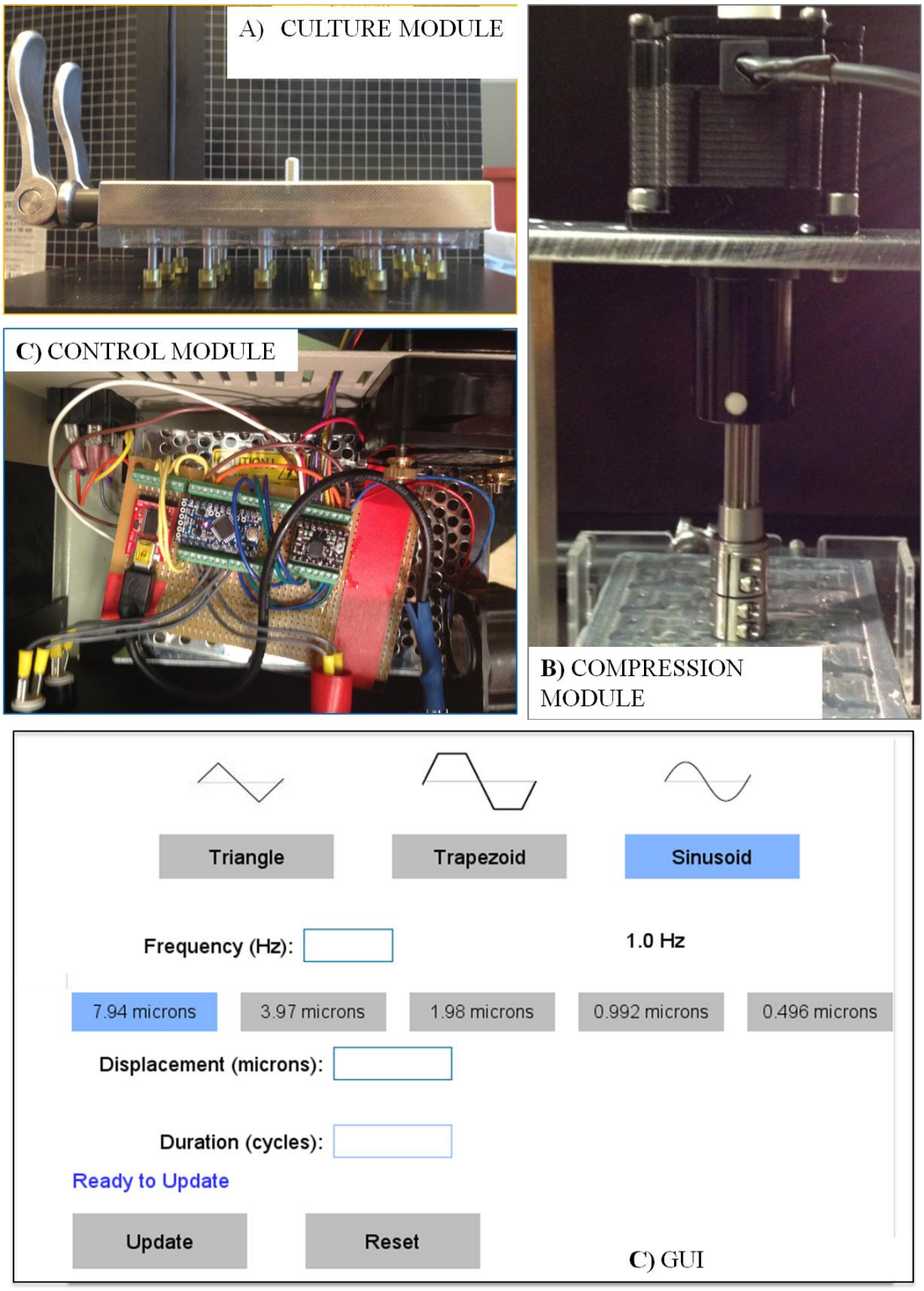

Figure 3.15. Overview of the main modules of the Bioreactor. (A) Culture module. (B) Compression module. (C) Control module. (D) GUI.

The Bioreactor's features previously described are resumed in Table 3.3.

Device:	Bioreactor
Function:	Compression loading to tissue engineered constructs
Type of motion	Linear
Maximum thrust [Kg]	90
Power supply [V]	12
Motion wave forms:	Trapezoid Triangle Sinusoid
Resolution [µm]	7.94 3.97 1.98 0.992 0.496
Displacement range [mm]	Min: 0.007 Max: 38.1
Frequency Range [Hz]	Min: 0.001 Max: 4
Main features	Quick and precise plunger positioning Fluid exchange system Completlely autoclavable Reduced number of assembly operations Accurate vertical motion Easy connection to the Culture module

Table 3.3. Data Sheet: Bioreactor main features

3.2.2 Technical validation

In order to employ the bioreactor for the pilot study, a technical validation was performed to assess the reliability of the device. It consisted in an evaluation of the accuracy of the *Lid's* displacement (measured value) compared to the value given as input by the operator (reference value). The frequency was fixed at 0.1 Hz and 8 different displacement values were measured (**fig.3.16)**.

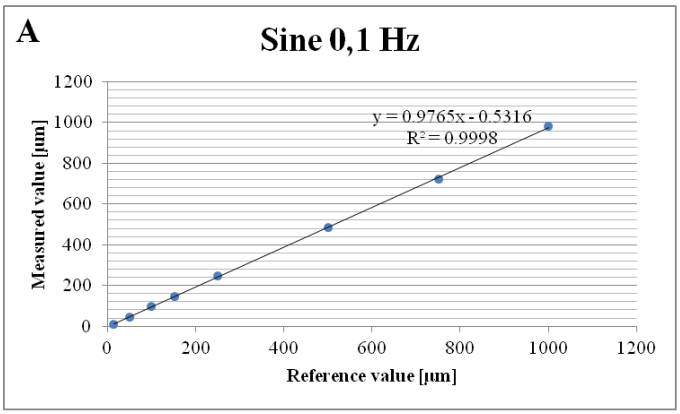

Reference value (µm)	Measured value (µm)	Accuracy
13.89	12.06896552	86.9%
49.6	47.96551724	96.7%
99.21875	96.93103448	97.7%
150.8125	148.4827586	98.5%
250.03125	246.7241379	98.7%
500.0625	485.1666667	97.0%
750.093	723.5714286	96.5%
1000.125	982.6666667	98.3%

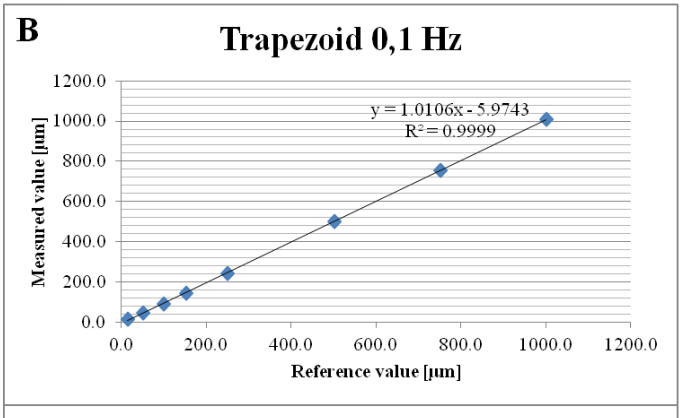

Reference value (µm)	Measured value (µm)	Accuracy
13.9	15.7	98.7%
49.6	44.9	90.5%
99.2	92.1	92.8%
150.8	143.1	94.9%
250.0	243.0	97.2%
500.1	497.8	99.6%
750.1	753.0	99.6%
1000.1	1006.4	99.4%

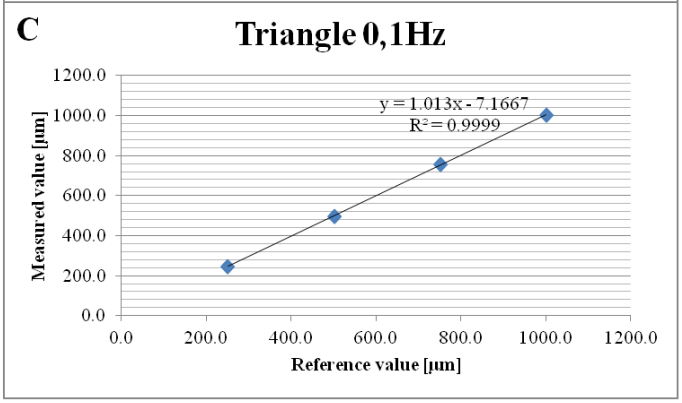

Reference value (µm)	Measured value (µm)	Accuracy
250.0	246.0	98.39%
500.1	497.9	99.56%
750.1	756.1	99.20%
1000.1	1004.2	99.59%

Figure 3.16. Displacement accuracy at 0.1 Hz frequency. (A) Sine waveform. (B) Trapezoid waveform. (C) Triangular waveform. For all the waveforms accuracy and determination coefficient were measured (n=5).

For all waveforms, the measured accuracy was always higher than 90%, but at the smallest displacement value of the sinusoidal motion it was equal to 86.9%. The coefficient of determination (R^2) was equal to 0.9999 for the triangular and trapezoidal motions and equal to 0.9998 for the sine waveform, confirming a high correlation between the outcomes and their predicted values.

The same experiment was performed at 1 Hz for the sine waveform, as shown in **figure 3.17**.

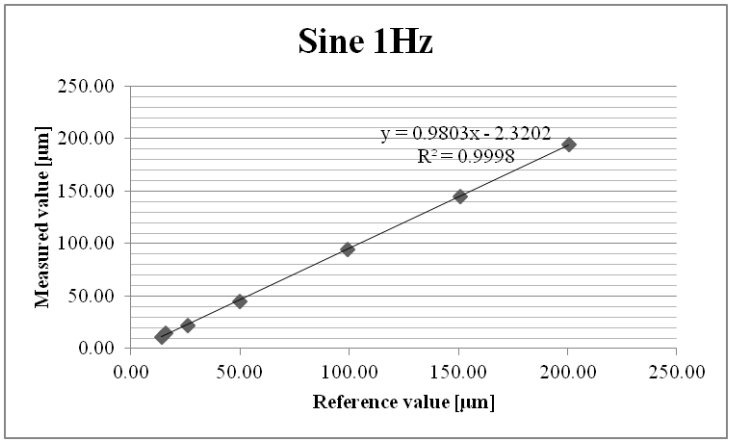

Reference value (µm)	Measured value (µm)	Accuracy
13.85	11.40	82%
15.88	14.93	94%
25.79	22.27	86%
49.60	45.13	91%
99.21	94.73	95%
150.81	145.10	96%
200.42	194.80	97%

Figure 3.17. Displacement accuracy at 1 Hz frequency. Sine waveform. Accuracy and determination coefficient were measured (n=5).

At 1 Hz the accuracy values are lower than in the 0.1 Hz experiment, but most of them are still higher than 90%. Moreover, the coefficient of determination is equal to 0.9998 indicating a high correlation between the reference and the measured values.

Taking together these data, it is then possible to suggest that the device, under the parameters described before, is accurate and that the outcome correlate with the expected values. Further testing and validation seems necessary to completely validate the system. In fact, it might be necessary to assess the temporal accuracy by fixing a displacement value and by measuring it at several frequencies. Lastly, it would also be very important to determine the consistency of the bioreactor during long periods of duty.

3.2.3 Finite element analysis of the stress field resulting from mechanical stimulation of trabecular bone

Using COMSOL® Multiphysics, a finite element analysis of the stress field arising in the bone scaffold as a response to dynamic compression was performed. In particular, as shown in **figure 3.18. A and B**, the trabecular bone was assumed linear elastic, with a Poisson ratio of 0.3 and a Young Modulus of 50 MPa [17]. The culture well, plunger, well insert and scaffold 3D geometry were recreated using the software's drawing tools. Furthermore, the plunger was forced to move in a sinusoidal motion, with a displacement amplitude of 14 μm (0.7% strain on a 2 mm thick scaffold), at 1 Hz frequency (**fig 3.18 C**). The chosen values have been considered to be in the physiological range according to Ozcivici *et al.* [94]. Therefore, because the plunger is in direct contact with the scaffold, its motion results in compression loading.

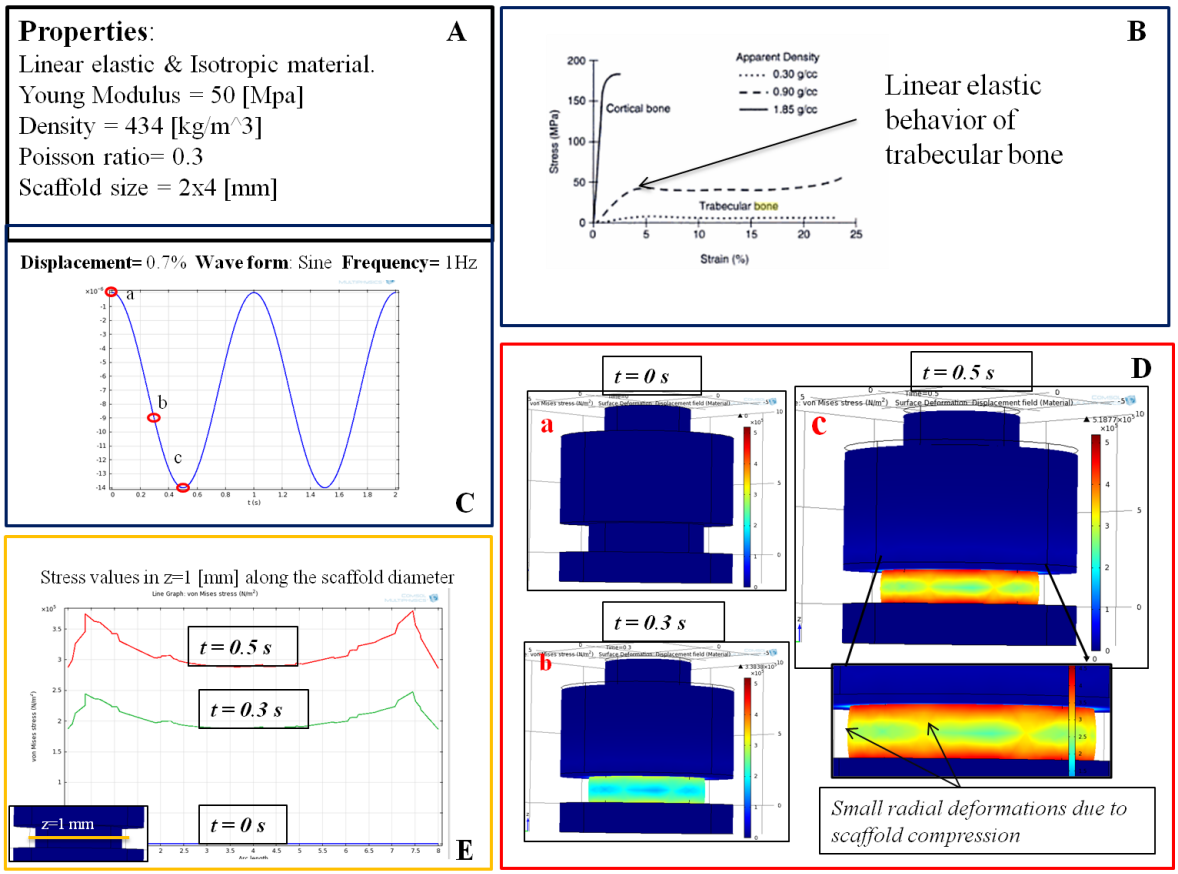

Figure 3.18. Finite element analysis of stress field resulting from dynamic compressive stimulation of tissue engineered bone.

In **figure 3.18 D** three snapshots at 0.0, 0.3 and 0.5 seconds are shown. Above all, it is possible to appreciate how the stresses through the entire scaffold increase according to the plunger's position. Solving Von Mises' tensor, the stress field generated in the construct was calculated and the stresses were in the range of $2.5x10^5$ - $5.0x10^5$ [Pa], depending on the position within the plug. It is most likely that the cells within the scaffold sense these physical stimuli, and that they integrate these signals activating the mechanotransduction process. It is hence interesting to evaluate whether or not tumor cells react to these stimuli, for example by expressing focal adhesion genes and by forming f-actin stress fibers.

3.3 Pilot Study

At last, in this section the two first aims of the project come together in the pilot study. As a matter of fact, it has been implied earlier in this thesis that mechanical stimuli sensed by cells, more specifically by tumor cells, can influence tumor's faith. In this pilot study it has – for the first time – been proposed to apply dynamic compression within physiological ranges (0.7% strain, 1 Hz frequency and sinusoidal waveform) to the TE-SK-N-MC by using the validated Bioreactor (**fig. 3.19**). The protocol used is reported in **figure 3.18 A.** Briefly after the model generation, the constructs were stimulated during 24 hours, three times, where every stimulation session lasted 30 minutes (1800 cycles). In the experiment the TE-SK-N-MC were compared to TE-Bone (n=3).

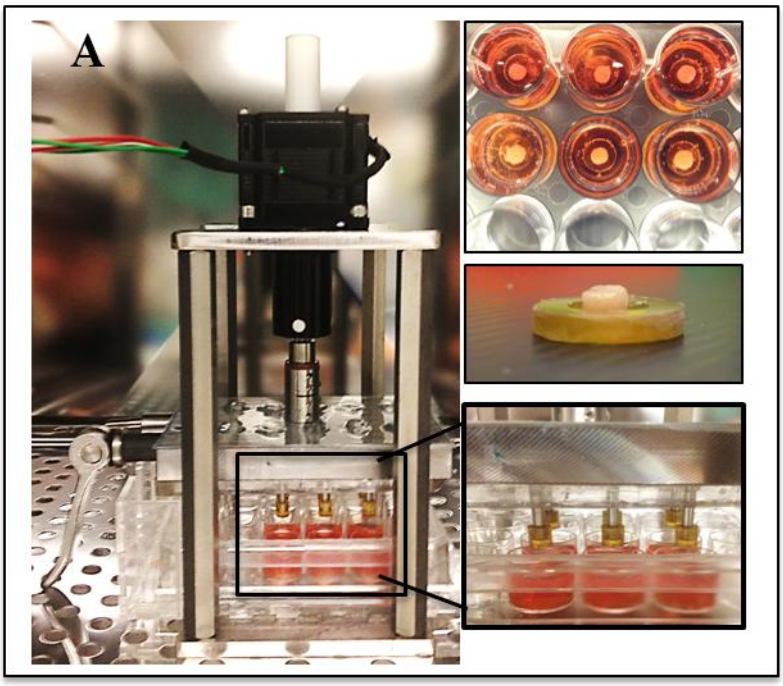

Figure 3.19. Experimental setup for the pilot study. (A) Compression bioreactor housing the TE-SK-N-MC and the TE-bone. (B) Stimulation protocol.

3.3.1 Gene expression: focal adhesion genes

One of the main features of the TE-ES previously described is that the 3D environment, along with the co-culture with osteoblast-like cells, induces the re-expression of 12 genes related to focal adhesion and cancer progression. Among these genes, CDC42 was found to be highly expressed in the tumor samples harvested from patients compared to the tumor cell lines. Furthermore, CDC42 and RHOA are both known to be involved into the mechanotransduction machinery (see **Chapter 1**). In particular, by regulating f-actin polymerization and the formation of stress fibers, they play an important role in several cellular functions including cell morphology and migration. In order to analyze the expression of CDC42 and RHOA, a qRT-PCR was performed, comparing the stimulated TE-SK-N-MC and the TE-bone to the respective counterparts not stimulated and to tumors harvested from patients. The expression was normalized to the expression of the SK-N-MC cell lines (**fig 3.20**).

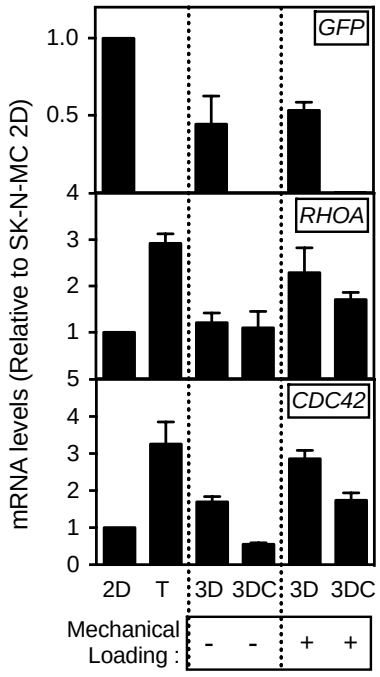

Figure 3.20. Re-expression of RHOA and CDC42. (Top panel) GFP expressed by tumor cells. (Middle panel) Re-expression of RHOA in the stimulated groups. (Bottom panel) Re-expression of CDC42 in both stimulated groups. 2D refers to SK-N-MC cell line, T refers to patients' tumor, 3D is the TE-SK-N-MC and 3DC the TE-bone. For the stimulated samples n=2, for the rest n=3.

The GFP expression was measured to ensure that there were viable tumor cells within the TE-ES and that there was not cross-contamination with the control (TE-bone). It is possible to see that the tumor cells express GFP and that in TE-bone there is no expression. The expression of RHOA is almost equal both in the TE-SK-N-MC and the TE-bone compared to 2D tumor cells. Whereas, in the stimulated group, the fold-change is greater than 2 for the TE-SK-N-MC and equal 2 for the TE-bone. Finally, the expression of CDC42 was almost 2 for the static TE-SK-N-MC and less than 1 for the static TE-bone. In contrast, the fold change of the same gene in the TE-SK-N-MC after the stimulation was 3 and for the TE-bone was 2. Taken together, these data show that 24 hours of stimulation is enough for the tumor cells to re-express focal adhesion-related genes.

3.3.2 F-actin immuno-staining

Focal adhesion genes, such as CDC42 and RHOA, have been previously linked to cell functions such as cell morphology and motility. It is known that these genes play a key role in the polymerization of the G-actin in F-actin, commonly referred as stress fibers [105]. In particular the polymerization of the F-actin leads to a reorganization of the cell's cytoskeleton and to changes of its morphology. As previously described, 24 hours of mechanical stimulation were enough to induce the re-expression of CDC42 and RHOA in the TE-SK-N-MC. Hence, F-actin immuno-staining was carry out to evaluate whether or not mechanical stimuli induce the formation of actin stress fibers in the TE-SK-N-MC compared to TE-bone.

In **figure 3.21** are represented both the TE-SK-N-MC and the TE-bone in static conditions (no mechanical loading), and it is manifest how the Ewing's sarcoma cells are round

shaped and form dense cluster, whereas the osteoblast-like cells have a typical mesenchymal morphology and are more sparse.

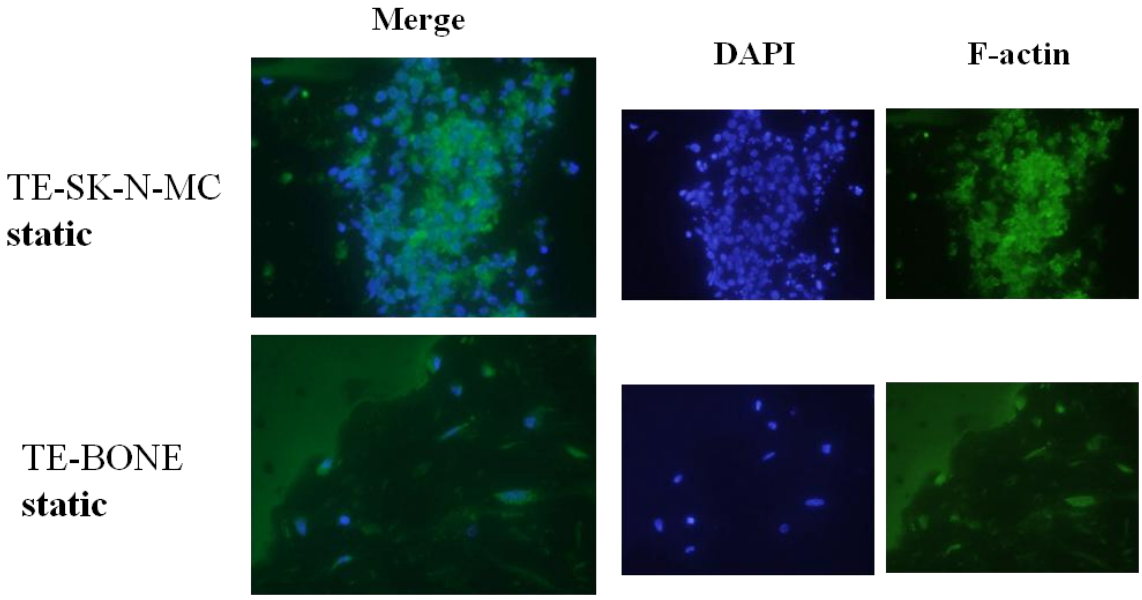

Figure 3.21. F-actin immuno-staining of TE-SK-N-MC and TE-bone in static condition. (Top) TE-SK-N-MC model. (Bottom) TE-bone model.

When stimulated for three times during 24 hours, the cells within the TE-SK-N-MC sense the mechanical cues, resulting in a higher expression of focal adhesion genes (such as CDC42 and RHOA) and with the formation of F-actin stress fibers (**fig 3.22**).

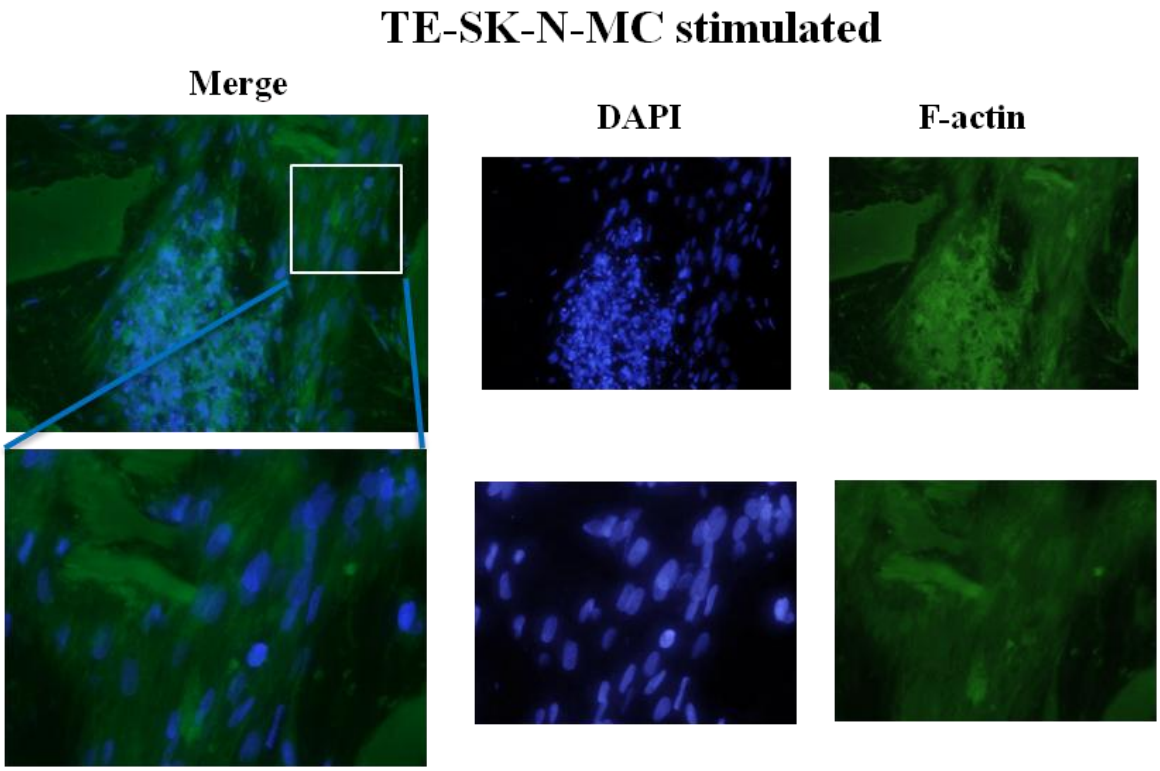

Figure 3.22. F-actin immuno-staining of stimulated TE-SK-N-MC.

In **figure 3.22**, groups of small rounded cells, most likely Ewing's sarcoma cells, are surrounded by elongated and highly orientated cells. This cluster of rounded cells and of polarized cells seems directed towards the center of the scaffold. It is unclear whether the elongated cells are the osteoblast-like, that might protect and lead the way to the cancer cells, or are the tumor cells themselves that after the mechanical stimulation switch to a more aggressive behavior that results in morphology changes and migration.

3.4 Discussion

An obvious goal of cancer engineers is to develop human tumor models predictive of native tumors *in vitro*. The most frequently used current models – spheroids of tumor cells and porous scaffolds – capture 3D aspects with some control of oxygen tension and pH [76] [77] [106] [107] [108] [109]. However, cancer is a complex disease where interactions between tumor cells and non-neoplastic cells play an important role in carcinogenesis [8]. Here, a step forward in modeling human tumors has been taken by incorporating Ewing's sarcoma cell spheroids into a bioengineered tridimensional bone niche, and thus enabling multiple interactions of tumor cells with other tumor cells, bone tissue matrix and bone cells. A large body of work has demonstrated that tumor cell lines cultured in 2D lose their transcriptional profiles and down-regulate many genes implicated in cell-cell and cell-ECM interactions, such as focal adhesion genes [2] [110]. Gene expression profiles of cell lines cultured in monolayers and native tumors were compared, with focus on differentially expressed focal adhesion genes and cancer pathways. The induction of 12 genes in both TE-RD-ES and TE-SK-N-MC models evidenced a major role of microenvironment in the acquirement of tumor expression profile. This model could therefore be used for the characterization of differentially expressed genes and could then help identify new tumor targets. Notably, induction of CDC42 and PPP1R12A was observed, both of which are related to Rho family of GTPases. Inhibition of some Rho pathway members through therapeutic compounds was successfully applied in preclinical studies [111] [112], suggesting that CDC42 and PPP1R12A are potential candidates for ES therapy. These results also show an important role of the bone niche in acquiring ESFT features to tumor cells, such as hypoxic and glycolytic phenotypes, angiogenesis potential and vasculogenic mimicry. Notably, the three ES cell lines tested in this study exhibited different behaviors in the bioengineered tumor model. The primary bone tumor RD-ES cell line seemed to perfectly mimic the ESFT signature, the *in vitro*-generated EWS-GFP cell line only in part and the metastatic SK-N-MC cell line was not able to recapitulate many of the tumor characteristics. These differences, correlated to the expression levels of HIF1-α (low in RD-ES cells, and high in SK-N-MC and EW-GFP cells), suggesting that HIF1-α might play a protective role in the adaptation of tumor cells to hypoxia. All the data point to a new direction in tumor modeling, where tumor cells are studied within the 3D niche – engineered to mimic the native host tissue. Some of the immediate needs include: the

inclusion of stromal cells, the incorporation of tumor microvasculature and the fine-tuned control of biochemical and biomechanical signals, all through the use of bioreactors.

For the last decade, bioreactors have been extensively employed in the Tissue Engineering field with the promise of obtaining implantable viable tissue constructs [11]. After a rapid improving and some optimistic results – mostly in the field of bone and cartilage tissue engineering [12, 13] – the transfer of experimental *in vitro* findings into a clinical approach still remains a vast challenge. Although their clinical applications in regenerative medicine tend to receive most of the attention, in this work an innovative application for bioreactors has been proposed. In fact, the second aim of this project is the design and development of a compression bioreactor for Cancer Tissue Engineering that could provide mechanical loading to 24 independent samples and suitable for drug studies. In this device, like in others [113], mechanical stimulation is achieved by the mean of plungers in direct contact with the scaffold. Precise plunger positioning upon the scaffold is ensured by a cam lever – springs mechanism preventing from experimental errors, therefore being an important feature in this device. Briefly, the plungers fall freely upon the scaffold when the operator pulls up the cam lever, releasing them from the clamping force provided by a set of stacked springs. An additional advantage is the *fluid exchange layer*; made with casted PDMS; it is characterized by 24 independent channels that allow drugs, growing factors or culture medium, to flow in or out each culture well. The *fluid exchange layer* and the cam lever-system are easily assembled together in the central core of the Culture module: the *Lid*. A further upper hand of this system is that every piece forming the *culture module,* when assembled, is autoclavable, thus ensuring sterility. Moreover, the *Lid* can be connected to a linear actuator coupled with a stepper motor that provides the vertical motion resulting in the compression loading. Ultimately, the motion is controlled by an Arduino mini and a stepper driver, that allow micro-stepping and, hence, very small displacements. The operator, after connecting the *Lid* to the linear, starts the stimulation program interfacing with a user-friendly GUI. In fact, just basic parameters such as motion waveform, amplitude and frequency are necessary to start the duty cycles. An important step in the developmental process of a bioreactor is the technical validation, where the consistency and the reliability of the system are assessed. For these reasons the device was tested for several displacement values at a fixed frequency (at 0.1 Hz or 1 Hz), denoting high accuracy for the three different waveforms (sinusoid, trapezoid and triangle). Furthermore,

the measured displacement was always correlated with the reference value. The validation process of the apparatus was then completed with the simulation of a possible experimental setup using COMSOL® Multiphysics. The geometry of the *Culture module* – comprising the insert well, the scaffold and the plunger – was recreated in the simulator. Afterward, a sinusoidal waveform with 14 μm of amplitude and 1 Hz frequency was generated. Finally, solving Von Mises' tensor, the stresses field at three different time points (0, 0.3, 0.5 seconds) was measured. With the resulting values it has been then possible to predict the stresses arising in the compressed bone scaffold used in the TE-ES and, most likely, sensed by the cells within it. This bioreactor represents an important tool that allows the simulation of some physical cues commonly present in the human bone. Since Ewing's sarcoma arises and spreads in the bone microenvironment, it is likely that tumor cells sense and transduce these mechanical stimuli that, on the other hand, influence the tumor fate. Hence, in the proposed pilot study, the TE-ES model was stimulated during 24 hours for three times at physiological values. The stimulation not only induced further expression of the already re-expressed CDC42 (compared to cell lines), but the fold change was comparable to the one seen in real tumors. Moreover, along with an increase of RHOA expression, F-actin staining demonstrated that the cells under mechanical compression – in TE-SK-N-MC but not in TE-bone – had a polarized shape and were highly oriented. It is unclear whether these polarized cells were only SK-N-MC cells or also osteoblast-like cells. For example in their work, Tse *et al.* showed that compressive stress stimulates migration of mammary carcinoma cells. The enhanced migration is accomplished by a subset of "leader cells" that extend filopodia at the leading edge of the cell sheet. Formation of these leader cells is dependent on cell micro-organization and is enhanced by compressive stress [20]. In **figure 3.23 A** is summarized the pathway involving the two small component of the Rho-GTPase family, CDC42 and RHOA, and their effect on F-actin fibers. Moreover, some studies have correlated the tumor cells change in morphology with an enhanced migration activity and hence with an increased aggressiveness of tumor cells (**fig 3.23 B and C**) [114].

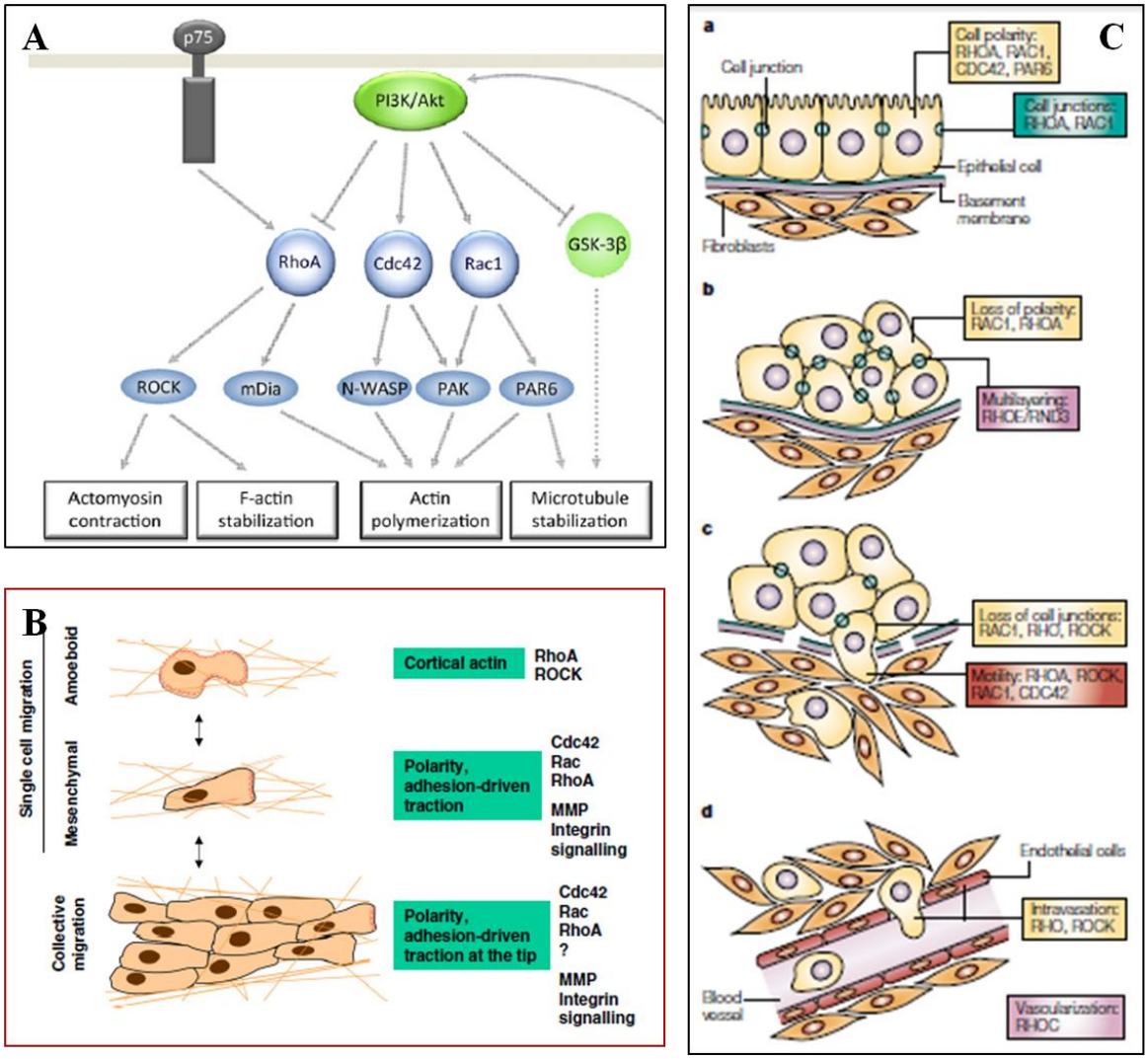

Figure 3.23. Expression of CDC42 and RHOA along with cells polarization enhances tumor motility. (A) CDC42 and RHOA induce actin polymerization and contraction. (B) RHOA and CDC42 play an important role in tumor cell shape and polarization. (C) CDC42 and RHOA are involved in tumors motility and aggressiveness. (a) Maintenance of normal epithelial polarity. (b) Benign tumors: loss of polarity and multi-layering. (c) Locally invasive tumors. (d) Metastasis to a distant site.

Taking together all these data, it seems straightforward that the novel TE-ES along with the compression bioreactor can be used as *in vitro* tools in the new born Cancer Tissue Engineering field, to closely mimic the complex tumor microenvironment. Eventually leading, in the future, to the identification of novel therapeutic targets currently neglected.

3.5 Conclusions and future work.

In this work, the first Ewing's sarcoma model has been developed, validated and characterized. Its capability to mimic tumor features most commonly seen in patients affected by Ewing's sarcoma such as hypoxia, glycolytic phenotype, secretion of angiogenic factors and vasculogenic mimicry , has been extensively demonstrated. Moreover, the 3D environment, along with the co-culture, induced in the TE-ES the re-expression of a cluster of genes related to focal adhesion and tumorigenesis when compared to tumor cell lines.

A great improving of the model could be achieved by introducing physiological and biophysical stimuli commonly present in the human bone, hence usually sensed by the tumor cells. For this reason, a novel compression bioreactor capable of stimulating 24 samples in parallel and providing a fluid-exchange system that allows drug studies has been designed and developed. Culturing the TE-ES in this bioreactor, under physiological stimuli, induced the polarization and orientation of the cells, most likely leading the tumor towards a more aggressive phenotype. More experiment and analysis are necessary to better understand and describe the effects of such stimuli on the TE-ES.

In the future, it will be important to optimize and fully validate both the Ewing's sarcoma experimental model and the compression bioreactor. The ultimate goal will be to establish an enabling technology for cancer research, in form of a bioengineering platform for studies of cancer biology and high-throughput screening of model *in vitro*. In order to develop the proposed platforms with bioengineered human tumors, for an advanced cancer research, it is possible to pursue three specific directions in a highly integrated fashion. First, to improve the actual model, the TE-bone should be pre-vascularized with HUVECs, as shown in previous studies [115] and then, by adding the ES spheroids, the TE-ES will be formed. In fact it was showed that under hypoxic conditions, the cells within the scaffold secreted angiogenic factors most likely attempting to form new blood vessels. This extra component would increase with great extent the complexity of the TE-ES allowing further insights in tumor mechanisms.

Second, it will be important to integrate the compression bioreactor with a perfusion system that could provide controlled oxygen and nutrient supply to the constructs. Hence, the integrated device would allow to study the effects of fluid shear stress and/or compression loading on pre-vascularized TE-ES. Last but not the least, it would be advisable to develop bioengineering platforms for high-throughput screenings of therapeutic ES targets, scaling down the TE-ES models (**fig.3.24**).

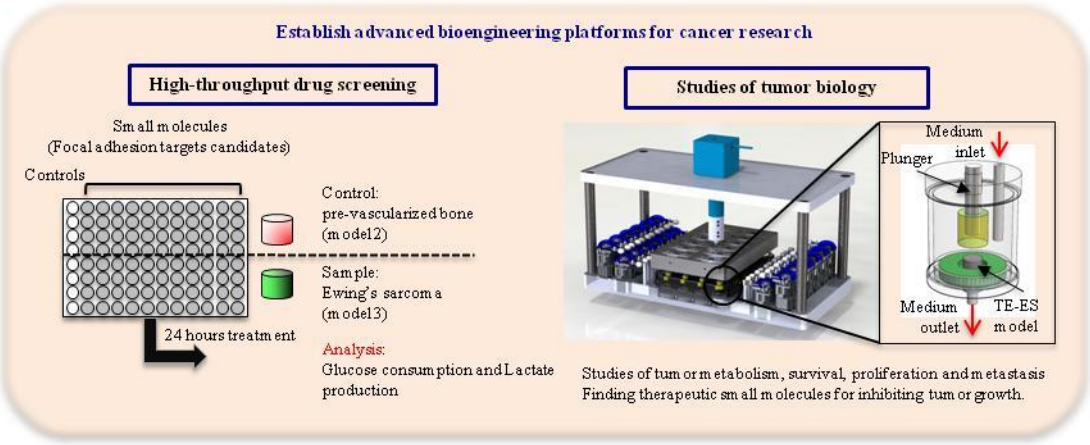

Figure 3.24. Bioengineering platform for cancer research.

In this project, innovative and powerful tools for tumor *in vitro* studies have been established, laying the basis for an avant-garde research in the newborn field of Cancer Tissue Engineering.

References

1. Chitcholtan, K., et al., *Differences in growth properties of endometrial cancer in three dimensional (3D) culture and 2D cell monolayer.* Exp Cell Res, 2013. **319**(1): p. 75-87.
2. Smalley, K.S., M. Lioni, and M. Herlyn, *Life isn't flat: taking cancer biology to the next dimension.* In Vitro Cell Dev Biol Anim, 2006. **42**(8-9): p. 242-7.
3. Seok, J., et al., *Genomic responses in mouse models poorly mimic human inflammatory diseases.* Proc Natl Acad Sci U S A, 2013. **110**(9): p. 3507-12.
4. van der Worp, H.B., et al., *Can animal models of disease reliably inform human studies?* PLoS Med, 2010. **7**(3): p. e1000245.
5. Yamada, K.M. and E. Cukierman, *Modeling tissue morphogenesis and cancer in 3D.* Cell, 2007. **130**(4): p. 601-10.
6. Kimlin, L.C., G. Casagrande, and V.M. Virador, *In vitro three-dimensional (3D) models in cancer research: an update.* Mol Carcinog, 2013. **52**(3): p. 167-82.
7. Nyga, A., U. Cheema, and M. Loizidou, *3D tumour models: novel in vitro approaches to cancer studies.* J Cell Commun Signal, 2011. **5**(3): p. 239-48.
8. Liotta, L.A. and E.C. Kohn, *The microenvironment of the tumour-host interface.* Nature, 2001. **411**(6835): p. 375-9.
9. Bissell, M.J. and W.C. Hines, *Why don't we get more cancer? A proposed role of the microenvironment in restraining cancer progression.* Nat Med, 2011. **17**(3): p. 320-9.
10. Geiger, B., J.P. Spatz, and A.D. Bershadsky, *Environmental sensing through focal adhesions.* Nat Rev Mol Cell Biol, 2009. **10**(1): p. 21-33.
11. Altman, G.H., et al., *Advanced bioreactor with controlled application of multi-dimensional strain for tissue engineering.* J Biomech Eng, 2002. **124**(6): p. 742-9.
12. Grayson, W.L., et al., *Engineering custom-designed osteochondral tissue grafts.* Trends Biotechnol, 2008. **26**(4): p. 181-9.
13. Mauck, R.L., et al., *Synergistic action of growth factors and dynamic loading for articular cartilage tissue engineering.* Tissue Eng, 2003. **9**(4): p. 597-611.
14. Marolt, D., et al., *Engineering bone tissue from human embryonic stem cells.* Proc Natl Acad Sci U S A, 2012. **109**(22): p. 8705-9.
15. Grayson, W.L., et al., *Effects of initial seeding density and fluid perfusion rate on formation of tissue-engineered bone.* Tissue Eng Part A, 2008. **14**(11): p. 1809-20.
16. Keaveny, T.M., et al., *Trabecular bone exhibits fully linear elastic behavior and yields at low strains.* J Biomech, 1994. **27**(9): p. 1127-36.
17. Marcos-Campos, I., et al., *Bone scaffold architecture modulates the development of mineralized bone matrix by human embryonic stem cells.* Biomaterials, 2012. **33**(33): p. 8329-42.
18. Hanahan, D. and J. Folkman, *Patterns and emerging mechanisms of the angiogenic switch during tumorigenesis.* Cell, 1996. **86**(3): p. 353-64.
19. van der Schaft, D.W., et al., *Tumor cell plasticity in Ewing sarcoma, an alternative circulatory system stimulated by hypoxia.* Cancer Res, 2005. **65**(24): p. 11520-8.
20. Tse, J.M., et al., *Mechanical compression drives cancer cells toward invasive phenotype.* Proc Natl Acad Sci U S A, 2012. **109**(3): p. 911-6.
21. Kim, Y., M.A. Stolarska, and H.G. Othmer, *The role of the microenvironment in tumor growth and invasion.* Prog Biophys Mol Biol, 2011. **106**(2): p. 353-79.
22. Hanahan, D. and R.A. Weinberg, *The hallmarks of cancer.* Cell, 2000. **100**(1): p. 57-70.
23. Warburg, O., *On the origin of cancer cells.* Science, 1956. **123**(3191): p. 309-14.

24. Kim, J.W. and C.V. Dang, *Cancer's molecular sweet tooth and the Warburg effect.* Cancer Res, 2006. **66**(18): p. 8927-30.
25. Jones, R.G. and C.B. Thompson, *Tumor suppressors and cell metabolism: a recipe for cancer growth.* Genes Dev, 2009. **23**(5): p. 537-48.
26. Mitchison, T.J. and L.P. Cramer, *Actin-based cell motility and cell locomotion.* Cell, 1996. **84**(3): p. 371-9.
27. Mundy, G.R., *Metastasis to bone: causes, consequences and therapeutic opportunities.* Nat Rev Cancer, 2002. **2**(8): p. 584-93.
28. Kenny, P.A., G.Y. Lee, and M.J. Bissell, *Targeting the tumor microenvironment.* Front Biosci, 2007. **12**: p. 3468-74.
29. Folkman, J., *Tumor angiogenesis: therapeutic implications.* N Engl J Med, 1971. **285**(21): p. 1182-6.
30. Cunha, G.R., et al., *Hormonal, cellular, and molecular regulation of normal and neoplastic prostatic development.* J Steroid Biochem Mol Biol, 2004. **92**(4): p. 221-36.
31. Dolberg, D.S. and M.J. Bissell, *Inability of Rous sarcoma virus to cause sarcomas in the avian embryo.* Nature, 1984. **309**(5968): p. 552-6.
32. Mueller, M.M. and N.E. Fusenig, *Friends or foes - bipolar effects of the tumour stroma in cancer.* Nat Rev Cancer, 2004. **4**(11): p. 839-49.
33. Joyce, J.A., *Tumour-Stroma Interactions at the Primary Site.* Nat review cancer, 2009.
34. Uccelli, A., L. Moretta, and V. Pistoia, *Mesenchymal stem cells in health and disease.* Nat Rev Immunol, 2008. **8**(9): p. 726-36.
35. Spaeth, E., et al., *Inflammation and tumor microenvironments: defining the migratory itinerary of mesenchymal stem cells.* Gene Ther, 2008. **15**(10): p. 730-8.
36. Karnoub, A.E., et al., *Mesenchymal stem cells within tumour stroma promote breast cancer metastasis.* Nature, 2007. **449**(7162): p. 557-63.
37. Marx, J., *Cancer biology. All in the stroma: cancer's Cosa Nostra.* Science, 2008. **320**(5872): p. 38-41.
38. Engler, A.J., et al., *Matrix elasticity directs stem cell lineage specification.* Cell, 2006. **126**(4): p. 677-89.
39. Paszek, M.J., et al., *Tensional homeostasis and the malignant phenotype.* Cancer Cell, 2005. **8**(3): p. 241-54.
40. Yu, H., J.K. Mouw, and V.M. Weaver, *Forcing form and function: biomechanical regulation of tumor evolution.* Trends Cell Biol, 2011. **21**(1): p. 47-56.
41. Butcher, D.T., T. Alliston, and V.M. Weaver, *A tense situation: forcing tumour progression.* Nat Rev Cancer, 2009. **9**(2): p. 108-22.
42. Helmlinger, G., et al., *Solid stress inhibits the growth of multicellular tumor spheroids.* Nat Biotechnol, 1997. **15**(8): p. 778-83.
43. Lynch, M.E., et al., *In Vivo tibial compression decreases osteolysis and tumor formation in a human metastatic breast cancer model.* J Bone Miner Res, 2013.
44. Heymann, D. and F. Rédini, *Bone sarcomas: pathogenesis and new therapeutic approaches.* IBMS BoneKEy, 2011. **8**(9): p. 402-414.
45. Subbiah, V., et al., *Ewing's sarcoma: standard and experimental treatment options.* Curr Treat Options Oncol, 2009. **10**(1-2): p. 126-40.
46. Riggi, N., et al., *EWS-FLI-1 Expression Triggers a Ewing's Sarcoma Initiation Program in Primary Human Mesenchymal Stem Cells.* Cancer Research, 2008. **68**(7): p. 2176-2185.
47. Riggi, N. and I. Stamenkovic, *The Biology of Ewing sarcoma.* Cancer Letters, 2007. **254**(1): p. 1-10.
48. Tora, L., et al., *Modeling Initiation of Ewing Sarcoma in Human Neural Crest Cells.* PLoS ONE, 2011. **6**(4): p. e19305.
49. Esiashvili, N., M. Goodman, and R.B. Marcus, Jr., *Changes in incidence and survival of Ewing sarcoma patients over the past 3 decades: Surveillance Epidemiology and End Results data.* J Pediatr Hematol Oncol, 2008. **30**(6): p. 425-30.

50. Bonassar, L.J. and C.A. Vacanti, *Tissue engineering: the first decade and beyond.* J Cell Biochem Suppl, 1998. **30-31**: p. 297-303.
51. Boden, S.D., *Bioactive factors for bone tissue engineering.* Clin Orthop Relat Res, 1999(367 Suppl): p. S84-94.
52. Lieberman, J.R., A. Daluiski, and T.A. Einhorn, *The role of growth factors in the repair of bone. Biology and clinical applications.* J Bone Joint Surg Am, 2002. **84-A**(6): p. 1032-44.
53. Wang, E.A., et al., *Recombinant human bone morphogenetic protein induces bone formation.* Proc Natl Acad Sci U S A, 1990. **87**(6): p. 2220-4.
54. Trivedi, N., et al., *Improved vascularization of planar membrane diffusion devices following continuous infusion of vascular endothelial growth factor.* Cell Transplant, 2000. **9**(1): p. 115-24.
55. Wang EA, *Recombinant human bone morphogenetic protein induces bone formation.* Proc. Natl Acad. Sci. USA, 1990. **87**: p. 2220.
56. Trivedi N et al, *Improved vascularization of planar diffusion devices following continuous infusion of vascular endothelial growth factor (VEGF).* Cell Transplant, 1999. **8**: p. 175.
57. Stoltz, J.F., et al., *Influence of mechanical forces on cells and tissues.* Biorheology, 2000. **37**(1-2): p. 3-14.
58. Burdett, E., et al., *Engineering tumors: a tissue engineering perspective in cancer biology.* Tissue Eng Part B Rev, 2010. **16**(3): p. 351-9.
59. Hutmacher, D.W., et al., *Can tissue engineering concepts advance tumor biology research?* Trends Biotechnol, 2010. **28**(3): p. 125-33.
60. Sawyers, C., *Targeted cancer therapy.* Nature, 2004. **432**(7015): p. 294-7.
61. Santini, M.T., et al., *MG-63 human osteosarcoma cells grown in monolayer and as three-dimensional tumor spheroids present a different metabolic profile: a (1)H NMR study.* FEBS Lett, 2004. **557**(1-3): p. 148-54.
62. Voskoglou-Nomikos, T., J.L. Pater, and L. Seymour, *Clinical predictive value of the in vitro cell line, human xenograft, and mouse allograft preclinical cancer models.* Clin Cancer Res, 2003. **9**(11): p. 4227-39.
63. Morin, P.J., *Drug resistance and the microenvironment: nature and nurture.* Drug Resist Updat, 2003. **6**(4): p. 169-72.
64. Morton, C.L. and P.J. Houghton, *Establishment of human tumor xenografts in immunodeficient mice.* Nat Protoc, 2007. **2**(2): p. 247-50.
65. Richmond, A. and Y. Su, *Mouse xenograft models vs GEM models for human cancer therapeutics.* Dis Model Mech, 2008. **1**(2-3): p. 78-82.
66. Johnson, J.I., et al., *Relationships between drug activity in NCI preclinical in vitro and in vivo models and early clinical trials.* Br J Cancer, 2001. **84**(10): p. 1424-31.
67. Talmadge, J.E., et al., *Murine models to evaluate novel and conventional therapeutic strategies for cancer.* Am J Pathol, 2007. **170**(3): p. 793-804.
68. Lin, R.Z. and H.Y. Chang, *Recent advances in three-dimensional multicellular spheroid culture for biomedical research.* Biotechnol J, 2008. **3**(9-10): p. 1172-84.
69. Kang, H.G., et al., *E-cadherin cell-cell adhesion in ewing tumor cells mediates suppression of anoikis through activation of the ErbB4 tyrosine kinase.* Cancer Res, 2007. **67**(7): p. 3094-105.
70. Kleinman, H.K., et al., *Basement membrane complexes with biological activity.* Biochemistry, 1986. **25**(2): p. 312-8.
71. Kleinman, H.K. and G.R. Martin, *Matrigel: basement membrane matrix with biological activity.* Semin Cancer Biol, 2005. **15**(5): p. 378-86.
72. Bissell, M.J. and D. Radisky, *Putting tumours in context.* Nat Rev Cancer, 2001. **1**(1): p. 46-54.
73. Sinha, D.K. and C.J. White, *Collagen gel culture of rat mammary tumor cells as an assay system for determination of therapeutic efficacy of chemotherapeutic agents.* In Vitro Cell Dev Biol, 1988. **24**(6): p. 525-9.

74. O'Keane, J.C., et al., *A three-dimensional system for long-term culture of human colorectal adenomas.* Am J Pathol, 1990. **137**(6): p. 1539-47.
75. Sahoo, S.K., A.K. Panda, and V. Labhasetwar, *Characterization of porous PLGA/PLA microparticles as a scaffold for three dimensional growth of breast cancer cells.* Biomacromolecules, 2005. **6**(2): p. 1132-9.
76. Fischbach, C., et al., *Engineering tumors with 3D scaffolds.* Nat Methods, 2007. **4**(10): p. 855-60.
77. Fong, E.L., et al., *Modeling Ewing sarcoma tumors in vitro with 3D scaffolds.* Proc Natl Acad Sci U S A, 2013. **110**(16): p. 6500-5.
78. Martin, I., D. Wendt, and M. Heberer, *The role of bioreactors in tissue engineering.* Trends Biotechnol, 2004. **22**(2): p. 80-6.
79. Seidel, J.O., et al., *Long-term culture of tissue engineered cartilage in a perfused chamber with mechanical stimulation.* Biorheology, 2004. **41**(3-4): p. 445-58.
80. Altman, G.H., et al., *Cell differentiation by mechanical stress.* FASEB J, 2002. **16**(2): p. 270-2.
81. Radisic, M., et al., *Cardiac tissue engineering using perfusion bioreactor systems.* Nat Protoc, 2008. **3**(4): p. 719-38.
82. Radisic, M., et al., *Optical mapping of impulse propagation in engineered cardiac tissue.* Tissue Eng Part A, 2009. **15**(4): p. 851-60.
83. Cimetta, E., et al., *Microfluidic bioreactor for dynamic regulation of early mesodermal commitment in human pluripotent stem cells.* Lab Chip, 2013. **13**(3): p. 355-64.
84. Vunjak-Novakovic, G., et al., *Microgravity studies of cells and tissues.* Ann N Y Acad Sci, 2002. **974**: p. 504-17.
85. Hung, C.T., et al., *A paradigm for functional tissue engineering of articular cartilage via applied physiologic deformational loading.* Ann Biomed Eng, 2004. **32**(1): p. 35-49.
86. Cigognini, D., et al., *Engineering in vitro microenvironments for cell based therapies and drug discovery.* Drug Discov Today, 2013.
87. Jagodzinski, M., et al., *Influence of perfusion and cyclic compression on proliferation and differentiation of bone marrow stromal cells in 3-dimensional culture.* J Biomech, 2008. **41**(9): p. 1885-91.
88. Sittichokechaiwut, A., et al., *Short bouts of mechanical loading are as effective as dexamethasone at inducing matrix production by human bone marrow mesenchymal stem cell.* Eur Cell Mater, 2010. **20**: p. 45-57.
89. Shachar, M., N. Benishti, and S. Cohen, *Effects of mechanical stimulation induced by compression and medium perfusion on cardiac tissue engineering.* Biotechnology Progress, 2012. **28**(6): p. 1551-1559.
90. de Peppo, G.M., et al., *Engineering bone tissue substitutes from human induced pluripotent stem cells.* Proc Natl Acad Sci U S A, 2013. **110**(21): p. 8680-5.
91. Wilson, W.R. and M.P. Hay, *Targeting hypoxia in cancer therapy.* Nat Rev Cancer, 2011. **11**(6): p. 393-410.
92. Savola, S., et al., *High Expression of Complement Component 5 (C5) at Tumor Site Associates with Superior Survival in Ewing's Sarcoma Family of Tumour Patients.* ISRN Oncol, 2011. **2011**: p. 168712.
93. Pasque, V., et al., *Histone variant macroH2A confers resistance to nuclear reprogramming.* EMBO J, 2011. **30**(12): p. 2373-87.
94. Ozcivici, E., et al., *Mechanical signals as anabolic agents in bone.* Nat Rev Rheumatol, 2010. **6**(1): p. 50-9.
95. Tzima, E., et al., *Activation of integrins in endothelial cells by fluid shear stress mediates Rho-dependent cytoskeletal alignment.* EMBO J, 2001. **20**(17): p. 4639-47.
96. Wozniak, M.A., et al., *ROCK-generated contractility regulates breast epithelial cell differentiation in response to the physical properties of a three-dimensional collagen matrix.* J Cell Biol, 2003. **163**(3): p. 583-95.

97. Provenzano, P.P. and P.J. Keely, *Mechanical signaling through the cytoskeleton regulates cell proliferation by coordinated focal adhesion and Rho GTPase signaling.* J Cell Sci, 2011. **124**(Pt 8): p. 1195-205.
98. Scotlandi, K., et al., *Insulin-like growth factor I receptor-mediated circuit in Ewing's sarcoma/peripheral neuroectodermal tumor: a possible therapeutic target.* Cancer Res, 1996. **56**(20): p. 4570-4.
99. O'Neill, A., et al., *Insulin-like growth factor 1 receptor as a therapeutic target in ewing sarcoma: lack of consistent upregulation or recurrent mutation and a review of the clinical trial literature.* Sarcoma, 2013. **2013**: p. 450478.
100. Wachsberger, P., R. Burd, and A.P. Dicker, *Tumor response to ionizing radiation combined with antiangiogenesis or vascular targeting agents: exploring mechanisms of interaction.* Clin Cancer Res, 2003. **9**(6): p. 1957-71.
101. Jiang, Y., et al., *A multiscale model for avascular tumor growth.* Biophys J, 2005. **89**(6): p. 3884-94.
102. Mueller-Klieser, W., *Tumor biology and experimental therapeutics.* Crit Rev Oncol Hematol, 2000. **36**(2-3): p. 123-39.
103. Carmeliet, P., et al., *Role of HIF-1alpha in hypoxia-mediated apoptosis, cell proliferation and tumour angiogenesis.* Nature, 1998. **394**(6692): p. 485-90.
104. Folberg, R., M.J. Hendrix, and A.J. Maniotis, *Vasculogenic mimicry and tumor angiogenesis.* Am J Pathol, 2000. **156**(2): p. 361-81.
105. Auer, M., B. Hausott, and L. Klimaschewski, *Rho GTPases as regulators of morphological neuroplasticity.* Ann Anat, 2011. **193**(4): p. 259-66.
106. Moreau, J.E., et al., *Tissue-engineered bone serves as a target for metastasis of human breast cancer in a mouse model.* Cancer Res, 2007. **67**(21): p. 10304-8.
107. Talukdar, S., et al., *Engineered silk fibroin protein 3D matrices for in vitro tumor model.* Biomaterials, 2011. **32**(8): p. 2149-59.
108. Sieh, S., et al., *Interactions between human osteoblasts and prostate cancer cells in a novel 3D in vitro model.* Organogenesis, 2010. **6**(3): p. 181-8.
109. Tan, P.H., et al., *Three-dimensional porous silk tumor constructs in the approximation of in vivo osteosarcoma physiology.* Biomaterials, 2011. **32**(26): p. 6131-7.
110. Zschenker, O., et al., *Genome-wide gene expression analysis in cancer cells reveals 3D growth to affect ECM and processes associated with cell adhesion but not DNA repair.* PLoS One, 2012. **7**(4): p. e34279.
111. Fritz, G. and B. Kaina, *Rho GTPases: promising cellular targets for novel anticancer drugs.* Curr Cancer Drug Targets, 2006. **6**(1): p. 1-14.
112. Lu, Q., et al., *Signaling through Rho GTPase pathway as viable drug target.* Curr Med Chem, 2009. **16**(11): p. 1355-65.
113. Waldman, S.D., et al., *Long-term intermittent compressive stimulation improves the composition and mechanical properties of tissue-engineered cartilage.* Tissue Eng, 2004. **10**(9-10): p. 1323-31.
114. Sahai, E. and C.J. Marshall, *RHO-GTPases and cancer.* Nat Rev Cancer, 2002. **2**(2): p. 133-42.
115. Correia, C., et al., *In vitro model of vascularized bone: synergizing vascular development and osteogenesis.* PLoS One, 2011. **6**(12): p. e28352.
116. Li, H., et al., *The Ink4/Arf locus is a barrier for iPS cell reprogramming.* Nature, 2009. **460**(7259): p. 1136-9.
117. Serrano, M., et al., *Oncogenic ras provokes premature cell senescence associated with accumulation of p53 and p16INK4a.* Cell, 1997. **88**(5): p. 593-602.
118. von Levetzow, C., et al., *Modeling initiation of Ewing sarcoma in human neural crest cells.* PLoS One, 2011. **6**(4): p. e19305.

Appendices

A1 Retroviral and Lentiviral transductions

Retroviral transductions were performed following a protocol previously reported [116] using a GFP retroviral vector (pBabe-Puro-GFP) provided by Dr. Manuel Serrano (CNIO, Madrid, Spain) [117]. Lentiviral transductions were performed as described previously [118]., 2011). EWS-FLI-GFP expression vector was generous provided by Dr. Elizabeth R. Lawlor (University of Michigan, Ann Arbor (MI), USA).

A2 Cytometry

Surface markers analysis by Fluorescence-activated cell sorting (FACS) was carried out as described previously (Marcos- Campos et al., 2012). Basically, hMSC and ES cell lines (RD-ES, SK-N-MC and EWSGFP) were harvested, centrifugated and incubated at 4°C for 1 hour with fluorochrome conjugated antibodies APC Mouse anti-human CD13 (BD Pharmingen, 557454), APC Mouse anti-human CD44 (BD Pharmingen, 560532), APC Mouse anti-human CD73 (BD Pharmingen, 560847), APC Mouse anti-human CD90 (BD Pharmingen, 559869) and APC Mouse anti-human CD105 (BD Pharmingen, 562408). Negative control cells were stained with APC mouse IgG1, k isotype control, Clone MOPC-21 (BD Pharmingen, 555751). CD99 expression was assed incubating cells with CD99 primary antibody (Signet antibodies, SIG-3620). FACS data were analyzed using FlowJo software version 7.6 (Tree Star Inc., Ashland, OR, USA)

A3 qRT-PCR protocol.

RNA EXTRACTION.

- Samples stored at -80 ^{o}C in Trizol. Thaw them on ice (13th floor)
- ARNase free area: Clean against RNA using RNAase kit. Clean bench and tools.

- Transfer Trizol with bone scaffolds to sarstedt tubes.They provide better resistance and break less often.
- Add 4 metal beads in each tube.
- Wrap the tubes in a napkin before using the MINI BEAD BEATER. (It prevents the tubes from moving in the machine.)
- Activate switch. CAREFUL! Tubes tend to break if shacked for a long time. (use 5 seconds on, 3 econds off as many times you need to desegregate the matrix completely).
- Transfer homogenate to 1.5mL eppendorf tubes
- If necessary dilute with Trizol. (if color tends to orange a dilution is needed, if the color is pinkish no).
- V_{fin} = 1mL; V_{try} = 0.5 mL; V_{sample} = 0.5 mL (operate under chemical hood).
- Add chloroform 200 μL (low viscosity fluid, cut the tip at the narrow extremity).
- Vortex carefully each sample. (has to be yellowish after).
- Centrifuge at 13,2 X 10^3 RPM, 15 min, 4 ^{o}C.
- After Centrifuge 3 layers are observable. From top to bottom. 1) RNA 2) Proteins & Lipids & DNA 3) general debris.
- Add Isopropanol 500 μL into a tube (general eppendorf 1.5 mL).
  Carefully extract the supernatant (layer 1) using a pipette and transfer into the tube with isopropanol.
- Don't disrupt or touch the other layers. If you do just go back to the vortex + centrifuge step.
- Put another rack on top of the samples and turn it upside down
- Centrifuge at 12.6 10^3 RPM, 10 min, RT (room temperature).
- Prepare EtOH 70%. Use a sterile container and use DEPC treated water. Use pipette for this operation.
- Remove supernatant from tube. Use a p1000 and do not touch the pellet on the bottom.
- Add 1 mL of EtOH 70%.
- Centrifuge 7.6 10^3 RPM, 5 min, RT

- Remove EtOH 70%. Add EtOH 70%. Remove EtOH as much as you can. Use p100 if necessary.
- Re-suspend in DEPC treated water.
- Add first DEPC treated water in a new 1.5 mL eppendorf tube
- Depending on the pellet size add: 30 μL (big), 20 μL (small), 10uL…5uL

RNA QUANTIFICATION (7^{th} floor)

- Bring samples in the bucket with ice.
- Use NanoDrop device.
- Add 1 μL of DEPC treated water (check if it works properly).
- Add 1 μL of DEPC treated water and click BLANK.
- Write sample name in the software and add 1 μL of RNA sample
- The ratio of absorbance at 260 nm and 280 nm is used to assess the purity of DNA and RNA. A ratio of ~1.8 is generally accepted as "pure" for DNA; a ratio of ~2.0 is generally accepted as "pure" for RNA. If the ratio is appreciably lower in either case, it may indicate the presence of protein, phenol or other contaminants that absorb strongly at or near 280 nm.
- Depending on the final concentration of RNA we extract a Volume of RNA sample to have 2 μg of RNA
- Freeze the rest of the samples at -80 ^{o}C.

A4 PRIMERS list

Gene Description	**PrimerBank ID**
beta actin (Actin)	4501885a1
EWS-Fli1 fusion isoform type 8 (EWS-FLI)	633772a1
Homo sapiens NK2 homeobox 2 (NKX2-2)	32307133b1
Homo sapiens tumor protein p53 (TP53)	371502118c1
ACTN4 Homo sapiens actinin, alpha 4 (ACTN4)	316660986c2

CCND2 Homo sapiens cyclin D2 (CCND2)	209969683c1
COL1A2 Homo sapiens collagen, type I, alpha 2 (COL1A2)	48762933c3
COL3A1 Homo sapiens collagen, type III, alpha 1 (COL3A1)	110224482c2
Homo sapiens collagen, type VI, alpha 1 (COL6A1)	87196338c2
COL6A2 Homo sapiens collagen, type VI, alpha 2 (COL6A2)	115527065c1
COL6A3 Homo sapiens collagen, type VI, alpha 3 (COL6A3)	240255534c1
FLNB Homo sapiens filamin B, beta (FLNB)	256222414c2
MYLK Homo sapiens myosin light chain kinase (MYLK	116008189c1
Homo sapiens 3-phosphoinositide dependent protein kinase-1 (PDPK1)	60498971c1
Homo sapiens protein phosphatase 1, regulatory subunit 12A (PPP1R12A)	219842213c1
Homo sapiens insulin-like growth factor 1 (somatomedin C) (IGF1)	163659898c1
VCL Homo sapiens vinculin (VCL)	50593538c1
CDKN1B Homo sapiens cyclin-dependent kinase inhibitor 1B (p27, Kip1) (CDKN1B)	207113192c3
Homo sapiens C-terminal binding protein 1 (CTBP1)	61743966c2
CTBP2 Homo sapiens C-terminal binding protein 2 (CTBP2)	145580576c1
ETS1 Homo sapiens v-ets erythroblastosis virus E26 oncogene homolog 1 (avian) (ETS1)	219689117c1
c-K-ras2 protein isoform a (KRAS)	15718763a1
PIAS1 Homo sapiens protein inhibitor of activated STAT, 1 (PIAS1)	7706636c2
Homo sapiens retinoid X receptor, alpha (RXRA)	207028087c3
Homo sapiens signal transducer and activator of transcription 3 (STAT3)	47080104c1
Homo sapiens cell division cycle 42 (GTP binding protein, 25kDa) (CDC42)	89903014c1

Homo sapiens collagen, type IV, alpha 2 (COL4A2)	116256353c1
Homo sapiens catenin (cadherin-associated protein), beta 1, 88kDa (CTNNB1)	148233337c2
Homo sapiens jun proto-oncogene (JUN)	44890066c1
laminin alpha 4 chain (LAMA4)	4504949a2
Homo sapiens laminin, beta 1 (LAMB1)	167614503c1
Homo sapiens laminin, gamma 1 (formerly LAMB2) (LAMC1)	145309325c3
Homo sapiens phosphoinositide-3-kinase, regulatory subunit 1 (alpha) (PIK3R1)	335057530c3
Homo sapiens phosphatase and tensin homolog (PTEN)	110224474c2
Homo sapiens hypoxia inducible factor 1, alpha subunit (HIF1A)	194473734c1
Homo sapiens vascular endothelial growth factor A (VEGFA)	NM_001101
Homo sapiens EPH receptor A2 (EPHA2)	296010835c1
Homo sapiens tissue factor pathway inhibitor (TFPI)	98991770c1
Homo sapiens laminin, gamma 2 (LAMC2)	157419139c1

A5 TUNEL assay protocol

- Fix cells in 1% PFA in PBS (pH 7.4) for 10 minutes at RT
- Wash in PBS twice for 5 minutes each
- Change to fresh PBS, parafilm, and store at 4°C until ready to proceed with staining
- Post-fix in cooled Ethanol: Acetic Acid (2:1) for 5 minutes at ‑20°C (perm eabilization)
- Wash in PBS twice for 5 minutes each.
- Apply Equilibration Buffer (13µl per cm2)

- Immediately add Working Strength TdT enzyme (77µl reaction buffer + 33µl TdT,
  vortex, store on ice) and incubate in humidified chamber at 37°C for 1 hour .
- Agitate for 15 seconds in Working Strength Stop/Wash Buffer (1ml Stop/Wash Buffer, 34ml dH20) and then incubate for 10 minutes.
- Remove an aliquot of Anti-digoxigenin conjugate and warm to RT in DARK .
- Wash in PBS 3 times for 1 minute each.
- Apply warmed Anti-Digoxigenin conjugate (13µl per cm2) and incubate in DARK humidified chamber at RT for 30 minutes.
- Wash in PBS 4 times for 2 minutes each.
- Mount with DAPI, seal coverslip, store at ‑20°C.Updated 12/30/10
- Working Strength TdT
  77µl Reaction Buffer
  33µl TdT (glycerol stock in ‑20)
  110µl Total
  Vortex and store on ice for up to 6 hours
- Working Strength Stop/Wash Buffer
  1ml Stop/Wash Buffer
  34ml dH20
  35ml Total
  Store at 4°C for up to a year
  Working Strength Anti-Digoxigenin Conjugate
  68µl Blocking Solution
  62µl Anti-Digoxigenin Conjugate
  130µl Total
  Vortex, store on ice for up to 3 hours, protect from light

A6 ELISA assay

(http://www.rndsystems.com/multiplex_assay_arrays_detail_objectname_li_cor_human_angiogenesis_array.aspx)

1. Prepare all reagents and samples as directed in the previous sections.
2. Pipette 2.0 mL of Array Buffer 7 into each well of the 4-Well Multi-dish to be used.
3. Using flat-tip tweezers, remove each membrane to be used from between the protective sheets. **Carefully cut off the stamped identification number on the membrane using scissors.** Membrane may be labeled with pencil in the empty space to the right side of the array. Pick up the membrane from this edge during all processing steps.
4. Place one membrane in each well of the 4-Well Multi-Dish.

Note: Upon contact with Array Buffer 7, the blue dye from the spots will disappear, but the capture antibodies are retained in their specific locations.

5. Incubate for one hour on a rocking platform. Orient the tray so that each array rocks end to end in its well. Array Buffer 7 serves as a block buffer.
6. While the membranes are blocking, prepare samples by adding up to 1 mL of each sample to 0.5 mL of Array Buffer 4 in separate tubes. Adjust to a final volume of 1.5 mL with Array Buffer 5 as necessary.
7. Add 15 µL of reconstituted Human Angiogenesis Array Detection Antibody Cocktail to each prepared sample. Mix and incubate at room temperature for one hour.
8. Aspirate Array Buffer 7 from the wells of the 4-Well Multi-dish and add sample/antibody mixtures prepared in step 6. Place the lid on the 4-Well Multi-dish.
9. Incubate overnight at 2 - 8° C on a rocking platform.

Note: A shorter incubation time may be used if optimal sensitivity is not required.

10. Carefully remove each membrane and place into individual plastic containers with 20 mL of 1X Wash Buffer. Rinse the 4-Well Multi-dish with deionized or distilled water and dry thoroughly.

11. Wash each membrane with 1X Wash Buffer for 10 minutes on a rocking platform shaker. Repeat two times for a total of three washes.

12. Dilute the IRDye 800CW Streptavidin (LI-COR, Catalog 926-32230) 1:2000 in Array Buffer 5. Pipette 1.5 mL of diluted IRDye 800CW Streptavidin into each well of the 4-Well Multi-Dish.

13. Carefully remove each membrane from its wash container. Allow excess buffer to drain from the membrane by blotting the lower edge onto absorbent paper. Return the membrane to the 4-Well Multi-dish containing the diluted IRDye 800CW Streptavidin. Cover the wells with the lid.

14. Incubate for 30 minutes at room temperature on a rocking platform.

15. Wash each array as described in steps 10 and 11.

16. Carefully remove each membrane from the wash container. Allow excess Wash Buffer to drain from the membrane by blotting the lower edge onto absorbent paper. Collect images with an Odyssey Imager.

A7 Stepper motor/ linear actuator specifications

Series	57000
Size	23
Stack Length	single
Mounting Footprint (in)	2.3
Actuator Type	captive
Captive Stroke Length (in)	1.5
Screw Length (Non-captive / External linear) (in)	n/a
Step Angle	1.8°
Linear Travel per Step (in)	0.0003125
Maximum Thrust (Chopper drive, 100% Duty Cycle) (lb)	200
Power	13 W
Winding Voltage	3.25 VDC
Current per Phase	2.0 amps
Resistance per Phase	1.63 ohms
Inductance per Phase	3.5 mH
Wiring	bipolar
Connection	12" Flying Leads
Temperature Rise (F)	135°
Insulation Resistance	20 Mohms
Price USD	$195.44

A8 Technical Drawings

57000 Series Size 23
Hybrid Stepper Motor
Linear Actuator

Part Number:
57H4A-3.25-807

Measurement Units = (mm) decimal inches

Captive Shaft

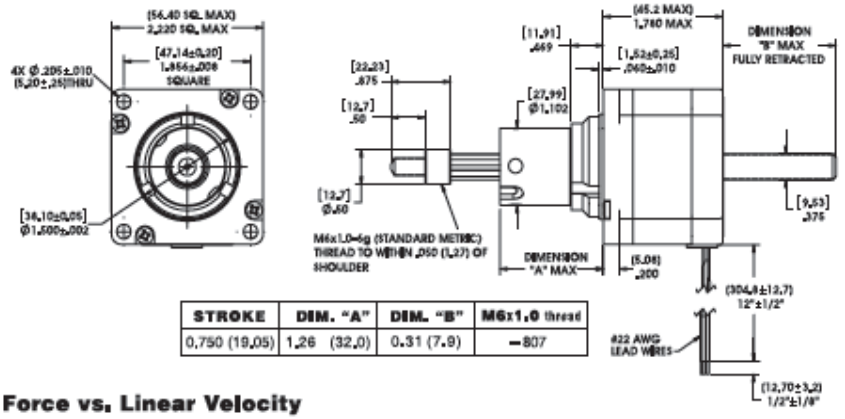

STROKE	DIM. "A"	DIM. "B"	M6x1.0 thread
0.750 (19.05)	1.26 (32.0)	0.31 (7.9)	–807

Force vs. Linear Velocity

Bipolar • Chopper • 100% Duty Cycle • Ø 0.375-in. (9.53 mm) Leadscrew

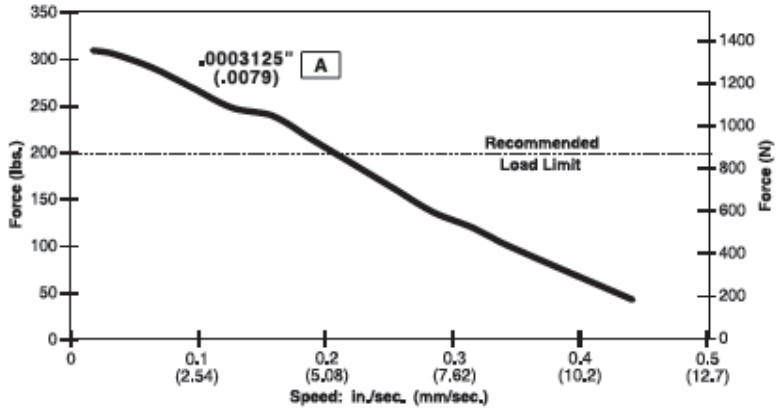

NOTE: All chopper drive curves were created with a 5 volt motor and a 40 volt power supply.

Ramping can increase the performance of a motor either by increasing the top speed or getting a heavier load accelerated up to speed faster. Also, deceleration can be used to stop the motor without overshoot.

NORTH AMERICA • EUROPE • ASIA
www.HaydonKerk.com
1.800.243.2715 International: 203.756.7441

A9 System capabilities

Maximum Displacement (mm)					
Frequency (Hz)	*Resolution (microns/step)*	*Triangle Waverform*	*Trapezoidal Waveform (50% hold time)*	*Trapezoidal Waveform (80% hold time)*	*Sinusoidal Waveform*
0.01	7.94	198	99	40	99
	3.97	99	50	20	50
	1.98	50	25	9.9	25
	0.99	25	12.4	5.0	12.4
	0.50	12.4	6.2	2.5	6.2
0.1	7.94	19.8	9.9	4.0	9.9
	3.97	9.9	5.0	2.0	5.0
	1.98	5.0	2.5	0.99	2.5
	0.99	2.5	1.24	0.50	1.24
	0.50	1.24	0.62	0.25	0.62
1	7.94	1.98	0.99	0.40	0.99
	3.97	0.99	0.50	0.20	0.50
	1.98	0.50	0.25	0.099	0.25
	0.99	0.25	0.124	0.050	0.124
	0.50	0.12	0.062	0.025	0.062
4	7.94	0.50	0.25	0.099	0.25
	3.97	0.25	0.124	0.050	0.124
	1.98	0.12	0.062	0.025	0.062
	0.99	0.062	0.031	0.012	0.031
	0.50	0.031	0.016	0.0062	0.016

A10 Arduino source code

```
#define MS1_PIN 12

#define MS2_PIN 11

#define MS3_PIN 10

#define STEP_PIN 7

#define DIR_PIN 8

#define UP_PIN 6

#define DOWN_PIN 4

#define GND_PIN_1 3

#define GND_PIN_2 5
```

```
#define up true
#define down false
void configTimer();
volatile float cyclesPerHalfPeriod;
volatile float stepCount;
volatile float cycleCount;
volatile int halfRevolutionCount;
volatile float slope;
volatile int duration;
volatile boolean dir = down;
volatile int waveform;
volatile int resolution;
volatile float period;
volatile float stepDisplacement;
volatile float duty;
volatile float holdCycles;
void setup() {
  Serial.begin(9600);
  configTimer();
  pinMode(MS1_PIN,OUTPUT);
  pinMode(MS2_PIN,OUTPUT);
  pinMode(MS3_PIN,OUTPUT);
```

```
  pinMode(STEP_PIN,OUTPUT);
  pinMode(DIR_PIN,OUTPUT);
  pinMode(UP_PIN,INPUT_PULLUP);
  pinMode(DOWN_PIN,INPUT_PULLUP);
  pinMode(GND_PIN_1, OUTPUT);
  pinMode(GND_PIN_2, OUTPUT);
  digitalWrite(MS1_PIN,LOW);
  digitalWrite(MS2_PIN,LOW);
  digitalWrite(MS3_PIN,LOW);
  digitalWrite(STEP_PIN,LOW);
  digitalWrite(DIR_PIN,dir);
  digitalWrite(GND_PIN_1,LOW);
  digitalWrite(GND_PIN_2,LOW);
 }
void loop()
{
  if (Serial.available()>=9)
  {
     int val1= Serial.read();
     int val2= Serial.read();
     int val3= Serial.read();
     int val4= Serial.read();
```

```
int val5= Serial.read();
int val6= Serial.read();
int val7= Serial.read();
int val8 = Serial.read();
int val9 = Serial.read();
waveform = val1;
resolution = val2;
period = 256*val3+val4;
stepDisplacement=256*val5+val6;
duty = val7;
duration = 256*val8+val9;
if (duration ==0) duration = -1;
switch(resolution)
{
  case (1):
  {
    digitalWrite(MS1_PIN,LOW);
    digitalWrite(MS2_PIN,LOW);
    digitalWrite(MS3_PIN,LOW);
    break;
  }
  case (2):
```

```
{
  digitalWrite(MS1_PIN,HIGH);
  digitalWrite(MS2_PIN,LOW);
  digitalWrite(MS3_PIN,LOW);
  break;
}
case (4):
{
  digitalWrite(MS1_PIN,LOW);
  digitalWrite(MS2_PIN,HIGH);
  digitalWrite(MS3_PIN,LOW);
  break;
}
case (8):
{
  digitalWrite(MS1_PIN,HIGH);
  digitalWrite(MS2_PIN,HIGH);
  digitalWrite(MS3_PIN,LOW);
  break;
}
case (16):
{
```

```
      digitalWrite(MS1_PIN,HIGH);
      digitalWrite(MS2_PIN,HIGH);
      digitalWrite(MS3_PIN,HIGH);
      break;
    }
  }
  stepCount=0;
  cycleCount=0;
  halfRevolutionCount=0;
  dir = down;
  digitalWrite(DIR_PIN,dir);
  cyclesPerHalfPeriod=period/4.0;  //divide period in half then in half again because we want to go from ms to timer cycles
  switch(waveform)
  {
    case (1):
    {
     slope = stepDisplacement/cyclesPerHalfPeriod;
     break;
    }
    case (2):
    {
```

```
            holdCycles = cyclesPerHalfPeriod*duty/100.0;
        slope = stepDisplacement/(cyclesPerHalfPeriod-holdCycles);
        break;
       }
       case (3):
       {
        break;
       }
         }
    TIMSK1 |= (1 << OCIE1A); //enable timer interrupt
   }
  delay(10);
}
ISR(TIMER1_COMPA_vect)
{
  //check for button control
  if (digitalRead(UP_PIN)==LOW)
  {
    digitalWrite(DIR_PIN, up);
    digitalWrite(STEP_PIN, HIGH);
    digitalWrite(STEP_PIN, LOW);
    return;
```

```
 }
if(digitalRead(DOWN_PIN)==LOW)
{
   digitalWrite(DIR_PIN, down);
   digitalWrite(STEP_PIN, HIGH);
   digitalWrite(STEP_PIN, LOW);
   return;
}
//move according to waveform
if (waveform==0)return;
if (halfRevolutionCount == duration)
{
  TIMSK1 |= (0 << OCIE1A);
  return;
}
  if (cycleCount==cyclesPerHalfPeriod)
{
    cycleCount = 0;
    halfRevolutionCount++;
    stepCount=0;
    dir=!dir;
    digitalWrite(DIR_PIN,dir);
```

```
}
switch (waveform)
{
  case (1):
  {
    if (slope*cycleCount - stepCount > 0.5)
    {
        digitalWrite(STEP_PIN,HIGH);
        stepCount++;
        digitalWrite(STEP_PIN, LOW);
    }
    cycleCount++;
    break;
  }
  case (2):
  {
    if ((slope*cycleCount - stepCount > 0.5)&&(slope*cycleCount < stepDisplacement))
    {
      digitalWrite(STEP_PIN,HIGH);
      stepCount++;
      digitalWrite(STEP_PIN, LOW);
    }
```

```
      cycleCount++;
      break;
    }
    case (3):
    {
      if ( (((-
stepDisplacement/2)*cos(cycleCount*PI/cyclesPerHalfPeriod)+(stepDisplacement/2))-
stepCount) > 0.5)
      {
          digitalWrite(STEP_PIN,HIGH);
          stepCount++;
          digitalWrite(STEP_PIN, LOW);
      }
      cycleCount++;
      break;
    }
  }
}
void serialEvent()
{
  TIMSK1 |= (0 << OCIE1A);//disable timer interrupt
}
void configTimer()
```

```
{
  //configure 2 ms interrupt on timer 1
  noInterrupts(); //disable all interrupts
  TCCR1A = 0;  //clear timer control registers
  TCCR1B = 0;
  TCNT1 = 0;  //preload timer to zero
  OCR1A = 4000; //output compare match register 16MHz/8/0.5 kHz
  TCCR1B |= (1<<WGM12); //clear timer on compare mode, output compare
  TCCR1B |= (1<<CS11);  //8 prescaler
  TIMSK1 |= (1 << OCIE1A);  //enable timer output compare interrupt
  interrupts();
}
```

A11 Circuit schematics

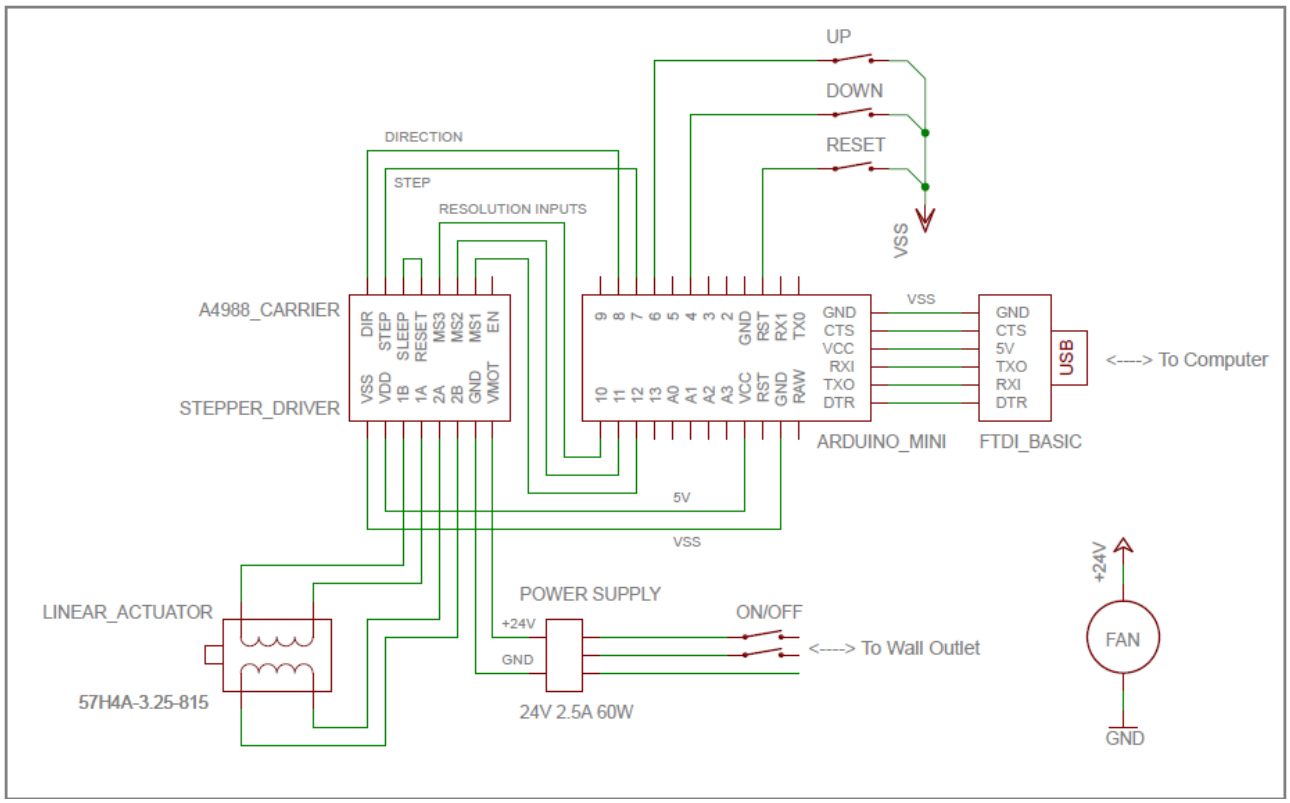

A12 F-actin staining

1. Wash cells twice with prewarmed phosphate-buffered saline, pH 7.4 (PBS).
2. Fix the sample in 3.7% formaldehyde solution in PBS for 10 minutes at room temperature. Note: Methanol can disrupt actin during the fixation process. Therefore, it is best to avoid any methanol containing fixatives. The preferred fixative is methanol-free formaldehyde.
3. Wash two or more times with PBS.
4. Place each coverslip in a glass petri dish and extract it with a solution of acetone at =–20°C or 0.1% Triton X-100 in PBS for 3 to 5 minutes.
5. Wash two or more times with PBS.

6. When staining with any of the fluorescent phallotoxins, dilute 5 µL methanolic stock solution into 200 µL PBS for each coverslip to be stained. To reduce nonspecific background staining with these conjugates, add 1% bovine serum albumin (BSA) to the staining solution. It may also be useful to pre-incubate fixed cells with PBS containing 1% BSA or with the Image-iT™ FX signal enhancer (I36933) for 20–30 minutes prior to adding the phallotoxin staining solution. When staining with biotin-XX phalloidin (B7474), dilute 10 µL of the methanolic stock solution into 200 µL PBS for each coverslip to be stained. When staining more than one coverslip, adjust volumes accordingly. For a stronger signal, use 2 or 3 units per coverslip.
7. Place the staining solution on the coverslip for 20 minutes at room temperature (generally, any temperature between 4°C and 37°C is suitable). To avoid evaporation, keep the coverslips inside a covered container during the incubation.
8. Wash two or more times with PBS.
9. When using biotin-XX phalloidin, incubate for 30 minutes with 100 µL of a 10 µg/mL solution of fluorescent or enzyme-conjugated streptavidin dissolved in 100 mM Tris-HCl, pH 7.5, 150 mM NaCl, 0.3% Triton X-100 and 1% BSA. Incubate for 15 minutes at room temperature. After incubation, wash the coverslip with PBS. To develop enzyme activity, follow a procedure recommended for the specific enzyme.
10. For long-term storage, the cells should be air dried and then mounted in a permanent mountant such as ProLong® Gold reagent or Cytoseal. Specimens prepared in this manner retain actin staining for at least six months when stored in the dark at 2–6°C.
11. 2. Simultaneous Fixation, Permeabilization, and Fluorescent Phallotoxin Staining
12. The phallotoxins appear to be stable for short periods in 4% formaldehyde fixation buffers. This permits a rapid one-step fixation, permeabilization, and labeling procedure as follows.
13. Prepare a 1 mL solution containing 50 to 100 µg/mL lysopalmitoylphosphatidylcholine and 3.7% formaldehyde and then add 5–10 units of fluorescent phallotoxin (approximately 25 to 50 µL of methanolic stock solution).

14. Place this staining solution on cells and incubate for 20 minutes at 4°C.
15. Rapidly wash three times with buffer.
16. Mount coverslips and view.

A13 Bioreactor set-up protocol

Material.

1) SS Lid + PDMS layer + plungers + spacers(n=12) (autoclave)
2) Ultem rings n=24 (autoclave)
3) Lever cams n=2 (autoclave)
4) 19g needles n>24 (sterile)
5) Injection adapters n>24 (sterile)
6) Bottom of housing (EtOH + overnight UV)
7) Standoff n=4 (auoclave)
8) Hex screw n=8 (autoclave)
9) Motor mounting plate + linear actuator (UV overnight).
10) Hex (autoclave)
11) Forceps n=2 (autoclave)
12) Paper towels (autoclave)
13) Petri dish p150 n=2 (sterile)
13) Modified 24 wp lid n=2.

Set-up.

1. Remember to leave the cells as long as possible in the incubator and reduce operation at room temperature.
2. Screw the 4 standoffs onto the SS bottom using the Hex and the Hex screws.
3. On top of the 4 stand offs put the motor mounting plate and use the 4 screw to tighten everything together.
4. Attach the lid to the shaft coupling and tight the last two screws of the shaft coupling

5. Add at each needle (19g) the injection adapter. Leave the needle in the paper and with the cap if needed to prevent contamination.
6. Insert the needles into each of the PTFE tube. Tube needle is meant to be a press fit so be careful with the needle not to break the tube.
7. Leave the injection adapters and the needle in the petri dishes keeping everything as sterile as possible.
8. Put the rings on the bottom of each well in the 24 well-plate. (use forceps)
9. TAKE CELLS FROM THE INCUBATOR.
10. Put the scaffold at the center of the ring.
11. Add cell medium in each well. Try not to move the scaffold from its position
12. Add the Modified 24 wp lid